Single Crystal Neutron Diffraction. What ‘s new?

Arsen Gukasov,

Laboratoire Léon Brillouin

CEA-CNRS, Saclay, France

OUTLINE

- Present state of SC Diffraction
- Recent Applications of SC Diffraction
- Polarized Neutron Diffraction
- Spin density and local susceptibility
- Polarization Analysis
- Future Challenges

2014 the Year of Cristallography

Solids of Platon

fire earth air water


2014 the Year of Cristallography
Cristallographie Elémentaire


Cristallographie
~~Elémentaire~~
Alimentaire

5 Two-Dimensional Bravais Lattices

Oblique *Rectangular*

Hexagonal *Square*

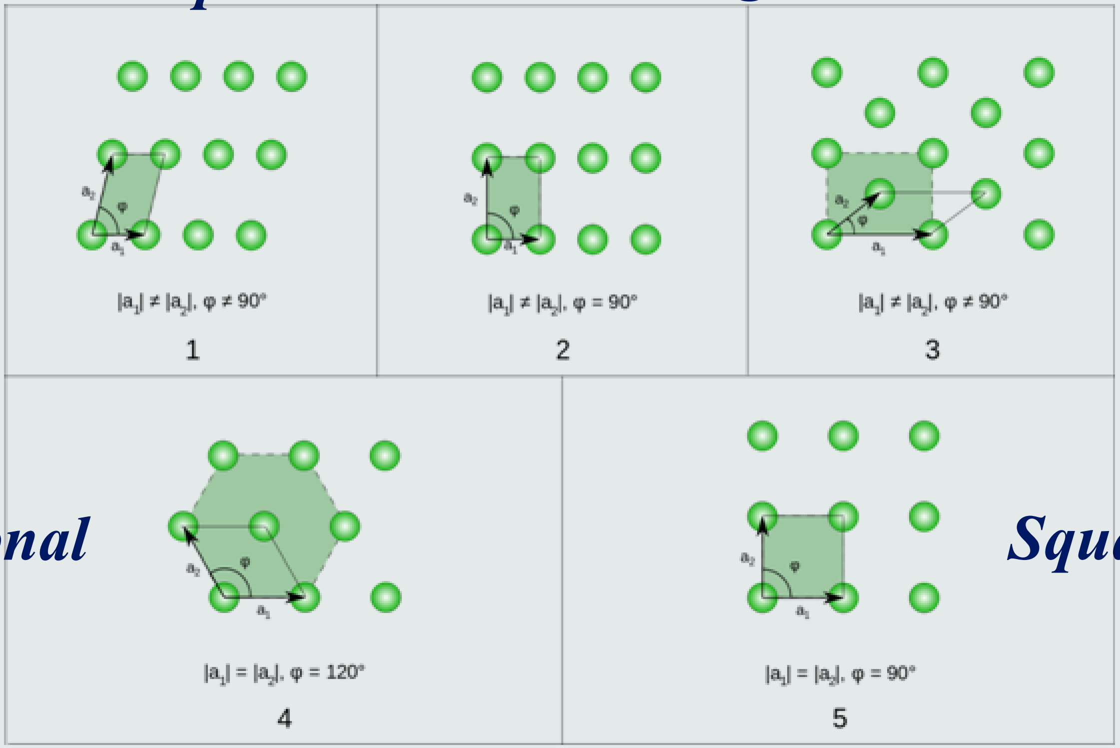

Two-Dimensional Bravais Lattices

Rectangular ***Rectangular*** ***Square*** ***Hexagonal***

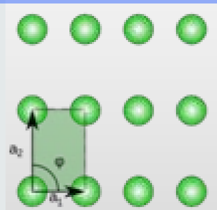

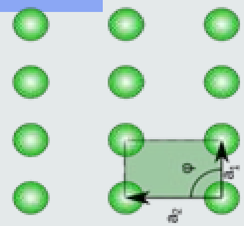

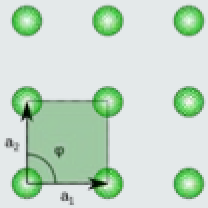

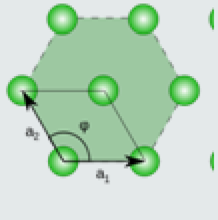

a=b

Two-Dimensional Bravais Lattices

Rectangular *Rectangular* *Square* *Hexagonal*

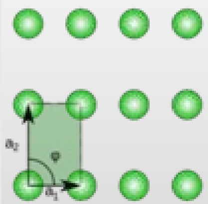

a=b

α=90° *α=120°*

Centered Bravais Lattices

$D_{min}=0.5*D_{max} = a_1$

$a_2=0.5*arctng(1/2)*a_1$

$\varphi=arcsin(1/2)$

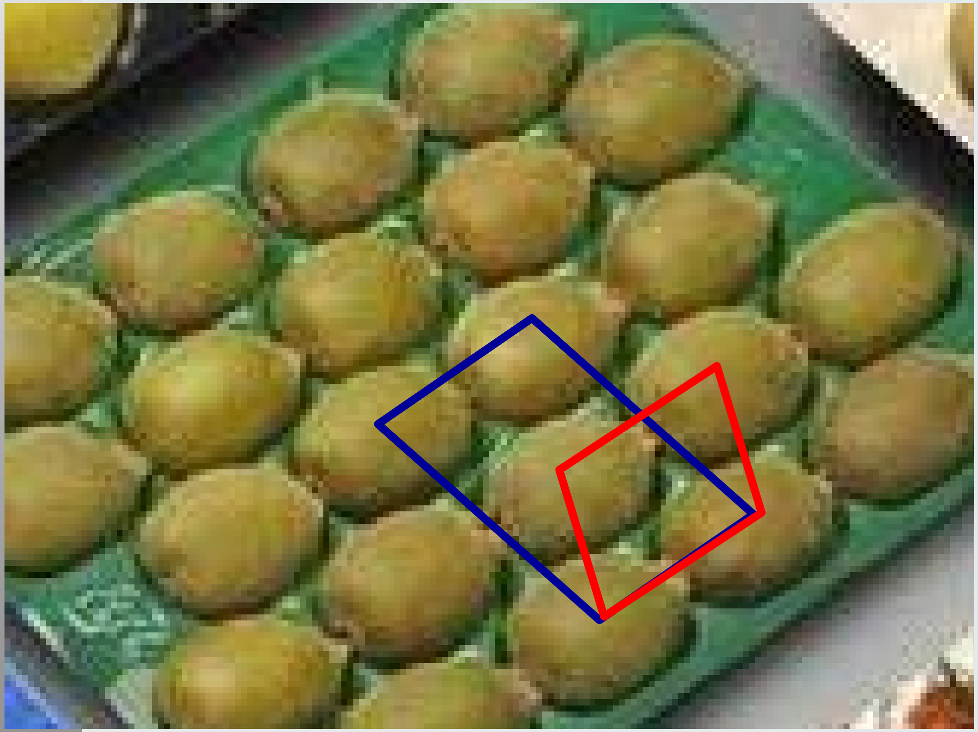

$a=b \qquad \alpha=90°$

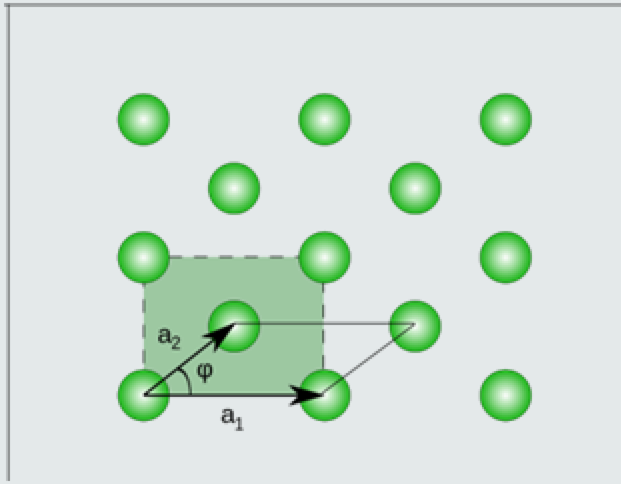

Two-Dimensional Space Groups

Square 2D Structures

P4

C4mm

14 3D Bravais Lattices

Bravais lattice	Parameters	Simple (P)	Volume centered (I)	Base centered (C)	Face centered (F)
Triclinic	$a_1 \neq a_2 \neq a_3$ $\alpha_{12} \neq \alpha_{23} \neq \alpha_{31}$	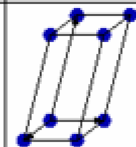			
Monoclinic	$a_1 \neq a_2 \neq a_3$ $\alpha_{23} = \alpha_{31} = 90°$ $\alpha_{12} \neq 90°$	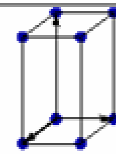	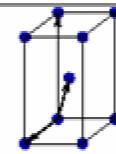		
Orthorhombic	$a_1 \neq a_2 \neq a_3$ $\alpha_{12} = \alpha_{23} = \alpha_{31} = 90°$	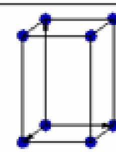	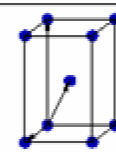	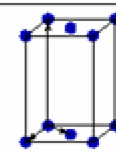	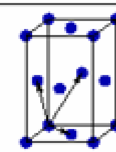
Tetragonal	$a_1 = a_2 \neq a_3$ $\alpha_{12} = \alpha_{23} = \alpha_{31} = 90°$	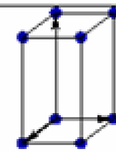	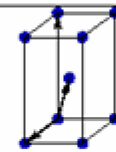		
Trigonal	$a_1 = a_2 = a_3$ $\alpha_{12} = \alpha_{23} = \alpha_{31} < 120°$	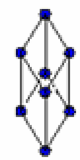			
Cubic	$a_1 = a_2 = a_3$ $\alpha_{12} = \alpha_{23} = \alpha_{31} = 90°$	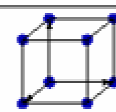	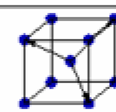		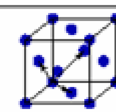
Hexagonal	$a_1 = a_2 \neq a_3$ $\alpha_{12} = 120°$ $\alpha_{23} = \alpha_{31} = 90°$	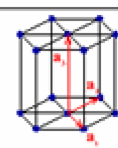			

230 Space Groupes

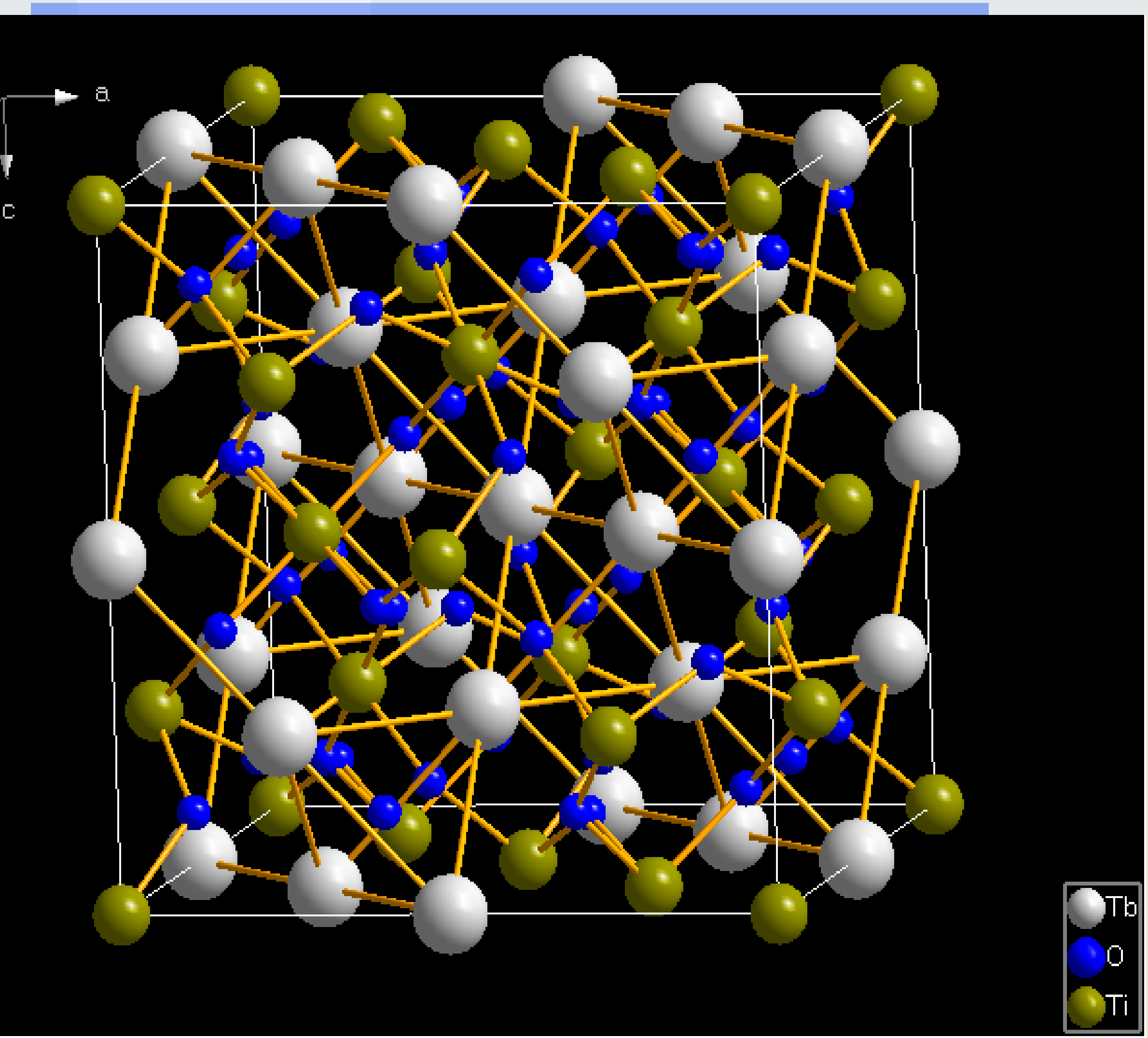

General

Bibliographic data

Phase data

Space-group	F d -3 m (227) - cubic
Cell	a=10.1400 Å V=1042.59 Å^3

Atomic parameters

Atom	Ox.	Wyck.	Site	S.O.F.	x/a	y/b	z/c	U [Å^2]
Tb1		16d	.-3m		1/2	1/2	1/2	
O1		48f	2.mm		0.33500	1/8	1/8	
O2		8b	-43m		3/8	3/8	3/8	
Ti		16c	.-3m		0	0	0	

Properties

Structure picture contents

Atomic parameters	4
Symmetry records	48
Atoms in unit cell	88
Explicitely defined bo...	0


HS

Cannonball problem

The problem of close-packing of spheres was first mathematically analyzed by Thomas Harriot around 1587, after a question on piling cannonballs on ships was posed to him by Sir Walter Raleigh on their expedition to America. Cannonballs were usually piled in a rectangular or triangular wooden frame, forming a three-sided or four-sided pyramid.

Both arrangements produce a face-centered cubic lattice – with different orientation to the ground.

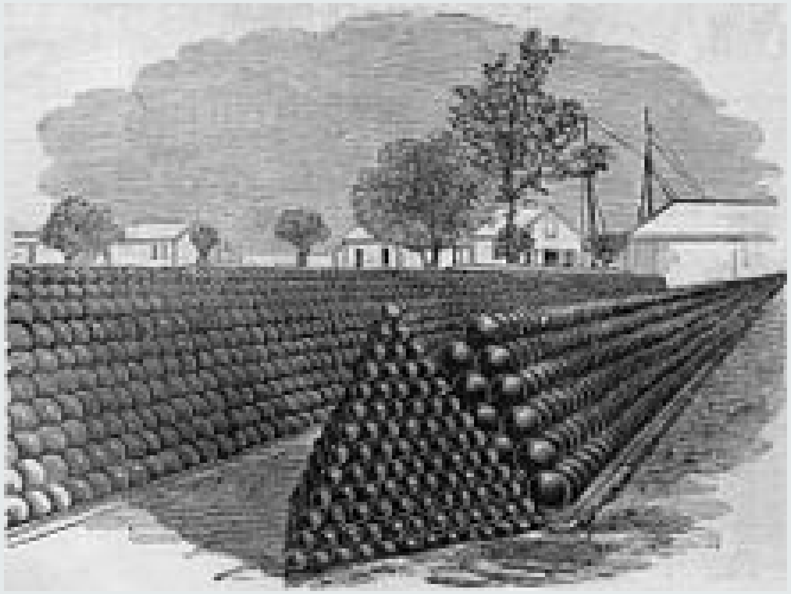

FCC and HCP structures

Density 0.74

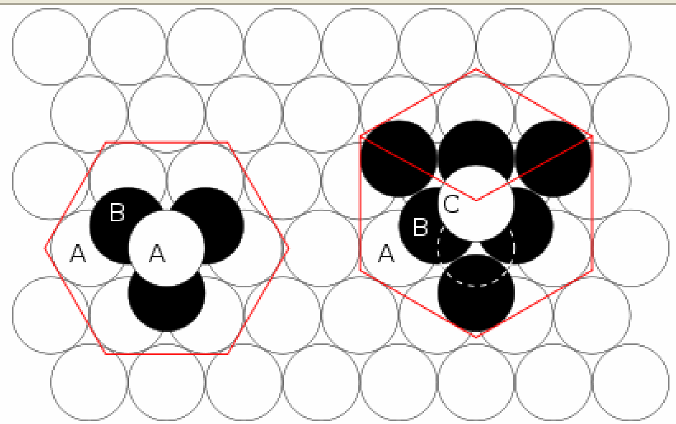

igure 1 – The hcp lattice (left) and the fcc lattice (right). The outline of each respective Bravais lattice is shown in red. The letters indicate which layers are the same. There re two "A" layers in the hcp matrix, where all the spheres are in the same position. All three layers in the fcc stack are different. Note the fcc stacking may be converted to the cp stacking by translation of the upper-most sphere, as shown by the dashed outline.

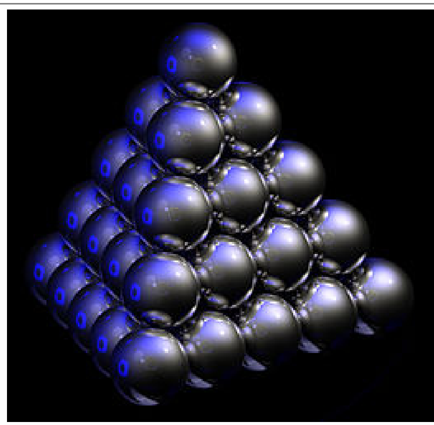

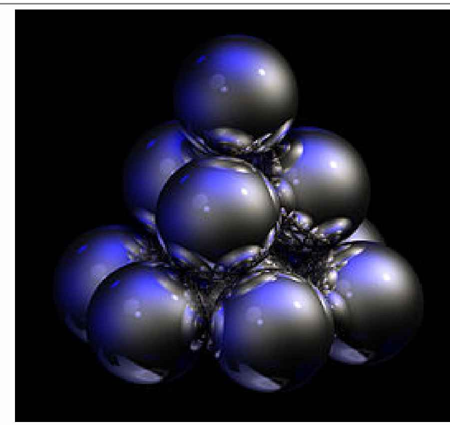

ure 2 – Thomas Harriot, circa 1585, first pondered the mathematics of the *cannonball* angement or *cannonball stack,* which has an **fcc** lattice. Note how adjacent balls along each je of the regular tetrahedron enclosing the stack are all in direct contact with one another.

Figure 3 – Shown here is a stack of eleven spheres of the **hcp** lattice illustrated in *Figure 1*. The hcp stack differs from the top 3 tiers of the fcc stack shown in *Figure 2* only in the lowest tier; it can be modified to fcc by an appropriate rotation

Three-Dimensional Space Groups

2D Rectangular and 3D Orthorhombic Structures

Tetragonal Rod Close Packings

Acta Cryst. (1977). A33, 914–923

Rod Packings and Crystal Chemistry

BY M. O'KEEFFE* AND STEN ANDERSSON
Kemicentrum, Lunds Universitet, Box 740, S-220 07 Lund 7, Sweden

The density is the same 0.7854.

P4/mmm

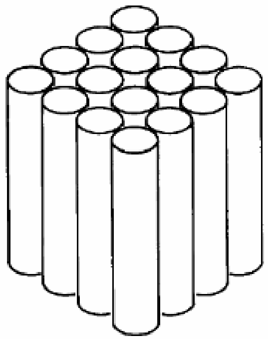

Fig. 2. Tetragonal packing of parallel cylinders.

$P4_2/mmc$

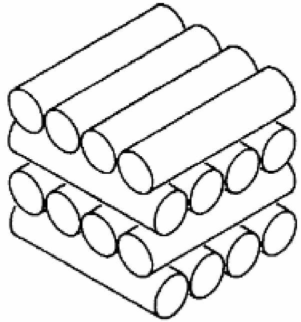

Fig. 3. Tetragonal layer packing of cylinders.

$I4_1/amd$

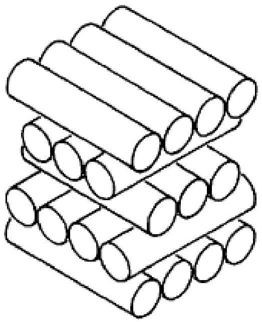

Fig. 5. Body-centred tetragonal layer packing of cylinders.

Cubic Rod Close Packings

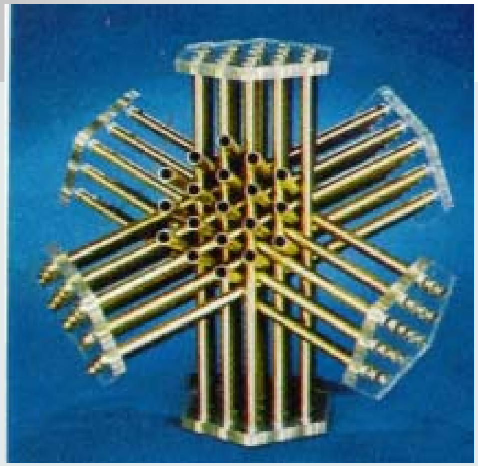

Density 0.5890

Pm3n

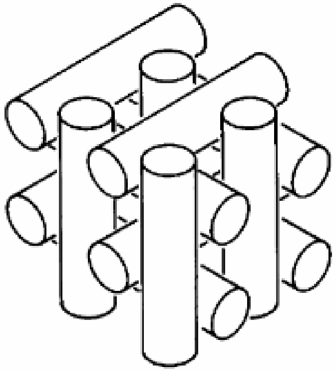

Fig. 9. Primitive cubic cylinder packing.

Density 0.6802

$I4_1/amd$

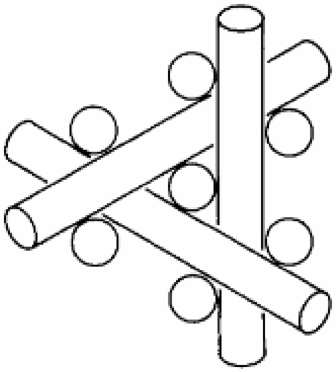

Fig. 12. An element of body-centred cubic rod packing viewed down a trigonal axis.

Rod Close Packings

Acta Cryst. (1977). A**33**, 914–923

Rod Packings and Crystal Chemistry

By M. O'Keeffe* and Sten Andersson
Kemicentrum, Lunds Universitet, Box 740, S-220 07 Lund 7, Sweden

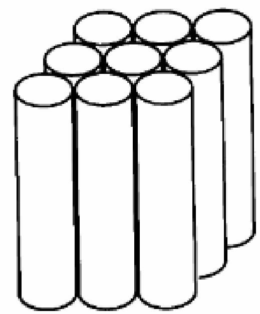

Fig. 1. Hexagonal (honeycomb) packing of parallel cylinders.

P6/mmm
The density is 0.9069.

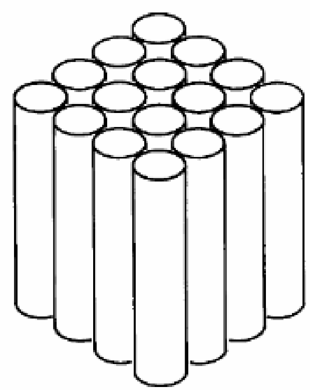

Fig. 2. Tetragonal packing of parallel cylinders.

P4/mmm
The density is 0.7854.

Fourier transform (*FT*) and Diffraction pattern

$$\rho_s = \sum F_M(q)e^{-iqr}$$

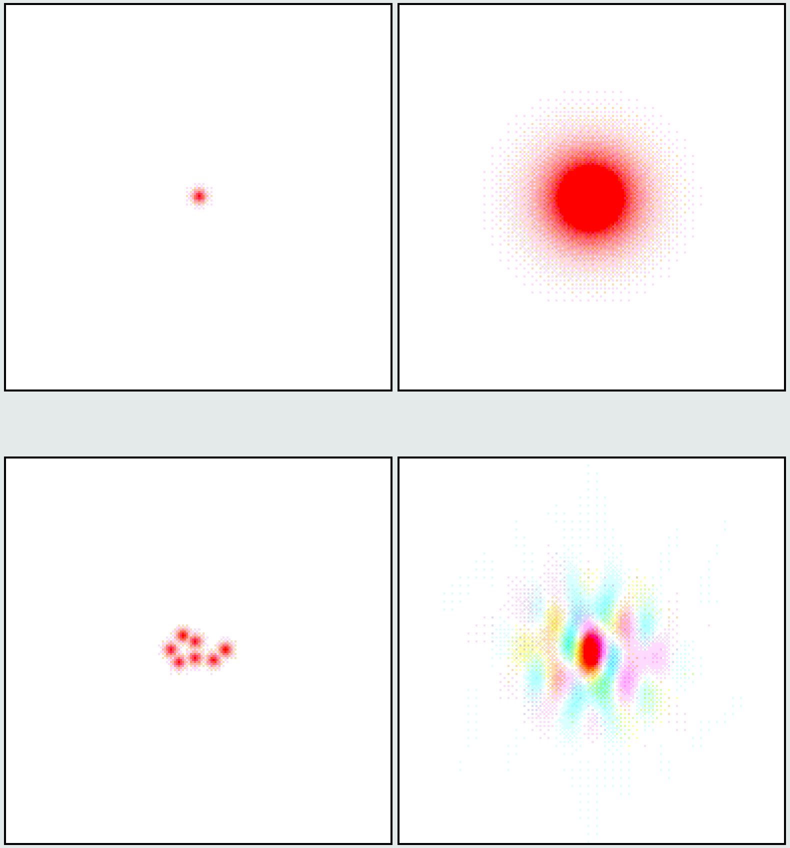

Fourier transform (*FT*) and Diffraction pattern

Lattice , and its FT :

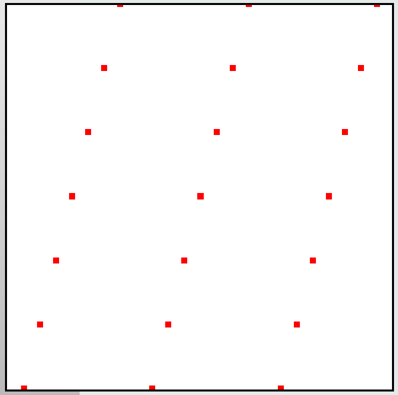

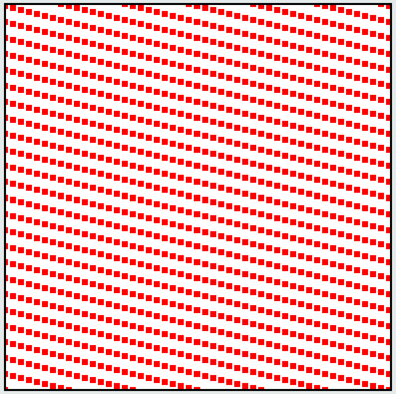

Crystal

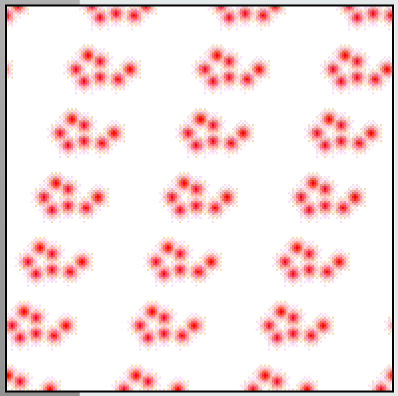

1 Molecule FT:

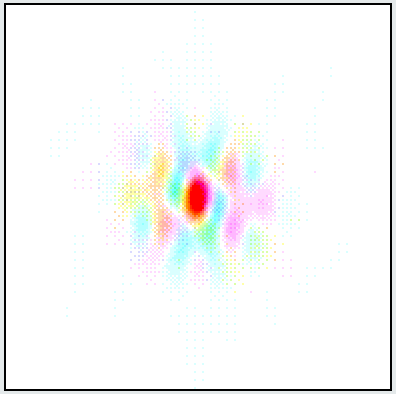

FT of the crystal =

Product of molecule FT and Rec. Latt. FT

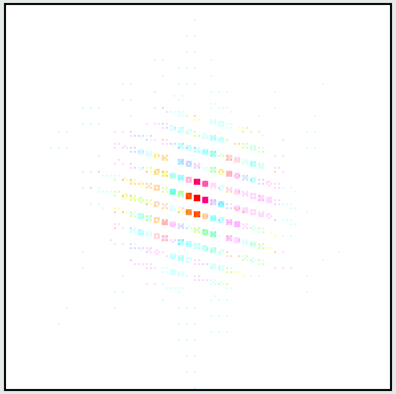

Time of flight (TOF) neutron Diffraction from a single crystal

Multiple reflections sorted by Time-Of-Flight

SXD at ISIS, TOPAZ at SNS **ESS Mag Diffractometer**

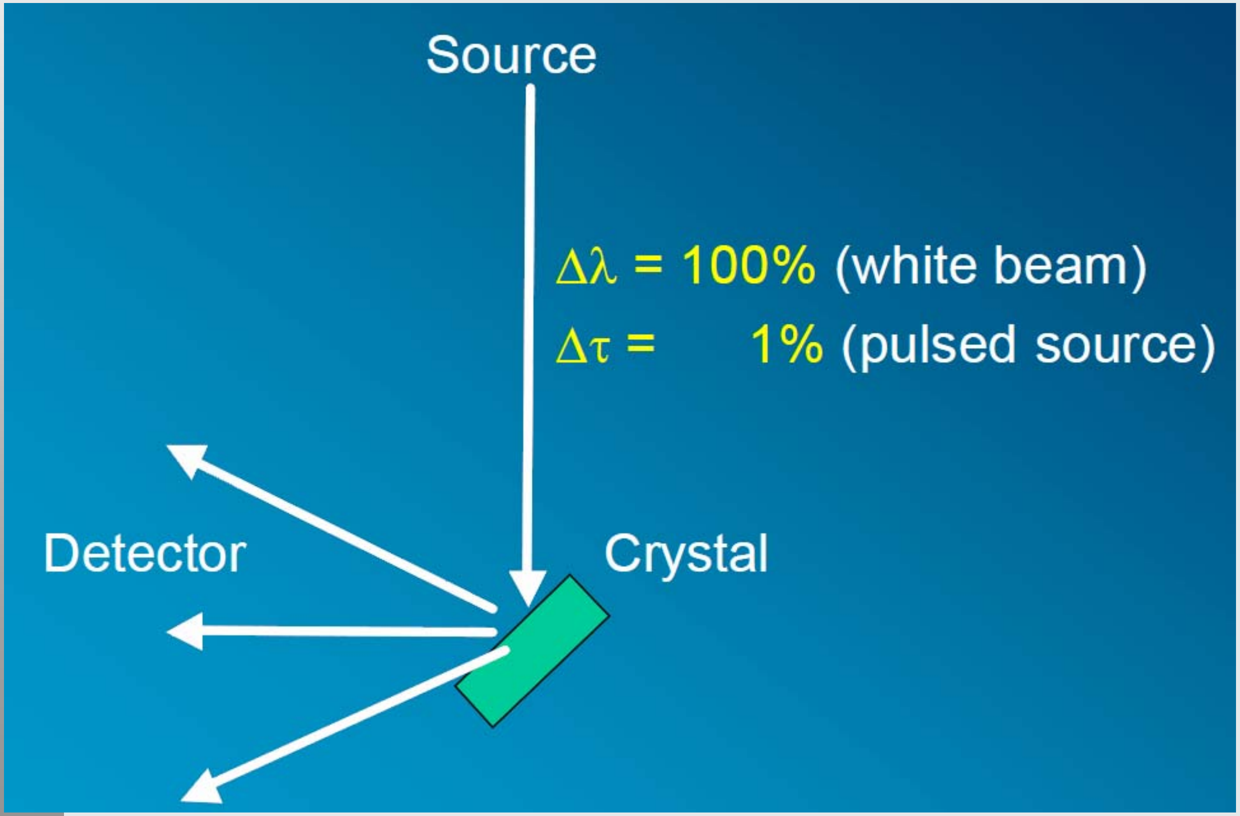

SINGLE COUNTER DIFFRACTION

$$sin(\theta_{hkl})=\lambda/2D_{hkl}$$

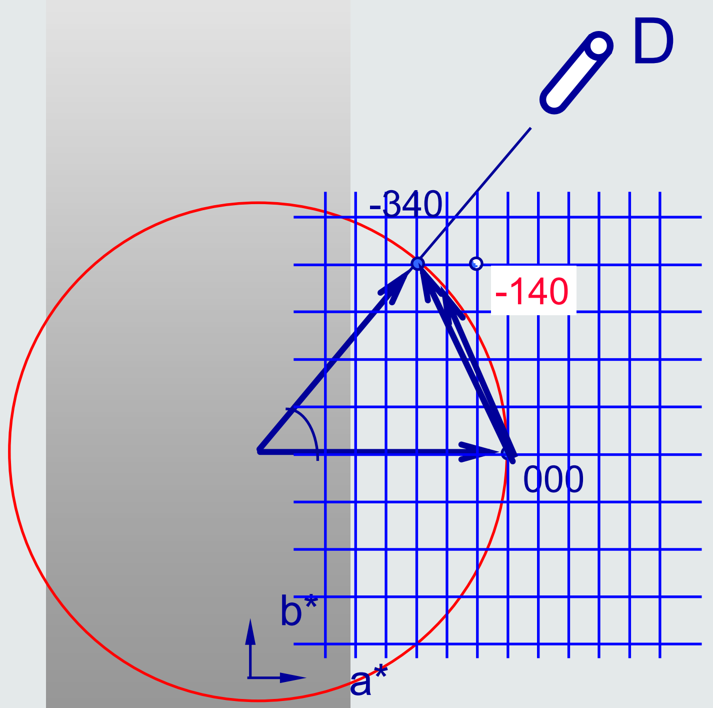

4-circles

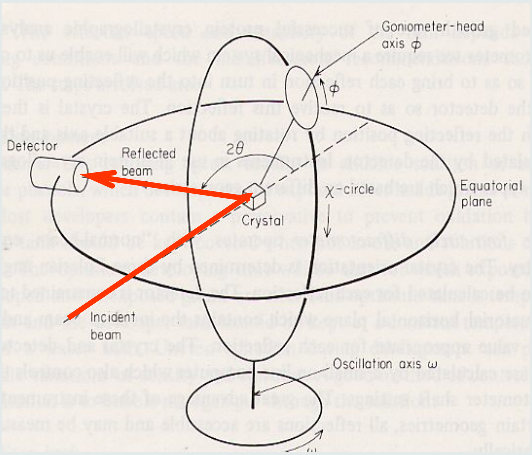

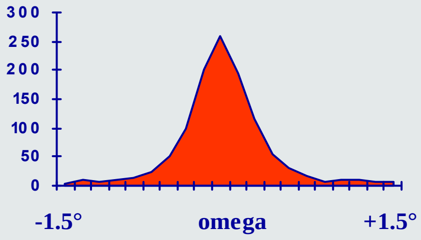

First generation neutron diffractometers

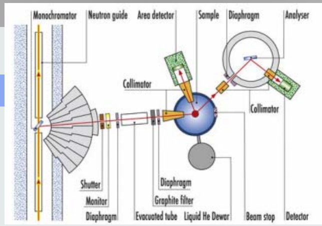

- **4- cercles : D9,D10, 6T2,5C2,TRICS (High resolution crystallography)**

- Bras levant : D3,D15, D23, 6T2, 5C1 (diffraction in extreme conditions)

UNPOLARISED NEUTRON DIFFRACTION 4-CIRCLES

- Structure determination
- Anharmonicity
- Microcrystals <0.05mm3 (PSD)
- Epitaxial layers(PSD)

DIFFRACTION USING PSD

Diffraction conventionnelle:

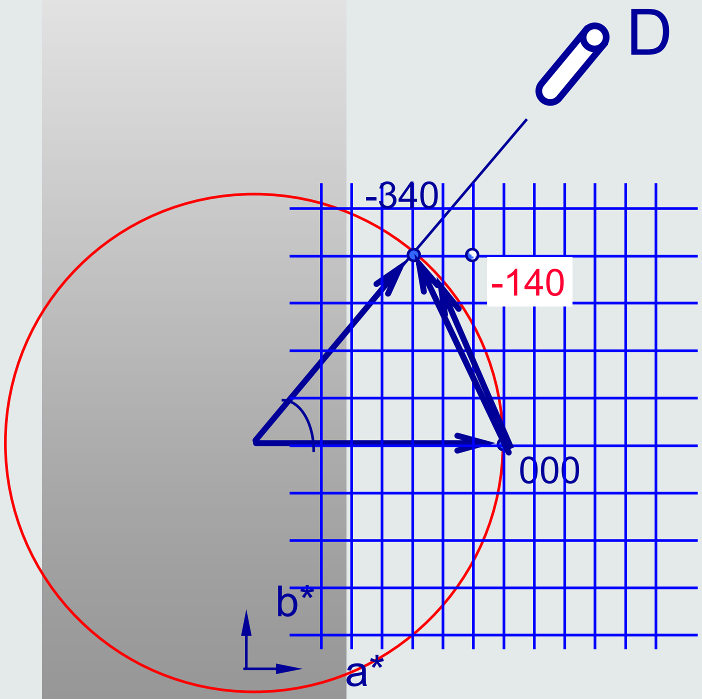

Diffraction using PSD :

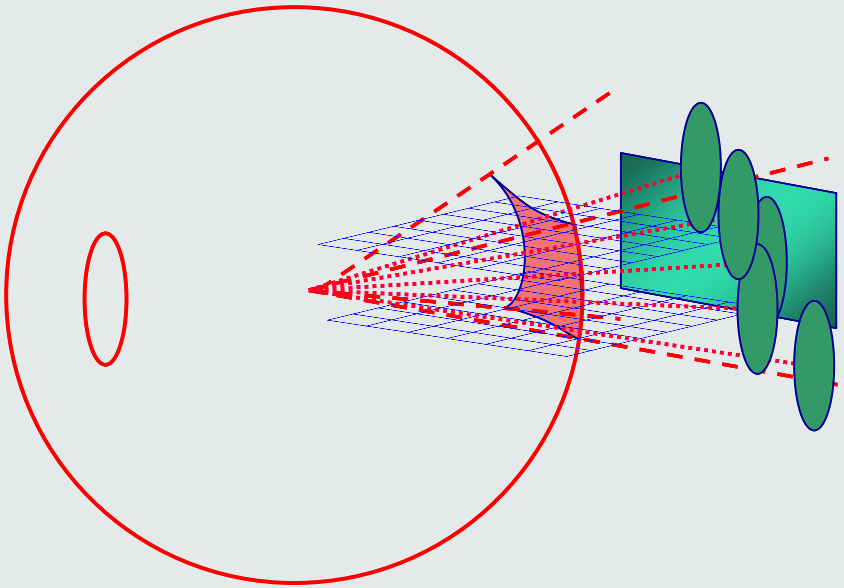

instrumentation program CAP2010

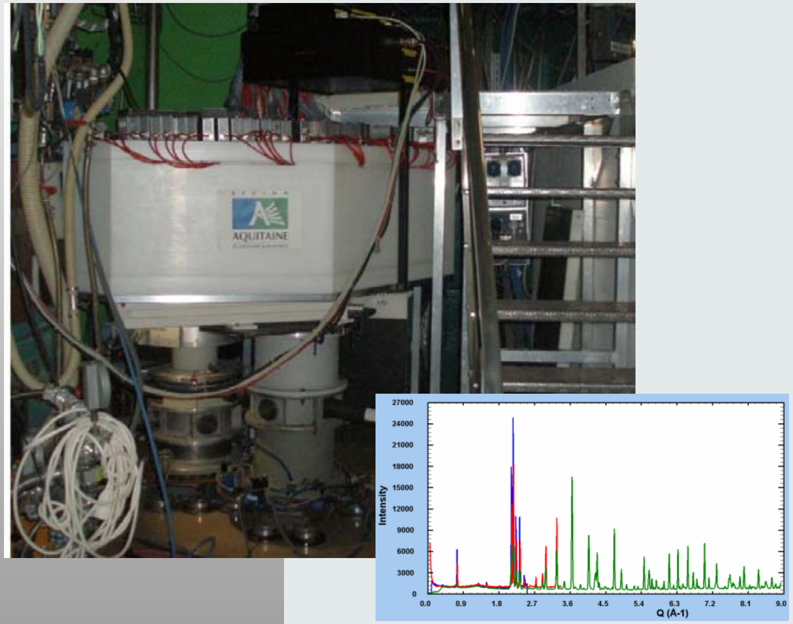

3T2 (2005)

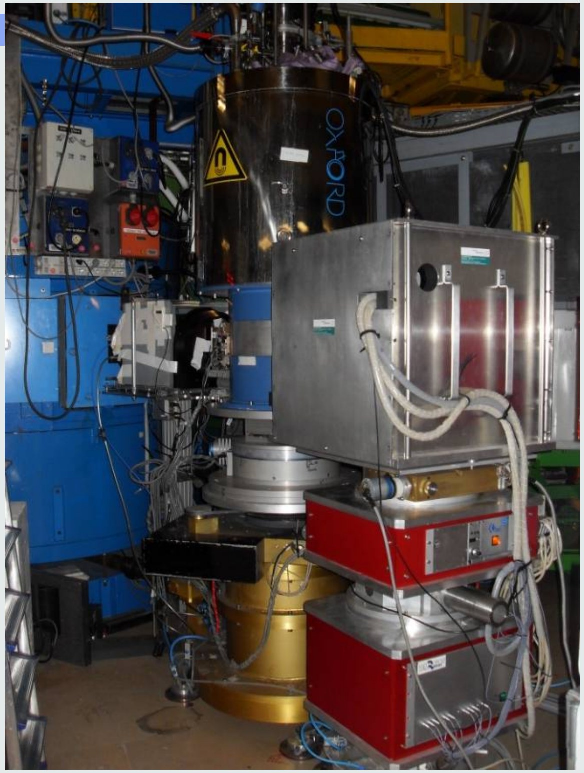

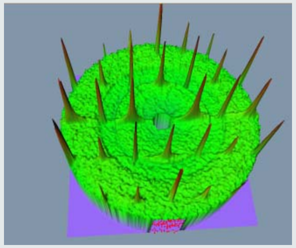

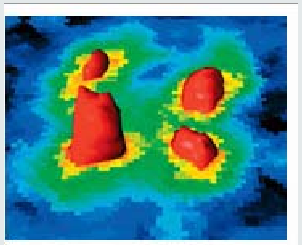

<0.1mm^3

Super-6T2(2006)

CAP2010-2015 commissioning Schedule

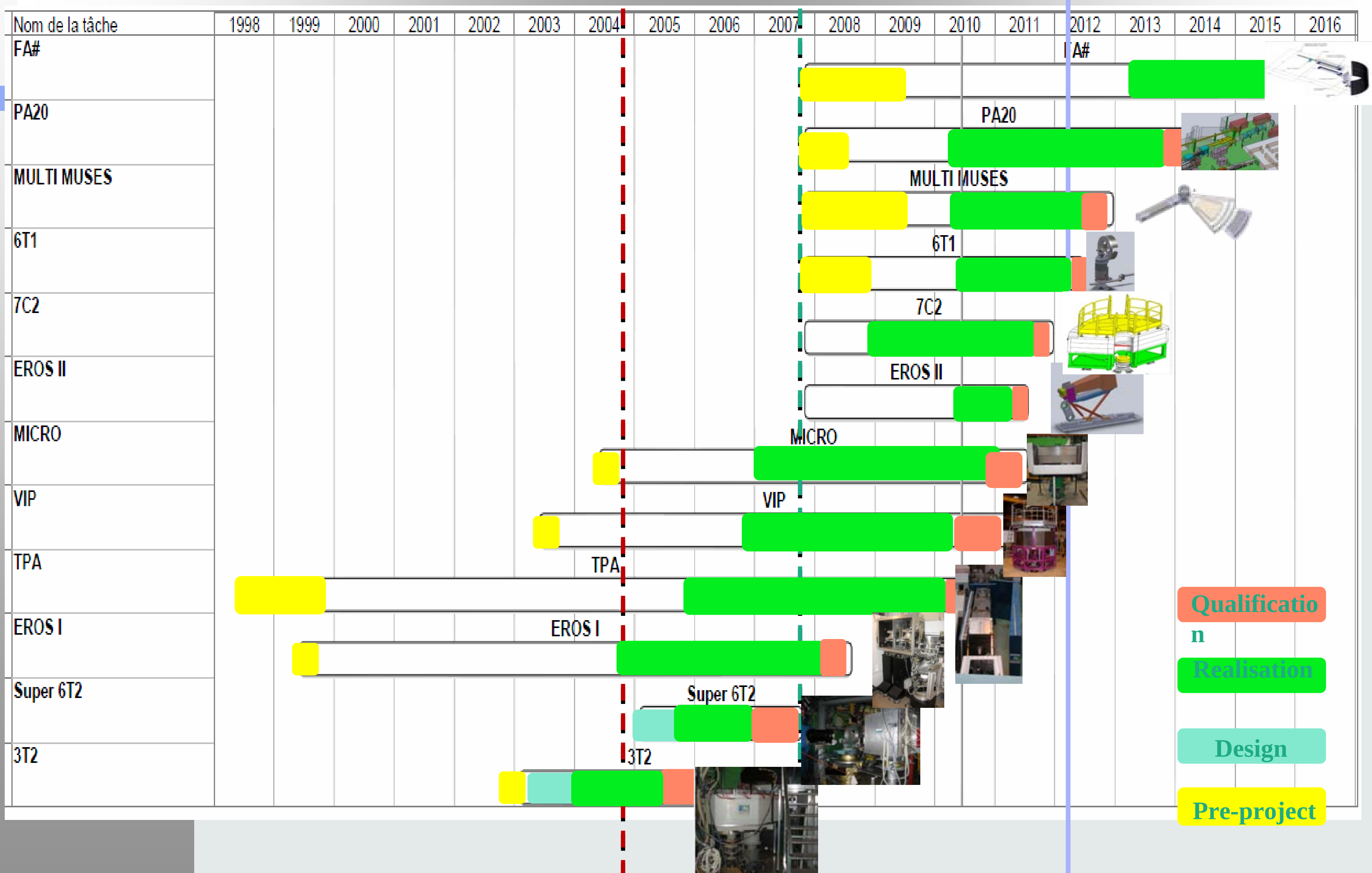

VIP

A. Goukassov, S. Rodrigues
Operational since February 2011

- Budget 380 k€ (50 kE Aquitaine Region)

Cap2010-2015 New 7C2

Liquid and Amorphous Diffractometer

B. Beuneu, B. Homatter, P. Lavie

- 256 **position sensitive tubes**

(Ø ~ 1.2cm) 30b ^{3}He

efficiency 76 % for 0.7Å

× 5

height 47 cm

× 5

} **25**

- **modular geometry**:

blocks of 16 paired tubes (2 tubes make one detector: less electronics and cables)

Opens to: 0.58Å measurements, more complex environments (HT), smaller samples, ...

Super 6T1: Texture/Contraintes

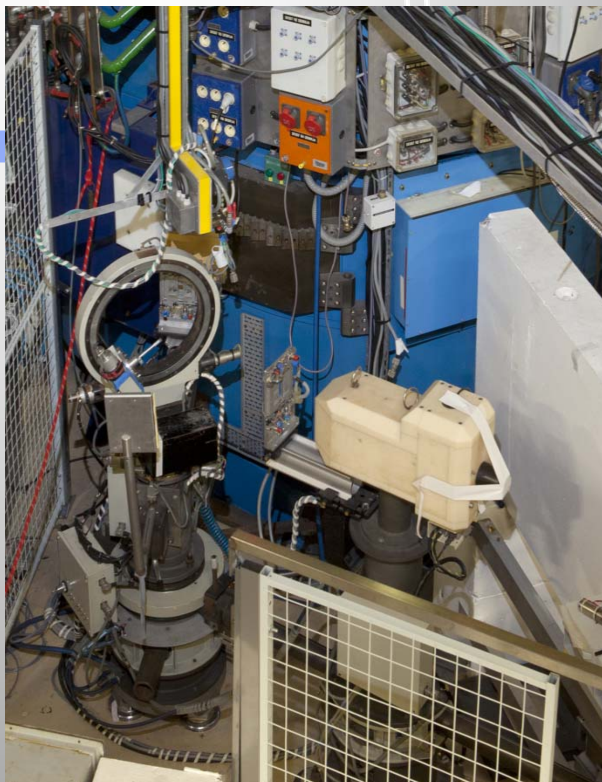

- Berceau équipé de tables x,y,z
- Support X,Y,Z
- λ variables
  (2 Monok avec foc vert, 3 take-off)
- Détecteur 2D

Take-off = 32°

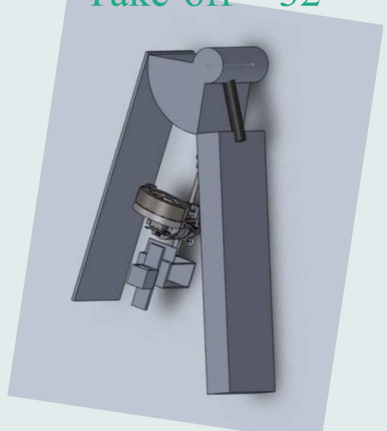

Take-off = 65°

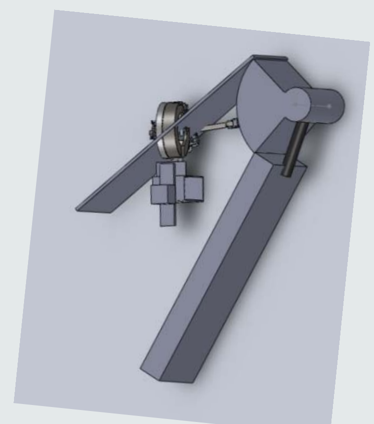

S. Gautrot
V. Klosek
M.H. Mathon

Cap2010

MICRO

I. Mirebeau, N. Rey, F. Porcher

Operational since March 2011

- ✓Conception (I. Goncharenko) : ~2004
- ✓Construction : 2008-2009
- ✓Operation started in march 2011

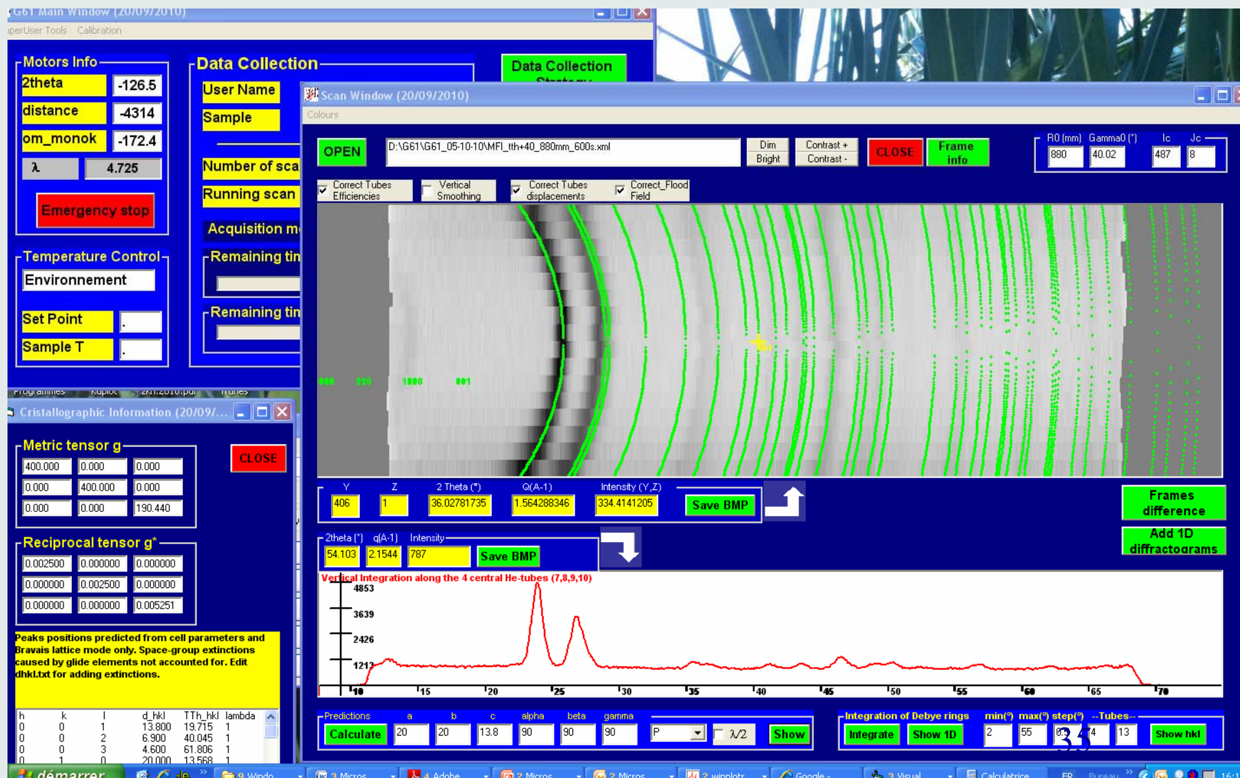

- 16 tubes
- L=100×2,54 cm
- P≈ 12 bar

ORPHEE guide hall

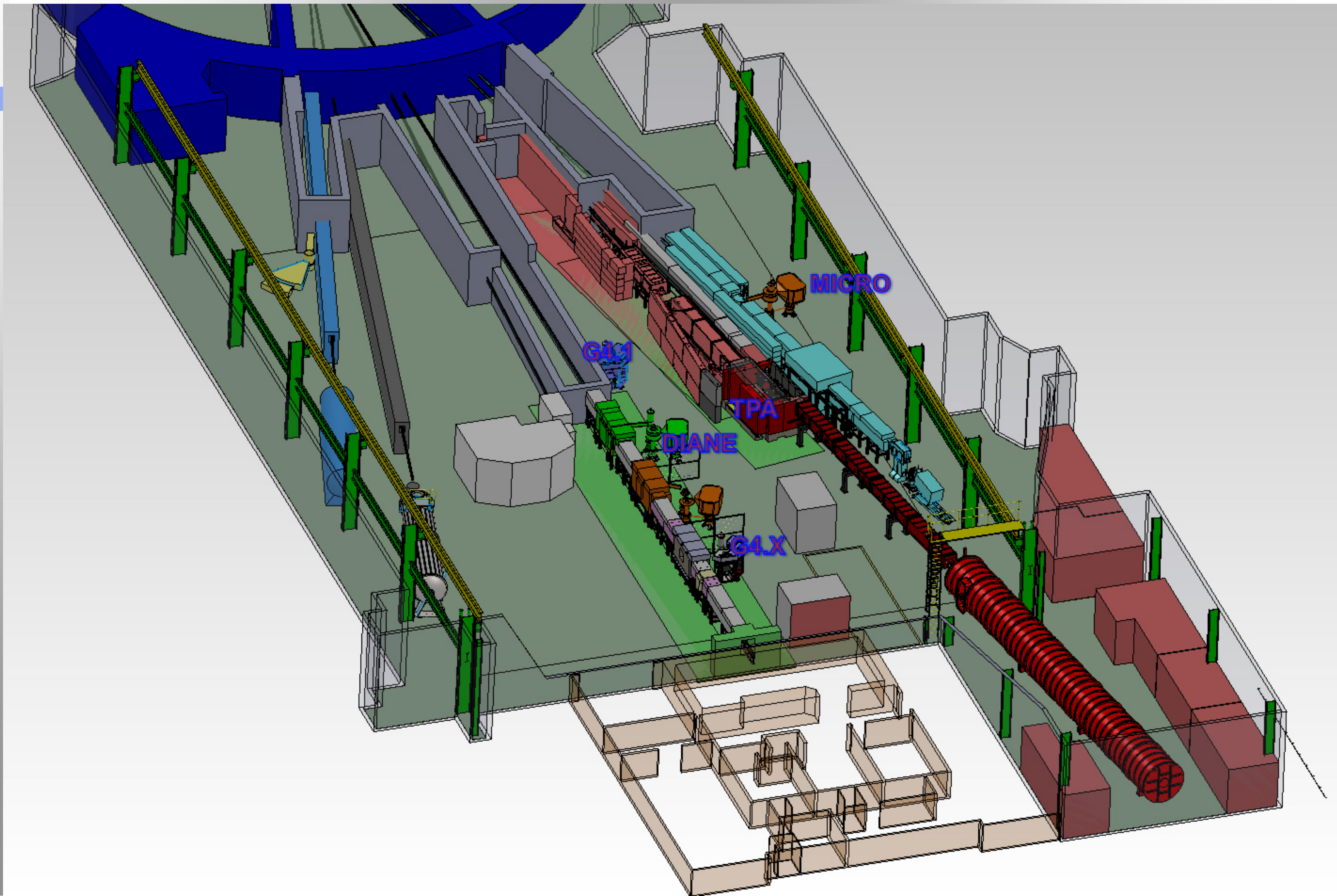

4*f* Magnetism and its Effects on Electronic Properties of $Dy_3Ru_4Al_{12}$

D.I. Gorbunov[1,2*], M.S. Henriques[3], A.V. Andreev[1], A. Gukasov[4], V. Petříček[1], N.V. Baranov[5], Y. Skourski[6], V. Eigner[1], M. Paukov[2]

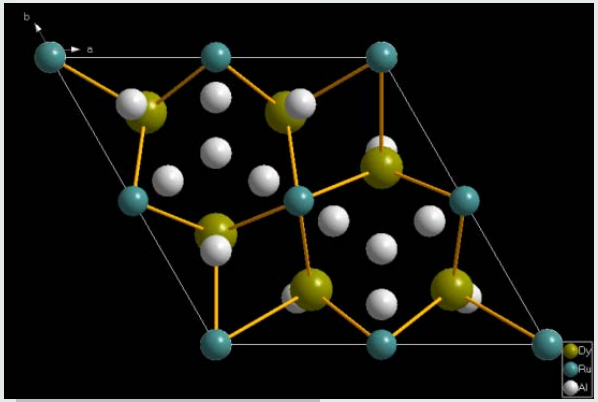

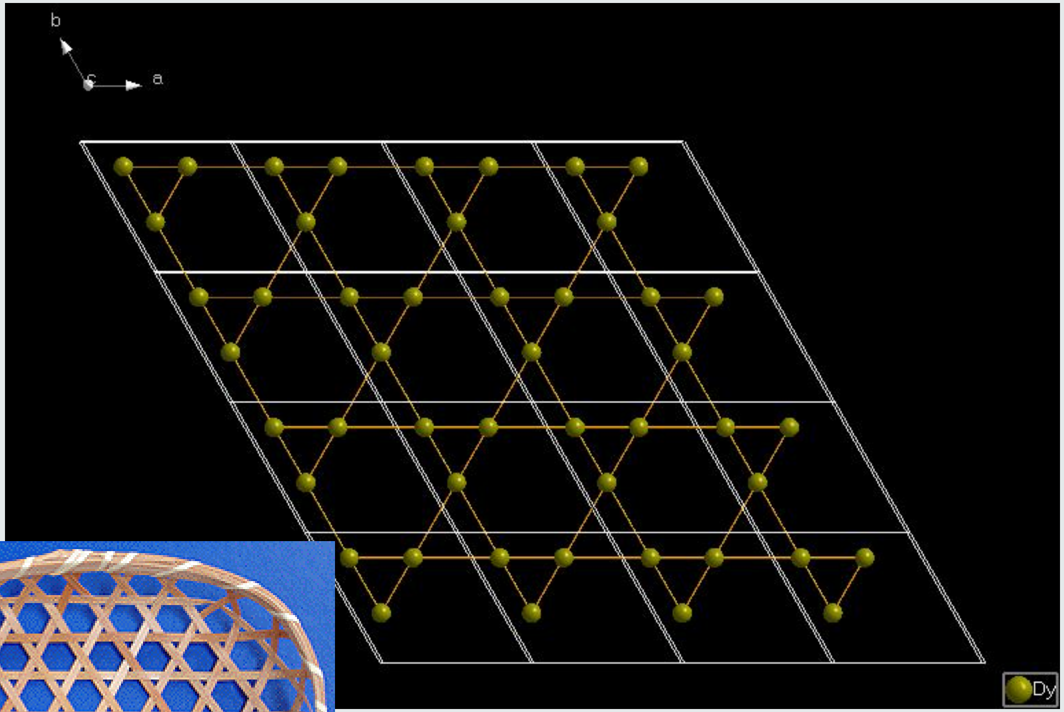

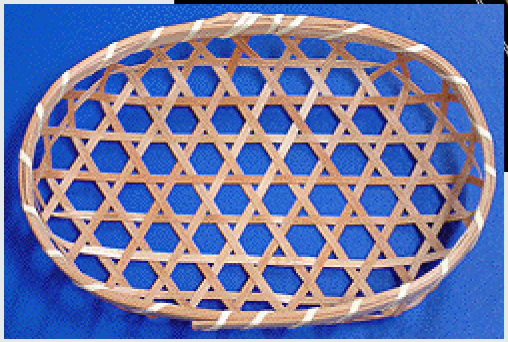

4*f* Magnetism and its Effects on Electronic Properties of $Dy_3Ru_4Al_{12}$

D.I. Gorbunov[1,2*], M.S. Henriques[3], A.V. Andreev[1], A. Gukasov[4], V. Petříček[1], N.V. Baranov[5], Y. Skourski[6], V. Eigner[1], M. Paukov[2]

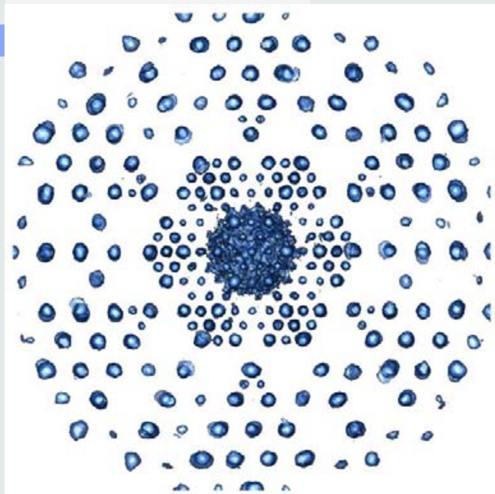

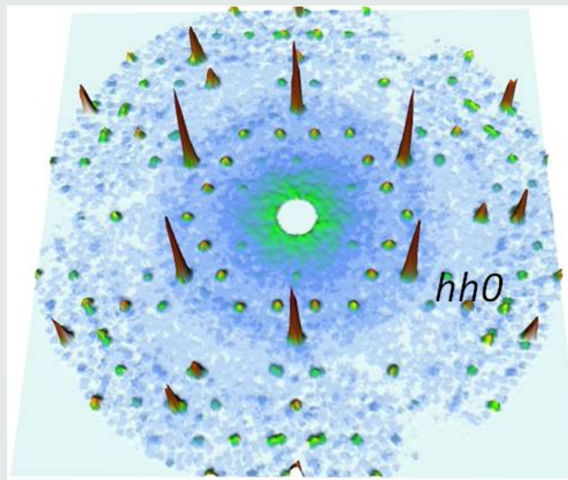

k=(1/2 0 1/2)

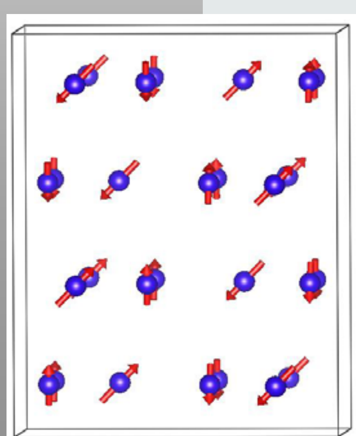

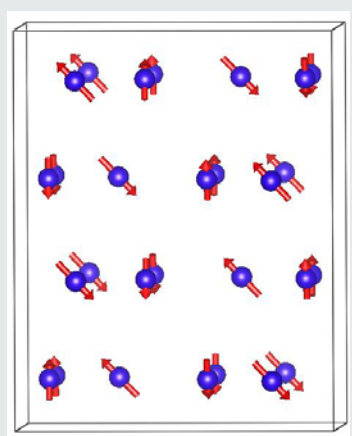

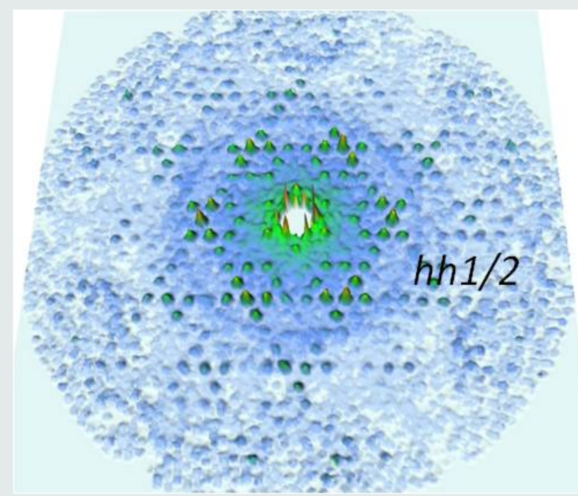

Minimum SC size for neutron studies?

a,b,c<10 A   V>0.01mm3   (X-rays >0.0001mm3)

PRL **100,** 227602 (2008) PHYSICAL REVIEW LETTERS week ending 6 JUNE 2008

Electric-Field-Induced Spin Flop in $BiFeO_3$ Single Crystals at Room Temperature

D. Lebeugle,[1] D. Colson,[1] A. Forget,[1] M. Viret,[1] A. M. Bataille,[2] and A. Gukasov[2]
[1]*Service de Physique de l'Etat Condensé, DSM/IRAMIS, CEA Saclay, F-91191 Gif-Sur-Yvette, France*
[2]*Laboratoire Leon Brillouin, DSM/IRAMIS, CEA Saclay, F-91191 Gif-Sur-Yvette, France*
(Received 24 January 2008; published 2 June 2008)

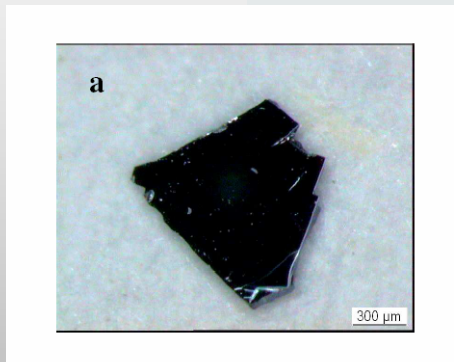

$BiFeO_3$, 0.7x0.7x4.10^{-2} mm^3

CYCLOID WITH D=640 Ǻ

High resolution mode

1.36 m instead of 56 cm

•Pixels (2x2 mm) → résolution de 0.2°x0.2°

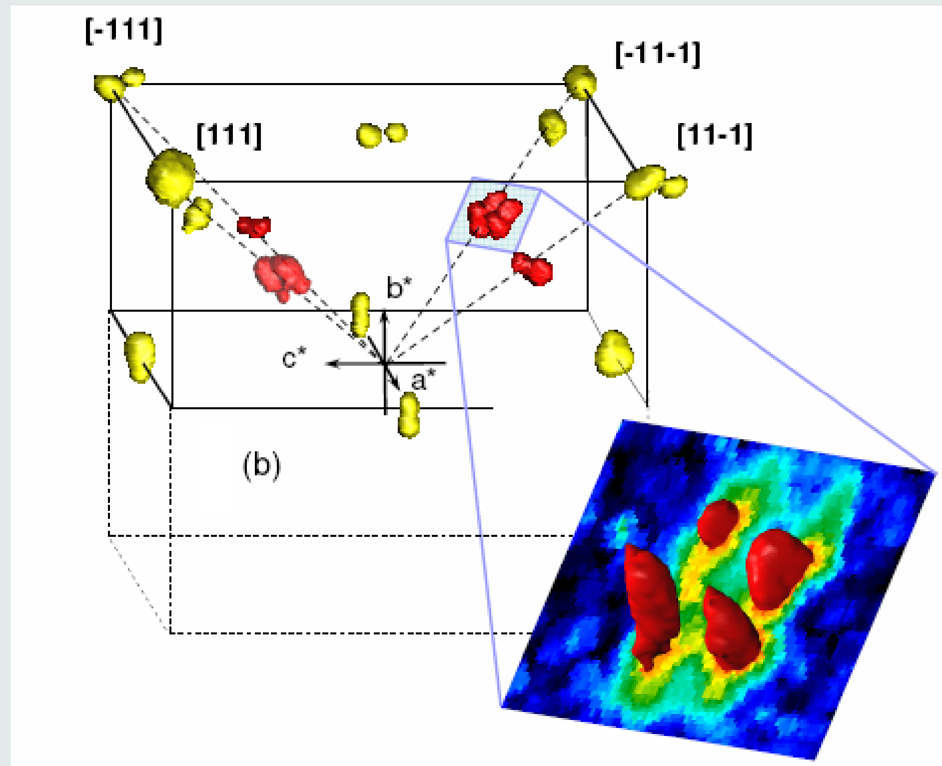

PRL **100**, 227602 (2008) PHYSICAL REVIEW LETTERS week ending 6 JUNE 2008

Electric-Field-Induced Spin Flop in $BiFeO_3$ Single Crystals at Room Temperature

D. Lebeugle,[1] D. Colson,[1] A. Forget,[1] M. Viret,[1] A. M. Bataille,[2] and A. Gukasov[2]
[1]*Service de Physique de l'Etat Condensé, DSM/IRAMIS, CEA Saclay, F-91191 Gif-Sur-Yvette, France*
[2]*Laboratoire Leon Brillouin, DSM/IRAMIS, CEA Saclay, F-91191 Gif-Sur-Yvette, France*

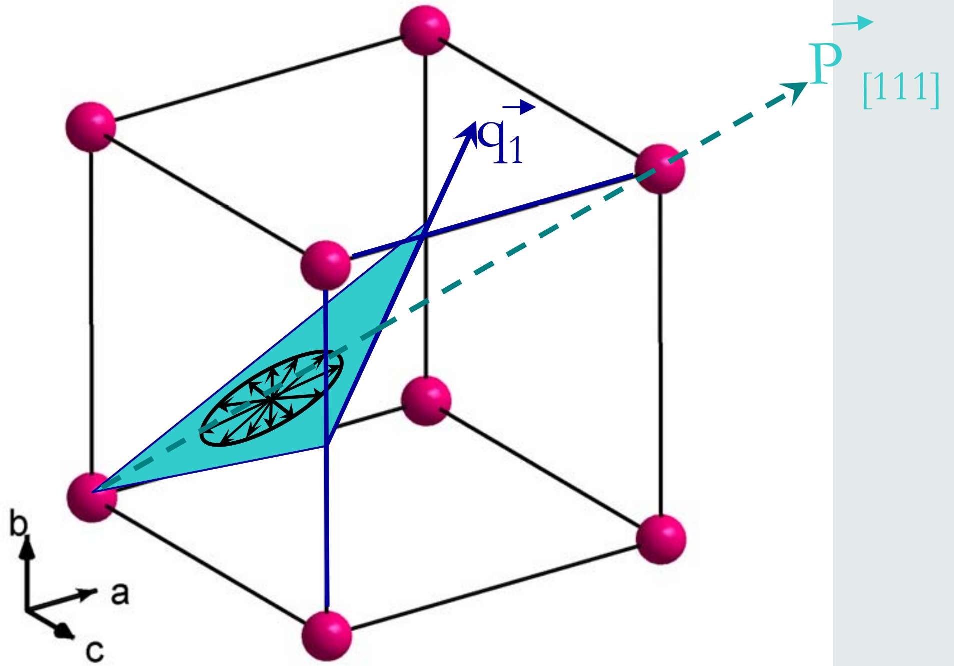

Domain I

Rotation plane : (-12-1) = $P_{[111]} \times q_1$

PRL **100,** 227602 (2008) PHYSICAL REVIEW LETTERS week ending 6 JUNE 2008

Electric-Field-Induced Spin Flop in $BiFeO_3$ Single Crystals at Room Temperature

D. Lebeugle,[1] D. Colson,[1] A. Forget,[1] M. Viret,[1] A. M. Bataille,[2] and A. Gukasov[2]
[1]*Service de Physique de l'Etat Condensé, DSM/IRAMIS, CEA Saclay, F-91191 Gif-Sur-Yvette, France*
[2]*Laboratoire Leon Brillouin, DSM/IRAMIS, CEA Saclay, F-91191 Gif-Sur-Yvette, France*

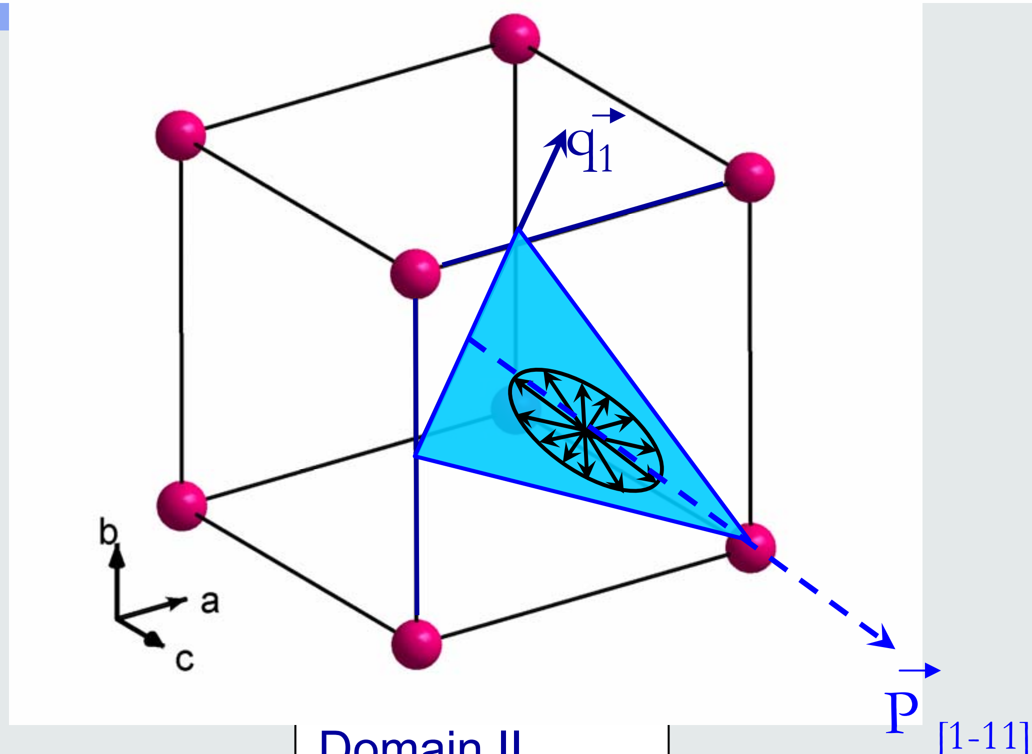

Domain II

Rotation plane : (121) = $P'_{[1-11]} \times q_1$

PRL **100,** 227602 (2008) PHYSICAL REVIEW LETTERS week ending 6 JUNE 2008

Electric-Field-Induced Spin Flop in $BiFeO_3$ Single Crystals at Room Temperature

D. Lebeugle,[1] D. Colson,[1] A. Forget,[1] M. Viret,[1] A. M. Bataille,[2] and A. Gukasov[2]
[1]*Service de Physique de l'Etat Condensé, DSM/IRAMIS, CEA Saclay, F-91191 Gif-Sur-Yvette, France*
[2]*Laboratoire Leon Brillouin, DSM/IRAMIS, CEA Saclay, F-91191 Gif-Sur-Yvette, France*
(Received 24 January 2008; published 2 June 2008)

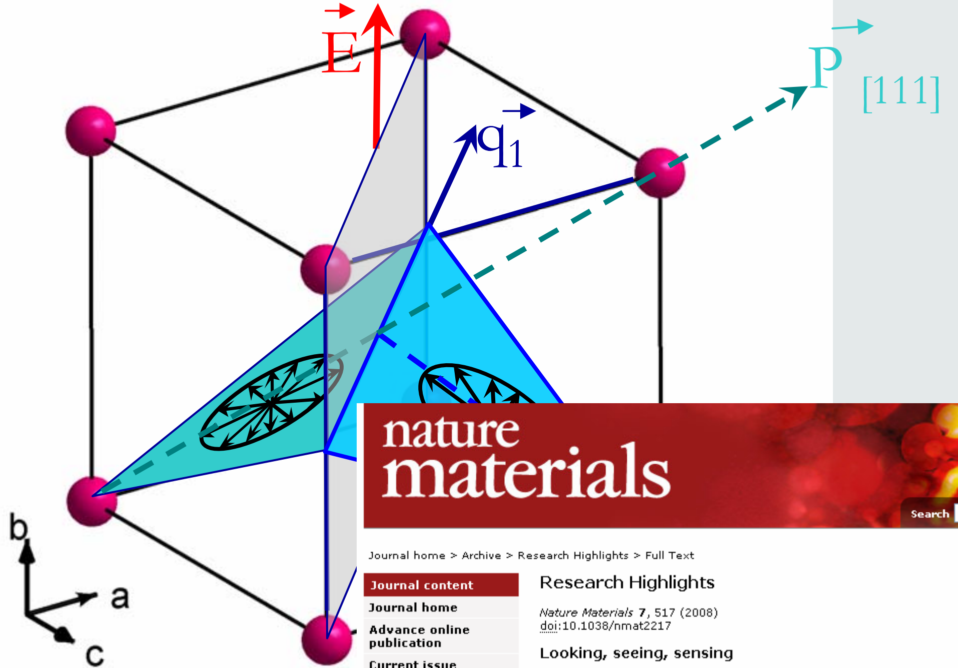

Research Highlights

Nature Materials **7**, 517 (2008)
doi:10.1038/nmat2217

Looking, seeing, sensing

A COUPLING, INDEED

top

Phys. Rev. Lett. **100**, 227602 (2008)

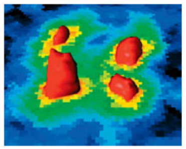
MICHEL VIRET

One of the most intensively studied multiferroic materials is $BiFeO_3$, mostly because it shows room-temperature multiferroic coupling with a large spontaneous electric polarization. Although the material has been known to be magnetoelectric since the 1960s, actual evidence of multiferroic coupling in bulk material has been missing, mainly owing to the lack of suitable high-quality crystals. Having achieved the growth of high-quality $BiFeO_3$ crystals, Delphine Lebeugle and co-workers now report on a neutron diffraction study into the coupling between magnetic and ferroelectric properties of $BiFeO_3$. They find that although the material has no linear magnetoelectric effect, the antiferromagnetic moments form a low-pitch spiral that creates an efficient multiferroic coupling. However, a more efficient switching of magnetic properties can be achieved not through a direct multiferroic coupling but if the antiferromagnetic moments of $BiFeO_3$ are used to switch the magnetic moments of a ferromagnet through the exchange interaction at the interface between the two materials. Therefore, an electric field applied to $BiFeO_3$ indirectly switches the ferromagnetic state of the adjacent layer, as has been demonstrated recently.

Neutron diffraction on thin films: what can we gain by using 2D detectors ?

V=0.02mm3

Cr 200 nm layer on Mg0

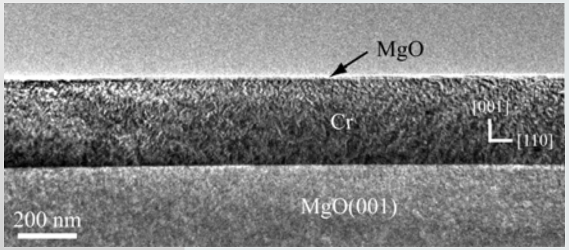

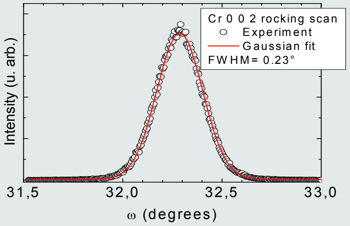

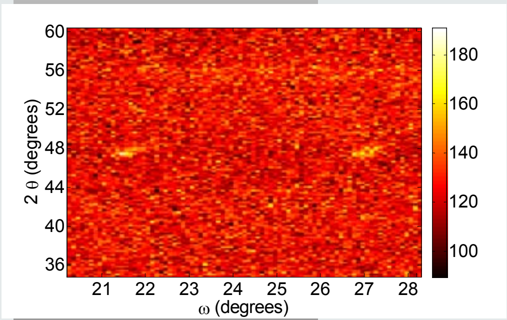

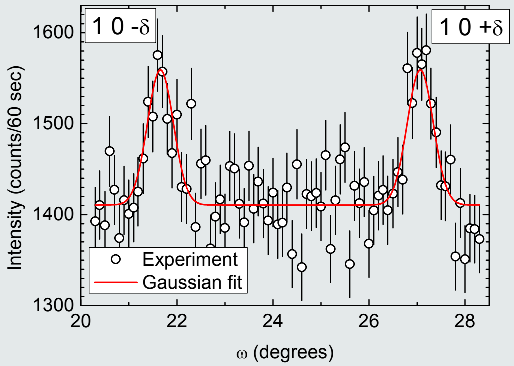

Laplacian of Gaussian filtering

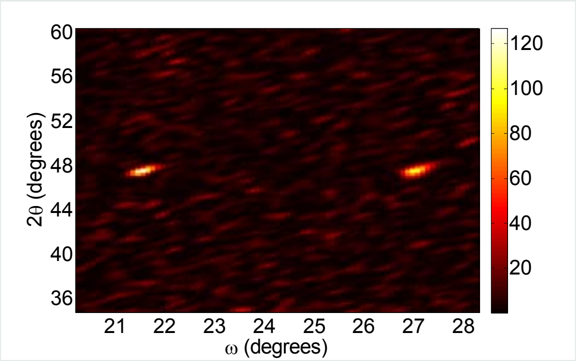

UNPOLARISED NEUTRON DIFFRACTION NORMAL BEAM GEOMETRY

- H, T phase diagramm
- High pressure
- photoexcitation
- Diifuse scattering (PSD)

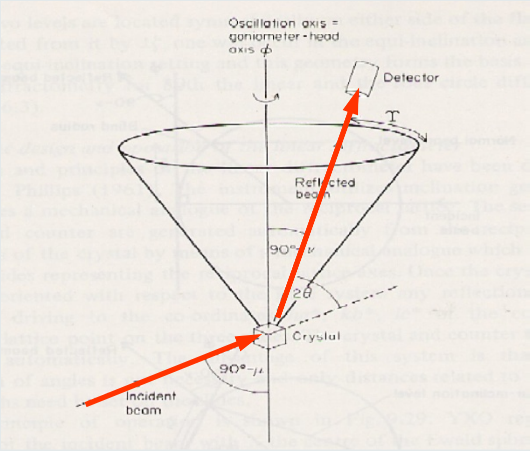

$Tb_2Ti_2O_7$a spin liquid single crystal under pressure and applied field

- 6T2, Lifting counter mode
- 7.5 T + 40 mK
- 7.5 T +10 Gpa+40 mK

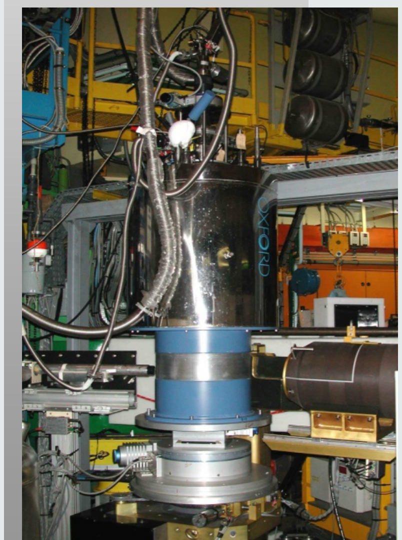

T=0.14K

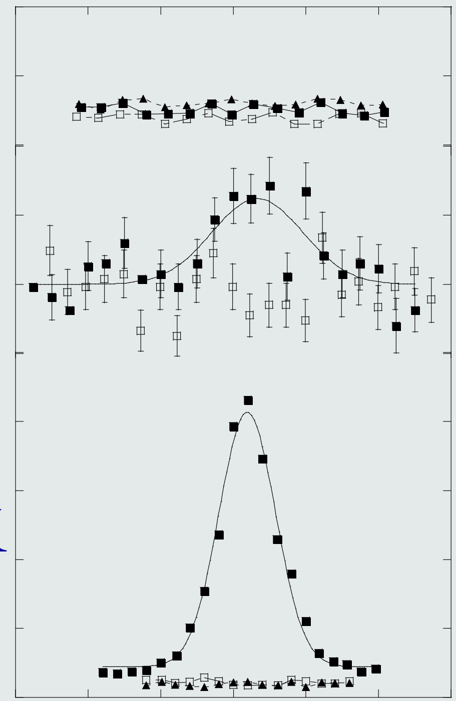

P_i=2.8 GPa;
P_u=0

P_i=2.0 GPa;
P_u=0.3 GPa
along 111

P_i=2.4 GPa;
P_u=0.3 GPa
along 011

I.Mirebeau, I. N. Goncharenko, G. Dhalenne, A. Revcolevschi, Phys. Rev. Lett. 93, 187204 (2004).

Mapping of Spin ice on the water ice

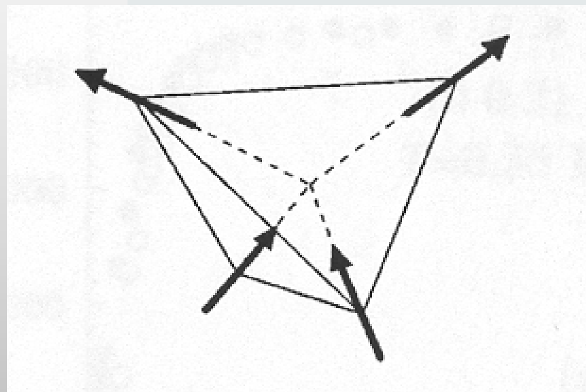

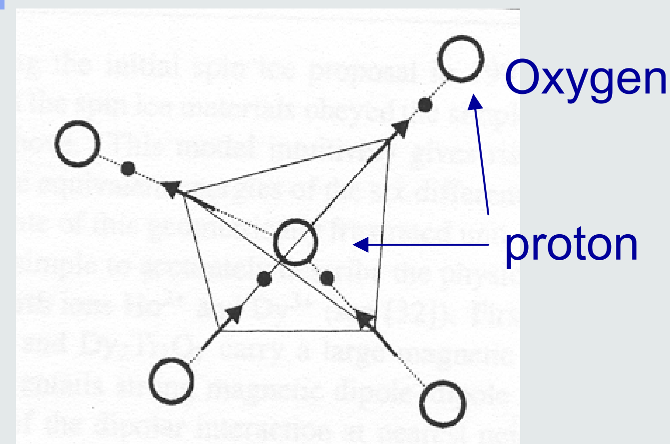

If ferromagnetic interactions,
the ground configuration is
« two in – two out » spins

$\Longrightarrow$

Similar to ice ground state:
« two close – two far » protons
with zero point entropy

Spin ice

M.Harris, S Bramwell. Nature **399** (1999) 311 & A.P.Ramirez *et al*, Nature **399** (1999) 333

- Residual low-T entropy: Pauling entropy for water ice $\mathcal{S}_0 = (1/2)\ln(3/2)$ Ramirez *et al.*:

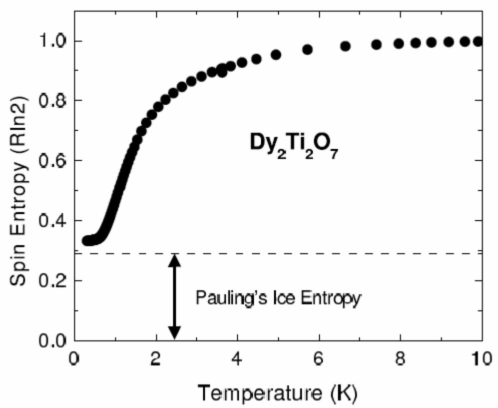

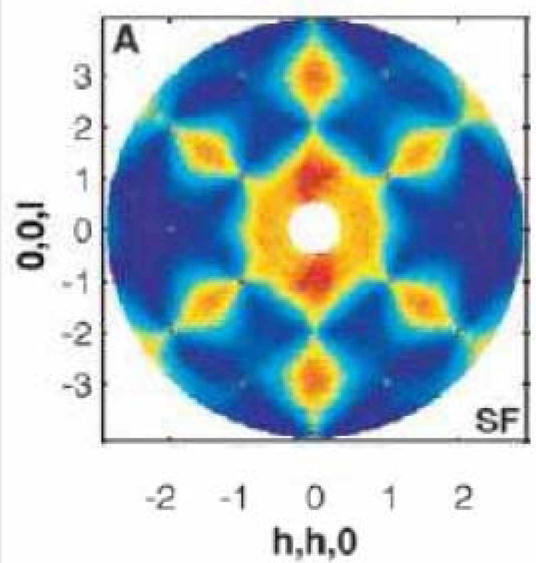

- Pauling estimate: ground-state constraints independent

$$N_{gs} = 2^n (6/16)^{n/2} = (3/2)^{n/2} \Rightarrow \mathcal{S}_0 = \frac{1}{2}\ln\frac{3}{2}$$

$$\vec{\nabla}.\vec{S}=0$$

Cooling of Spin ice in field takes longer than without it

nature Vol 451|3 January 2008|doi:10.1038/nature06433

Magnetic monopoles in spin ice

C. Castelnovo[1], R. Moessner[1,2] & S. L. Sondhi[3]

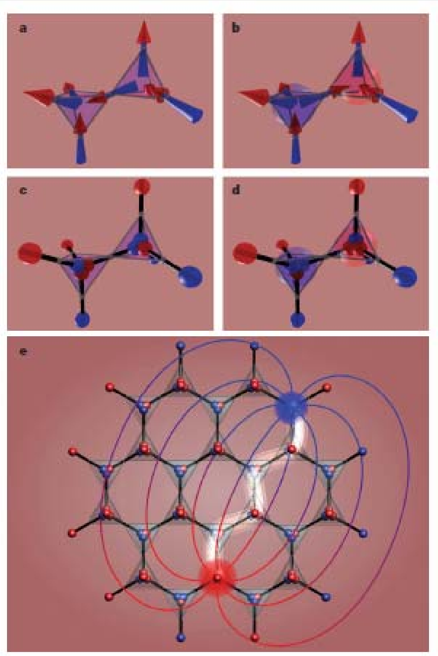

Journal of Experimental and Theoretical Physics, Vol. 101, No. 3, 2005, pp. 481–486.
Translated from Zhurnal Eksperimental'noi i Teoreticheskoi Fiziki, Vol. 128, No. 3, 2005, pp. 559–566.

ORDER, DISORDER, AND PHASE TRANSITIONS IN CONDENSED SYSTEMS

Magnetic Relaxation in Rare-Earth Oxide Pyrochlores

I. A. Ryzhkin

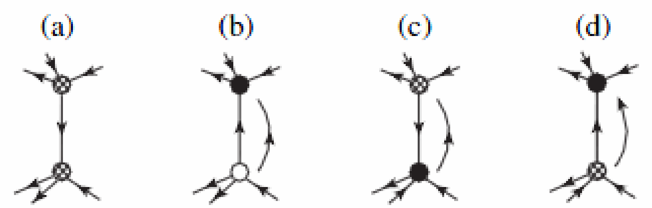

Fig. 3. Fragments of magnetic lattices with (a) no defects, (b) a pair of magnetic defects created by flipping a spin on the vertical bond, and (c, d) displacement of a magnetic defect downwards by a lattice spacing caused by a spin flip on the vertical bond. Hatched, closed, and open circles represent defect-free vertices and positive and negative magnetic defects, respectively.

Double layered monopole structure in spin liquide

A Sazonov, A Gukasov, I Mirebeau and P Bonville.

Phys. Rev. B 85, 214420 (2012)

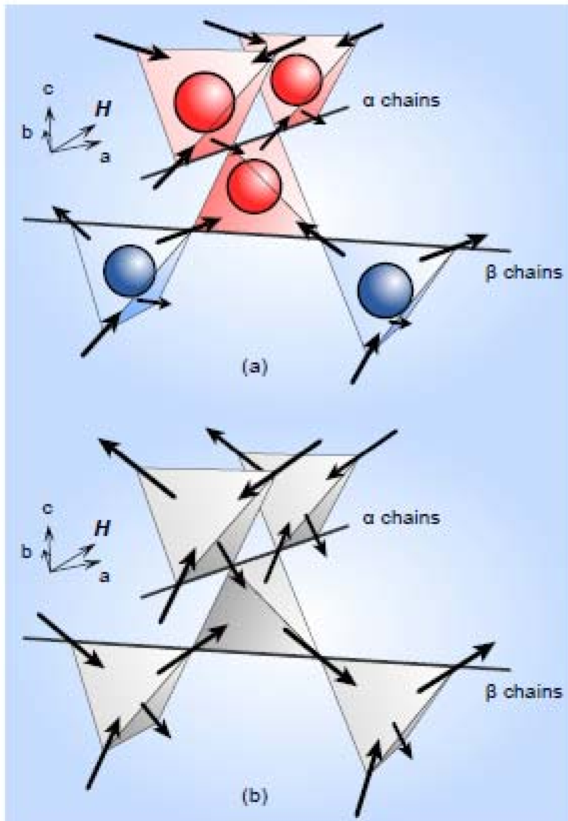

FIG. 3. Magnetic structures of $Tb_2Ti_2O_7$ spin liquid and $Ho_2Ti_2O_7$ spin ice in a [110] field. (a) Antimonopolar (double-layered monopolar) structure of $Tb_2Ti_2O_7$. (b) Magnetically vacuum state of $Ho_2Ti_2O_7$.

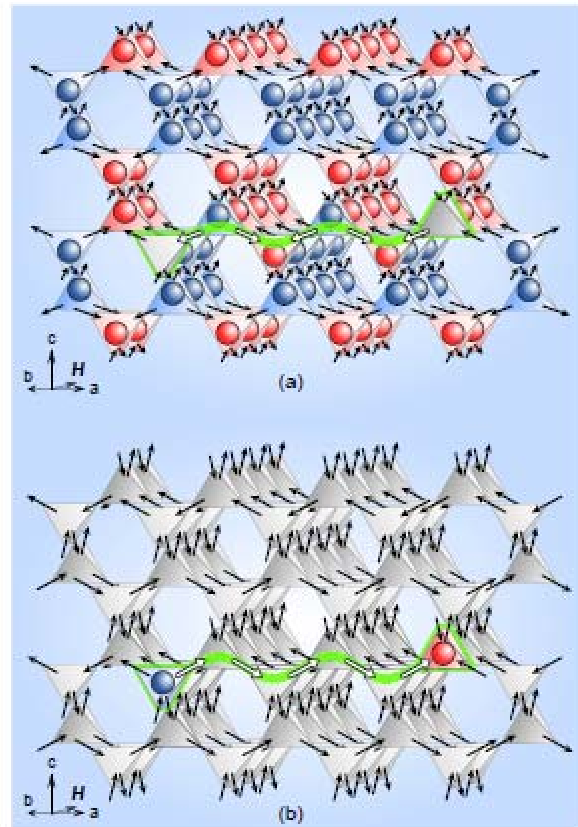

FIG. 4. Elementary excitations in $Tb_2Ti_2O_7$ spin liquid and $Ho_2Ti_2O_7$ spin ice. (a) Antimonopolar (double-layered monopolar) structure of $Tb_2Ti_2O_7$ with vacuum pair excitations. (b) Magnetically vacuum state of $Ho_2Ti_2O_7$ with

Field-induced magnetic structures in $Tb_2Ti_2O_7$ spin liquid under field $H \parallel [111]$

A. P. Sazonov,[1,2,*] A. Gukasov,[3] H. B. Cao,[4] P. Bonville,[5] E. Ressouche,[6] C. Decorse,[7] and I. Mirebeau[3]

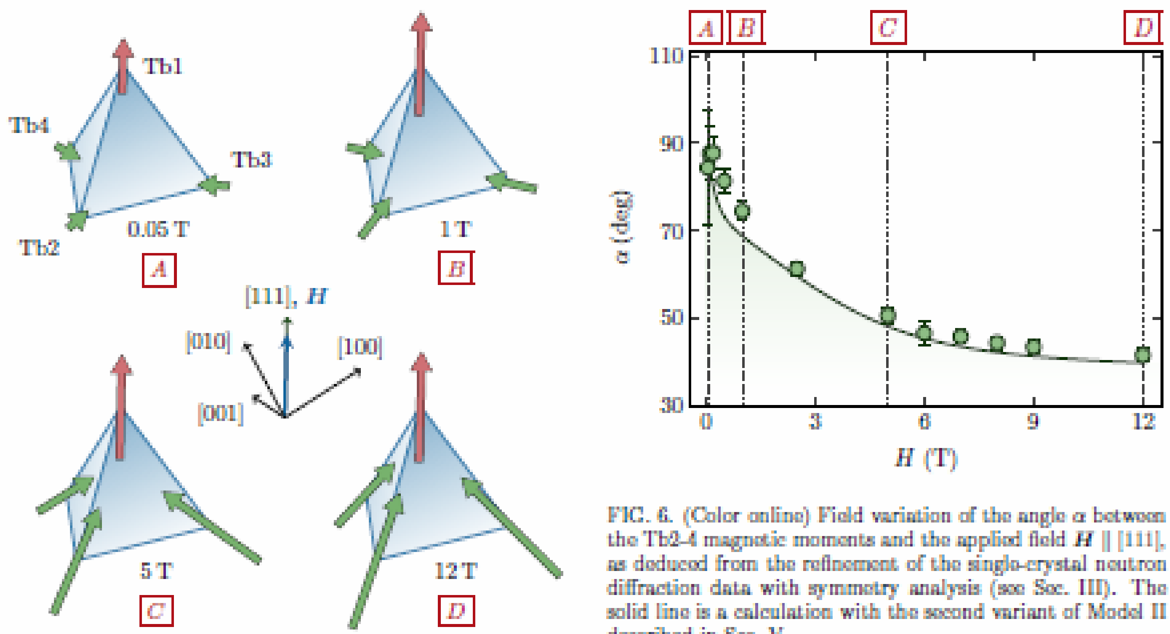

FIG. 6. (Color online) Field variation of the angle α between the Tb2-4 magnetic moments and the applied field $H \parallel [111]$, as deduced from the refinement of the single-crystal neutron diffraction data with symmetry analysis (see Sec. III). The solid line is a calculation with the second variant of Model II described in Sec. V.

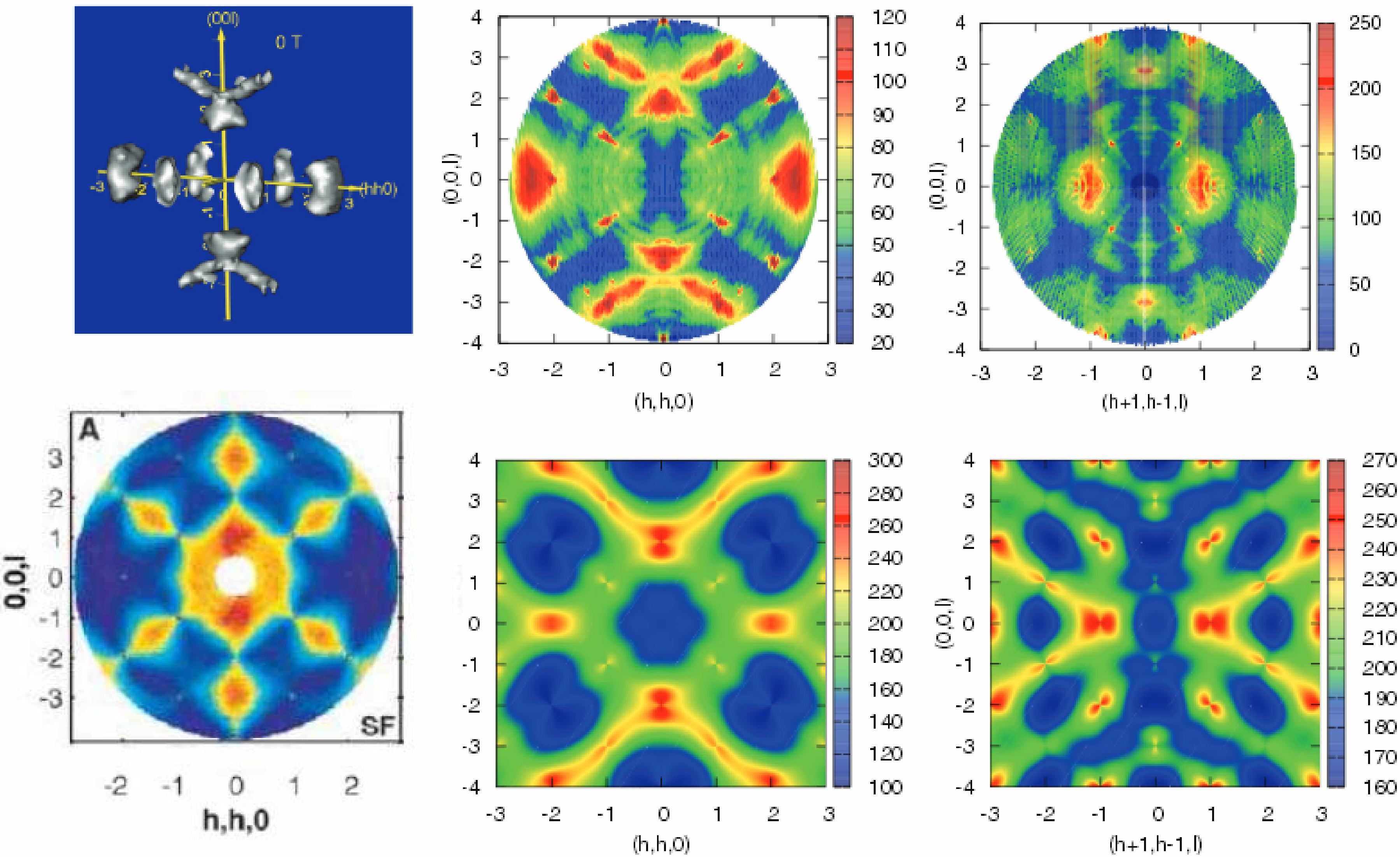

FIG. 1. (Color online) Zero-field neutron diffuse scattering maps in reciprocal space at 0.16 K in $Tb_2Ti_2O_7$: 3D equal intensity surface (left), experimental (upper central) and calculated (lower central) scattering in the (hhl) plane, experimental (right upper) and calculated (right lower) scattering in the $(h+1, h-1, l)$ plane. The simulations were made in the presence of dynamic Jahn-Teller effect, with the anisotropic exchange tensor $\mathcal{J}_a = -0.068$ K, $\mathcal{J}_b = -0.196$ K, $\mathcal{J}_c = -0.091$ K, and $\mathcal{J}_{DM}=0$.

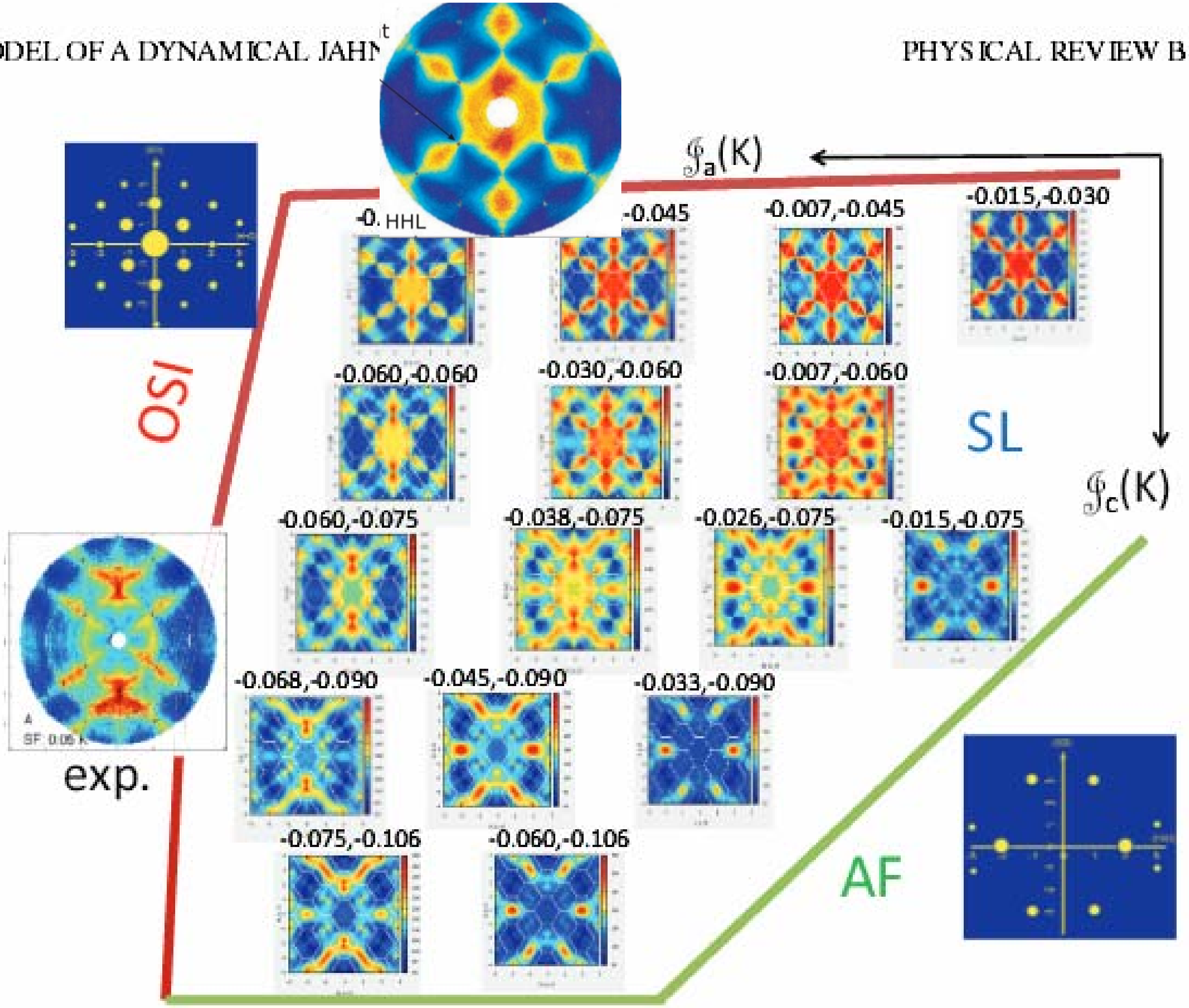

FIG. 4. (Color online) Calculated diffuse scattering maps in the (hhl) plane of the reciprocal space for the spin-flip channel at 0.05 K, according to the geometrical setup of Ref. [20]. The q maps are represented in the spin liquid (SL) phase of our model (see Ref. [39]), which stands as a wedge between the antiferromagnetic (AF) phase and the ordered spin ice (OSI) phase. The figure is a sketch of a cut in the exchange parameter phase space for $\mathcal{J}_b = -0.196$ K [65]; the numbers above each map are the values (in K) of $\mathcal{J}_a$ and $\mathcal{J}_c$. The map on the left labeled "exp." is the experimental spin-flip diffuse scattering in $Tb_2Ti_2O_7$ at 0.05 K from Ref. [20]; it has been placed close to the bottom left corner of

POLARIZED NEUTRON DIFFRACTION

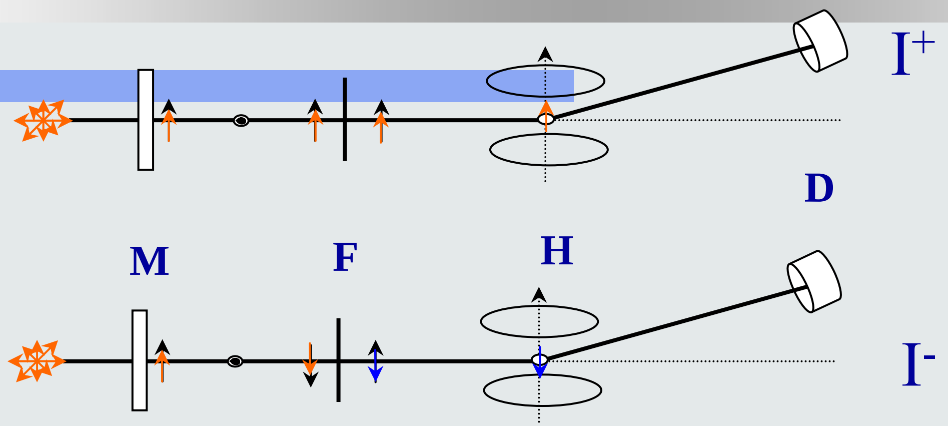

P_0 parallel to H

P_0 antiparallel to H

$$R = I^+ / I^- = (F_N + F_M)^2 / (F_N - F_M)^2$$

$$R = (1+\gamma)^2 / (1-\gamma)^2, \qquad \text{where } \gamma = F_M / F_N$$

$$R \cong 1 + 4\gamma \qquad\qquad F_M(q) = \gamma * F_N(q)$$

PND APPLICATIONS

- Spin Densities
- Magnetic structure refinement
- Local Susceptibility Parameters (LSP)
- Formfactors, L/S ratio

5C1 polarised neutron diffractometer (LLB)

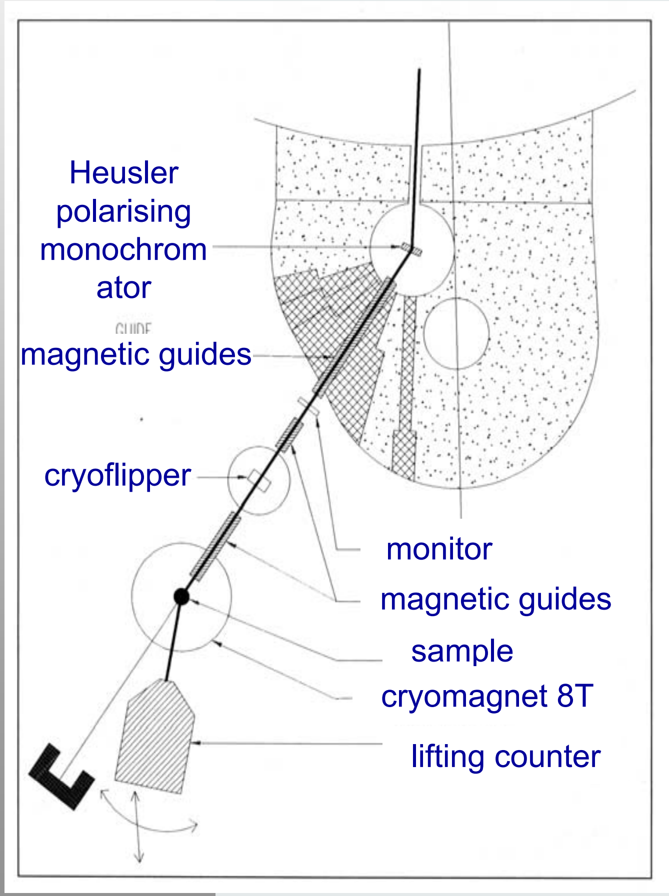

SPIN DENSITY OF Mn(dca)2(pym)H2O

pym=N2(CH)4 (pirimidine) *dca=N(CN)$_2$ (dicianamide)*

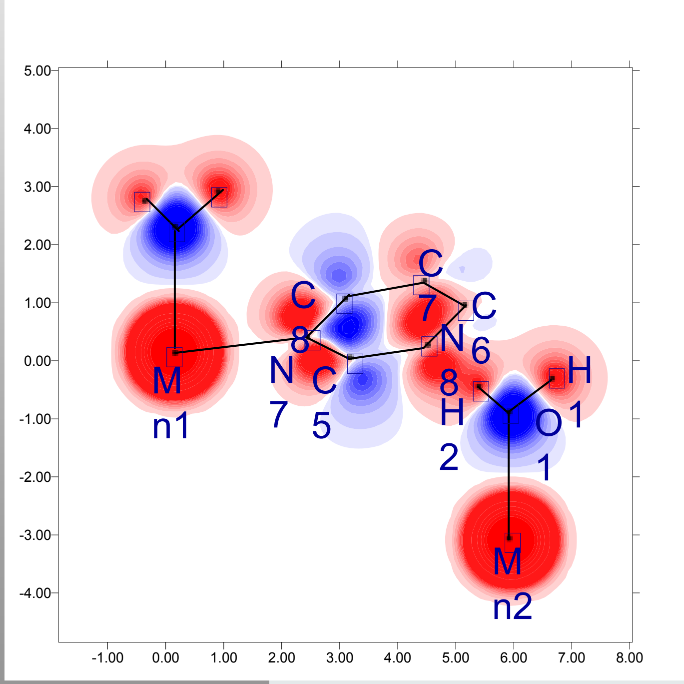

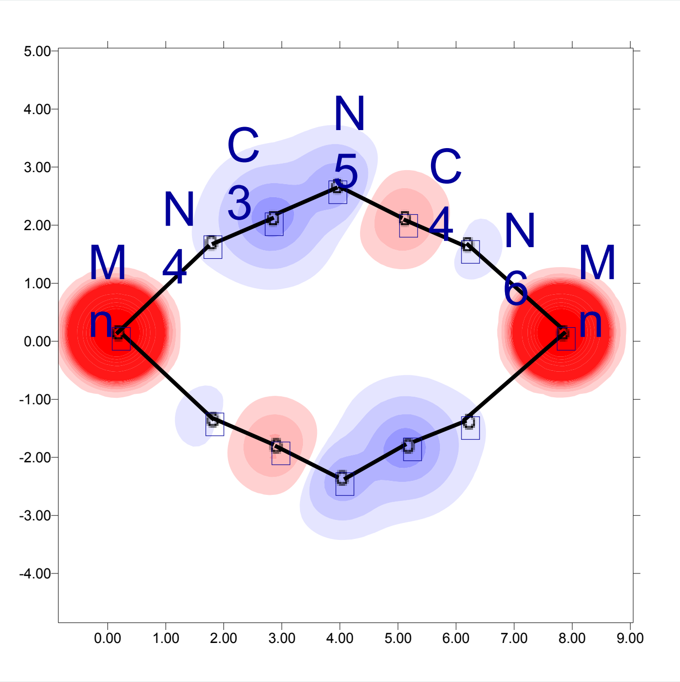

NON-COLLINEAR SPIN DENSITIES

Bulk magnetisation $M_i(r) = \chi_{ij} H_j$

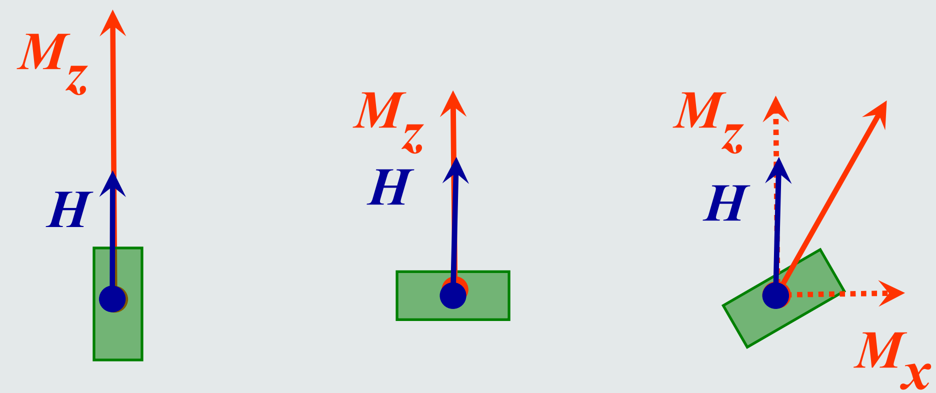

$$I^{\pm} \propto F^2_N \pm 2(\underline{P}_0 * \underline{F}_M)\, F_N + F_M^2$$

$$I^{\pm} \propto F^2_N \pm 2 F_{Mz}\, F_N + F_M^2$$

ANISOTROPIC SYSTEMS UNDER MAGNETIC FIELD

F. Wang; A Gukasov et al., PRL, 2003 **ORIGIN OF THE FIELD INDUCED METALIC STATE OF $(La_{0.4}\ Pr_{0.6})_{1.2}Sr_{1.8}Mn_2O_7$**

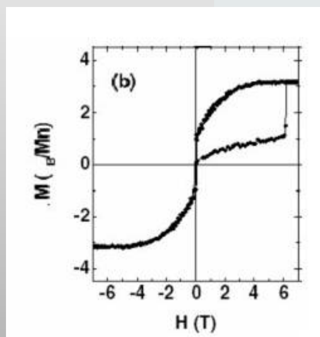

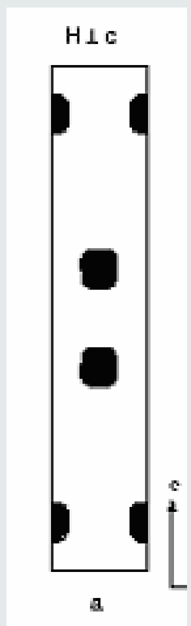

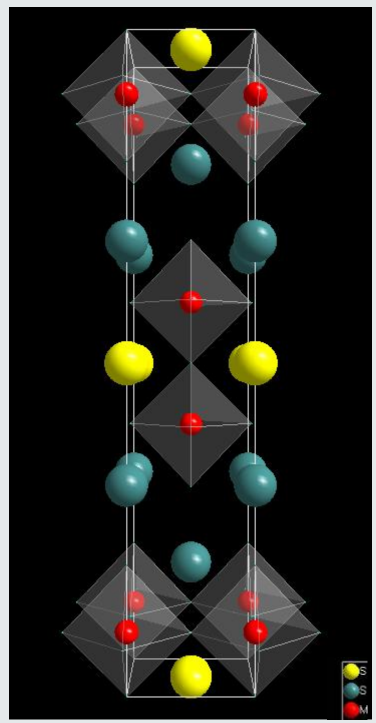

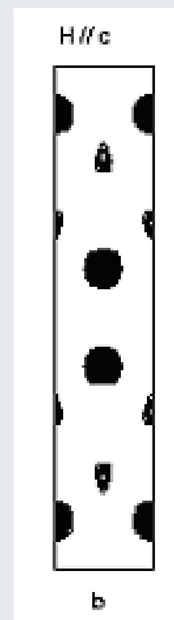

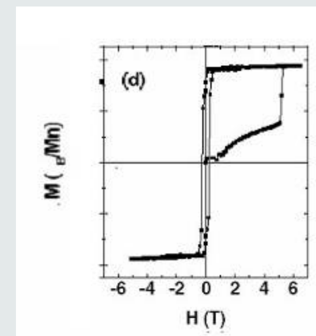

ANISOTROPIC SUSCEPTIBILITIES

$$\chi_{ij} = \begin{pmatrix} \chi_{11} & \chi_{12} & \chi_{13} \\ & \chi_{22} & \chi_{23} \\ & & \chi_{33} \end{pmatrix}$$

Bulk magnetisation $M_i(r) = \chi_{ij} H_j$

The number of independent components of χ_{ij} is determined by the crystal symmetry class:

cubic groups	1	parameter
all uniaxial groups	2	parameters
Orthorhombic	3	...
Monoclinic	4	...
Triclinic	6	

ANISOTROPIC BULK SUSCEPTIBILITY

CUBIC, $\chi_{11} = \chi_{22} = \chi_{33}$

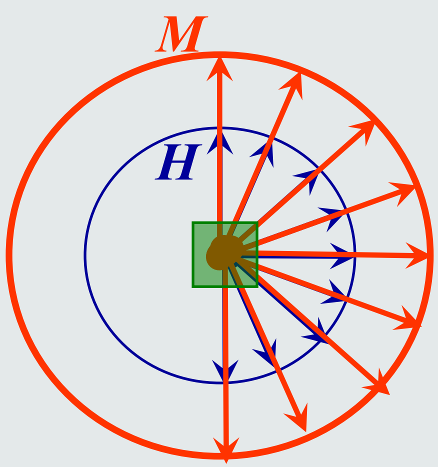

$$\chi_{ij} = \begin{pmatrix} \chi_{11} & 0 & 0 \\ 0 & \chi_{11} & 0 \\ 0 & 0 & \chi_{11} \end{pmatrix}$$

UNIAXIAL $\chi_{11} = \chi_{22} < \chi_{3}$

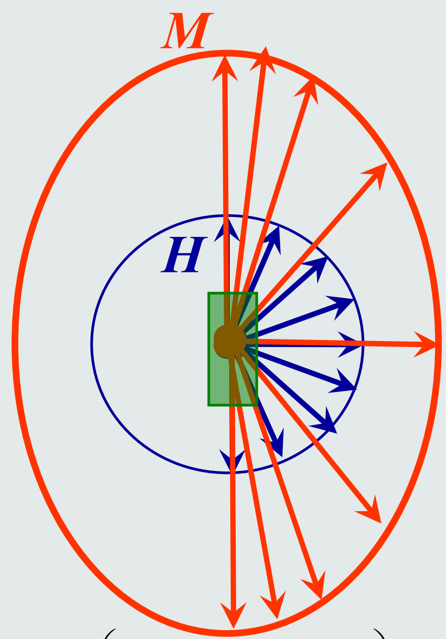

$$\chi_{ij} = \begin{pmatrix} \chi_{11} & 0 & 0 \\ 0 & \chi_{11} & 0 \\ 0 & 0 & \chi_{33} \end{pmatrix}$$

LOCAL SUSCEPTIBILITIES

$$I^{\pm} \propto N^2 \pm 2\, P_{0z}\, N\, M_z + M_z^2$$

$$\boldsymbol{M}_i = \Sigma_a\, \chi^a_{ij} \boldsymbol{H}_j$$

$$I^{\pm} \propto N^2 \pm 2 F_N (P_0 * \Sigma \chi^a_{ij} \boldsymbol{H}_j) + |\Sigma \chi^a_{ij} \boldsymbol{H}_j|^2$$

$R = I^+ / I^-$, CHILSQ (CCSL)

A Gukasov and P J Brown, J Phys C, 14, 8831, 2002

Field-Induced Spin-Ice-Like Orders in Spin Liquid $Tb_2Ti_2O_7$

H. Cao,[1] A. Gukasov,[1] I. Mirebeau,[1] P. Bonville,[2] and G. Dhalenne.[3]

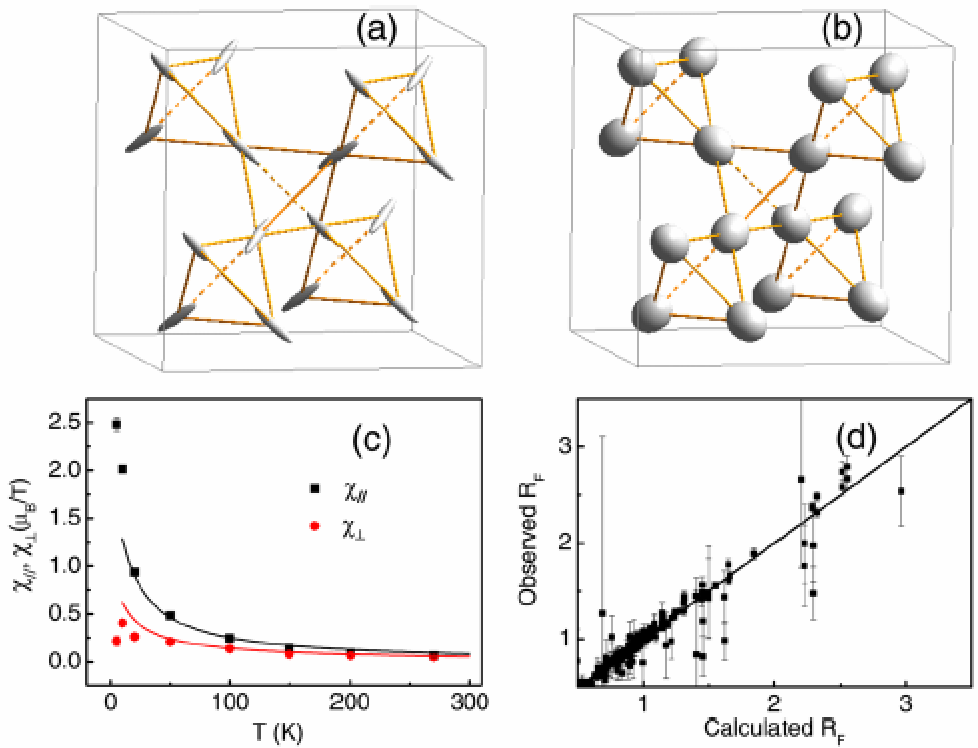

FIG. 1 (color online). $Tb_2Ti_2O_7$: Local anisotropic susceptibility ellipsoids $\chi_{ij}T$, measured at 10 K (a) and 270 K (b). Ellipsoids were scaled by temperature to compensate the Curie behavior. (c) Susceptibility components $\chi_{\parallel}$ and $\chi_{\perp}$ versus T. The lines are CF calculations. (d) Measured versus calculated flipping ratio at 10 K.

MAGNETIC ELLIPSOIDS in TbTi H II [111]

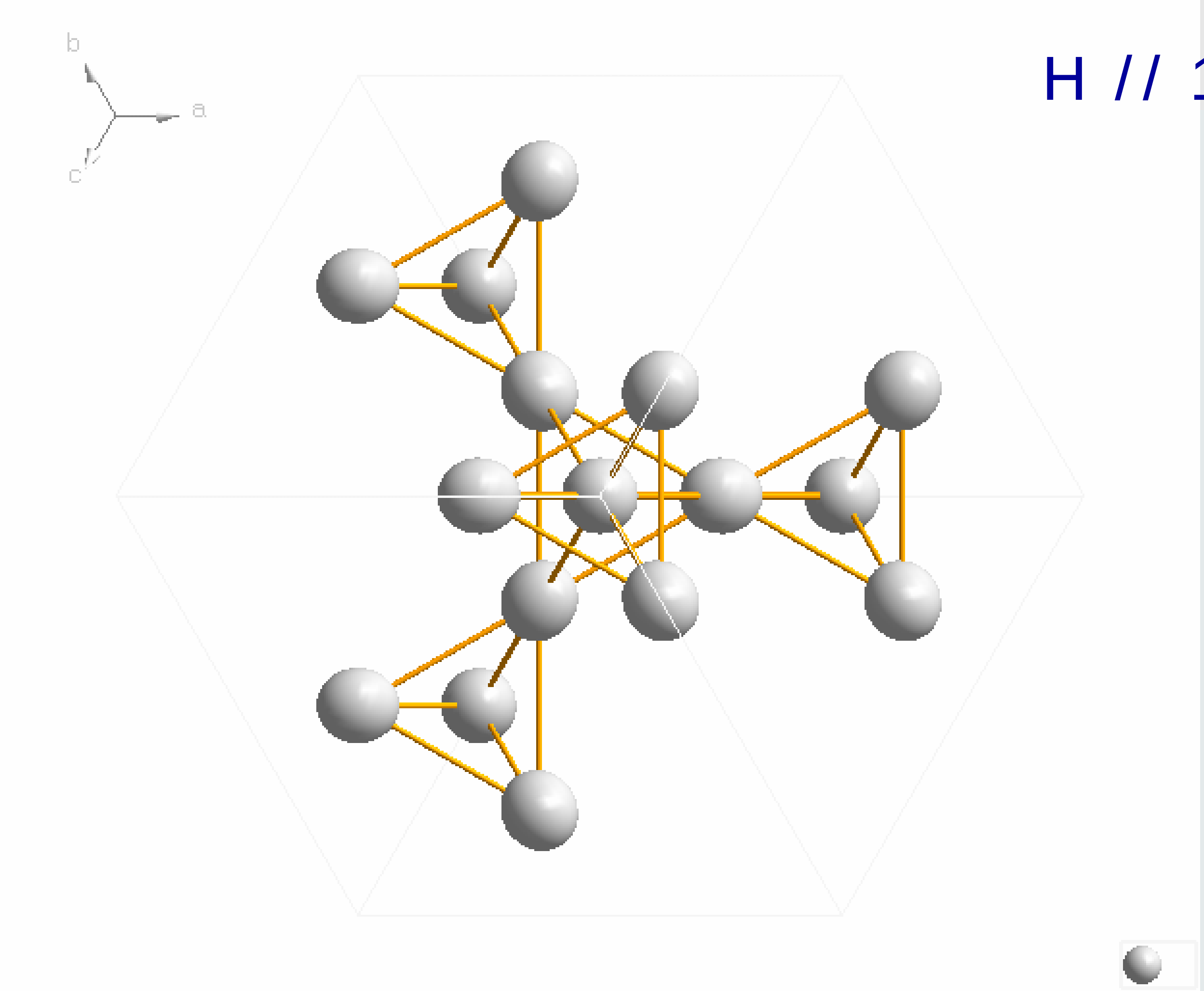

H // 111

270 K 1 T, 100 FR

MAGNETIC ELLIPSOIDS in TbTi H II [111]

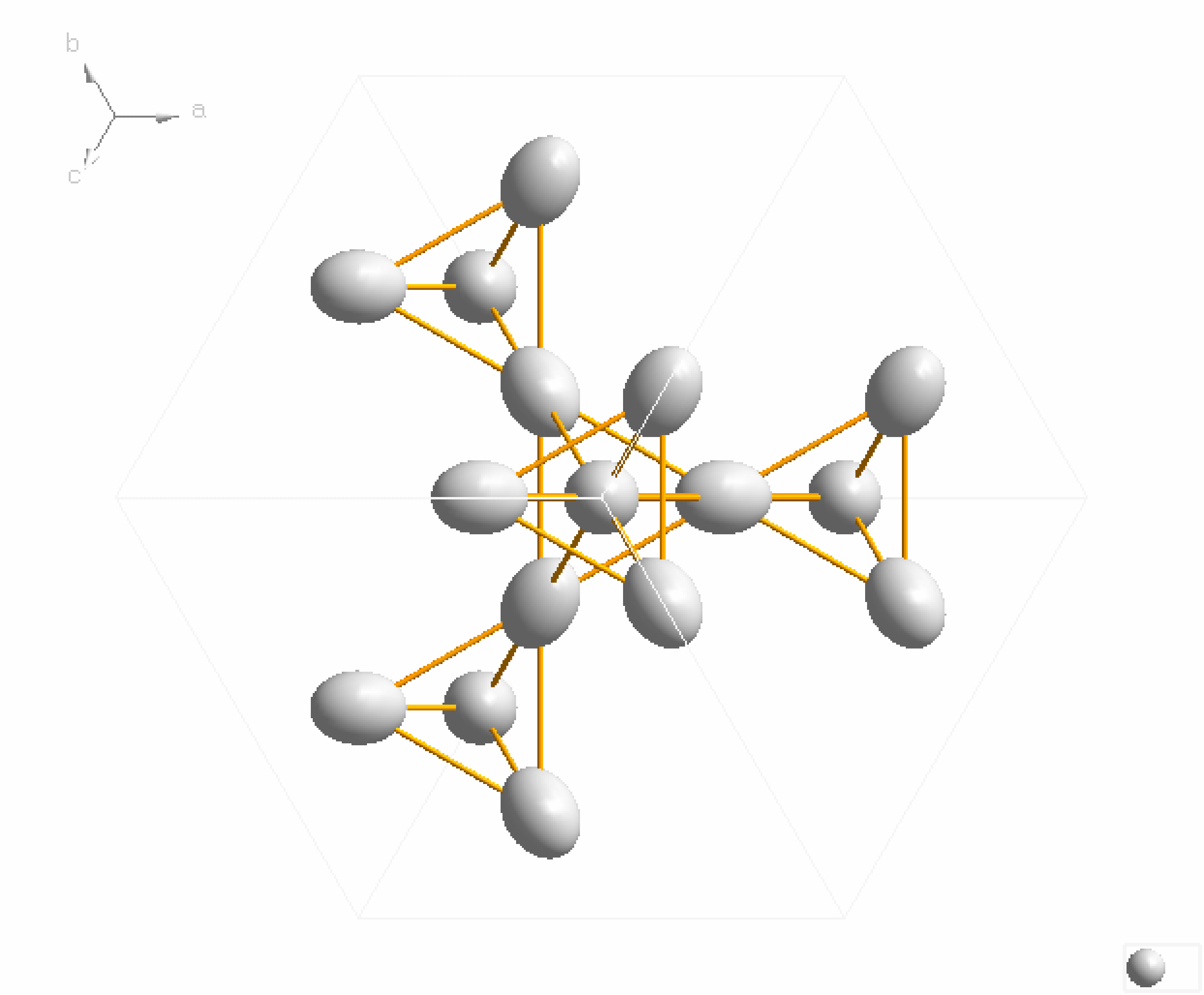

100 K 1 T, 100 FR

MAGNETIC ELLIPSOIDS in TbTi H II [111]

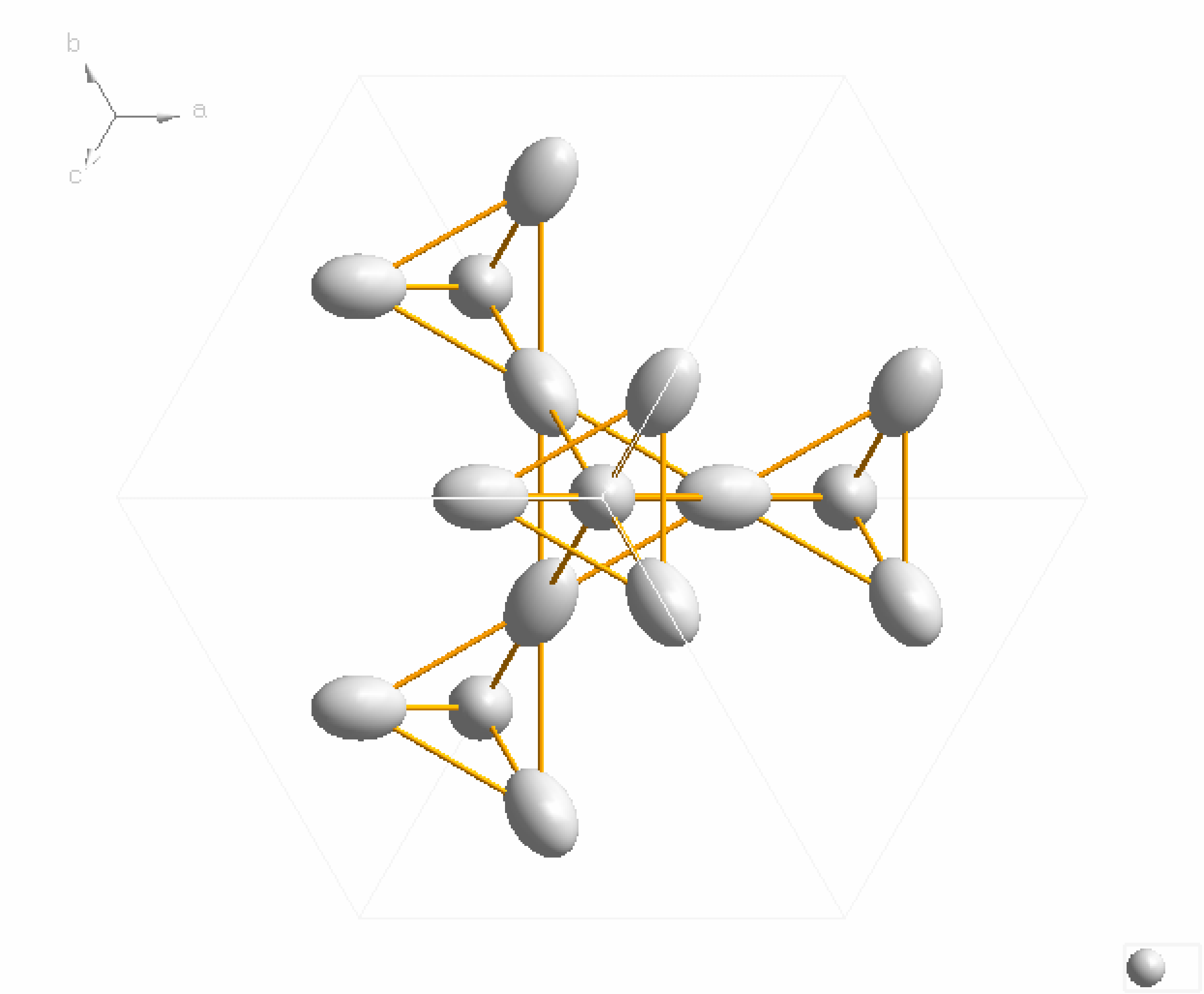

50 K 1 T, 100 FR

MAGNETIC ELLIPSOIDS in TbTi H II [111]

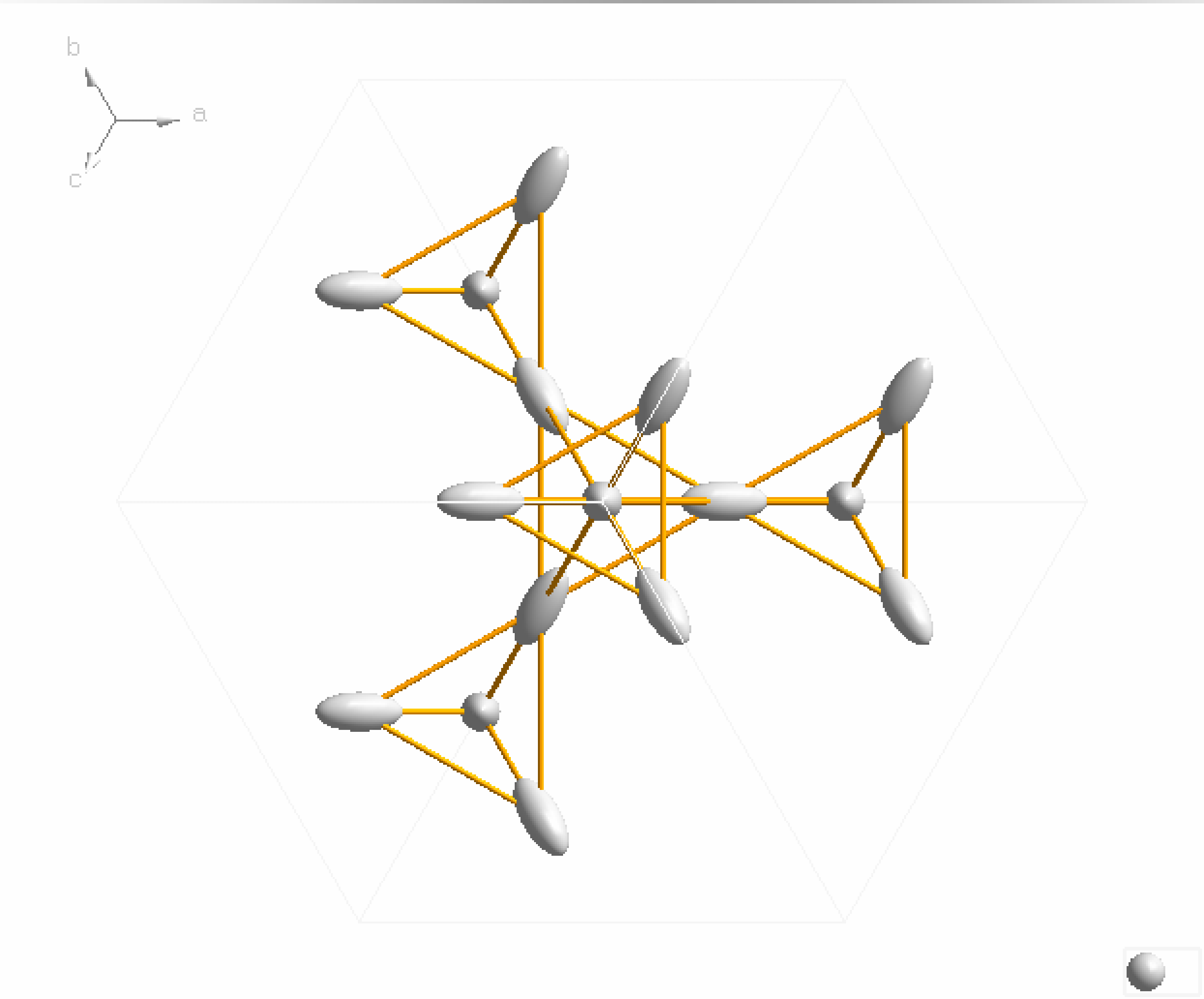

10 K 1 T, 150 FR

MAGNETIC ELLIPSOIDS in TbTi H II [111]

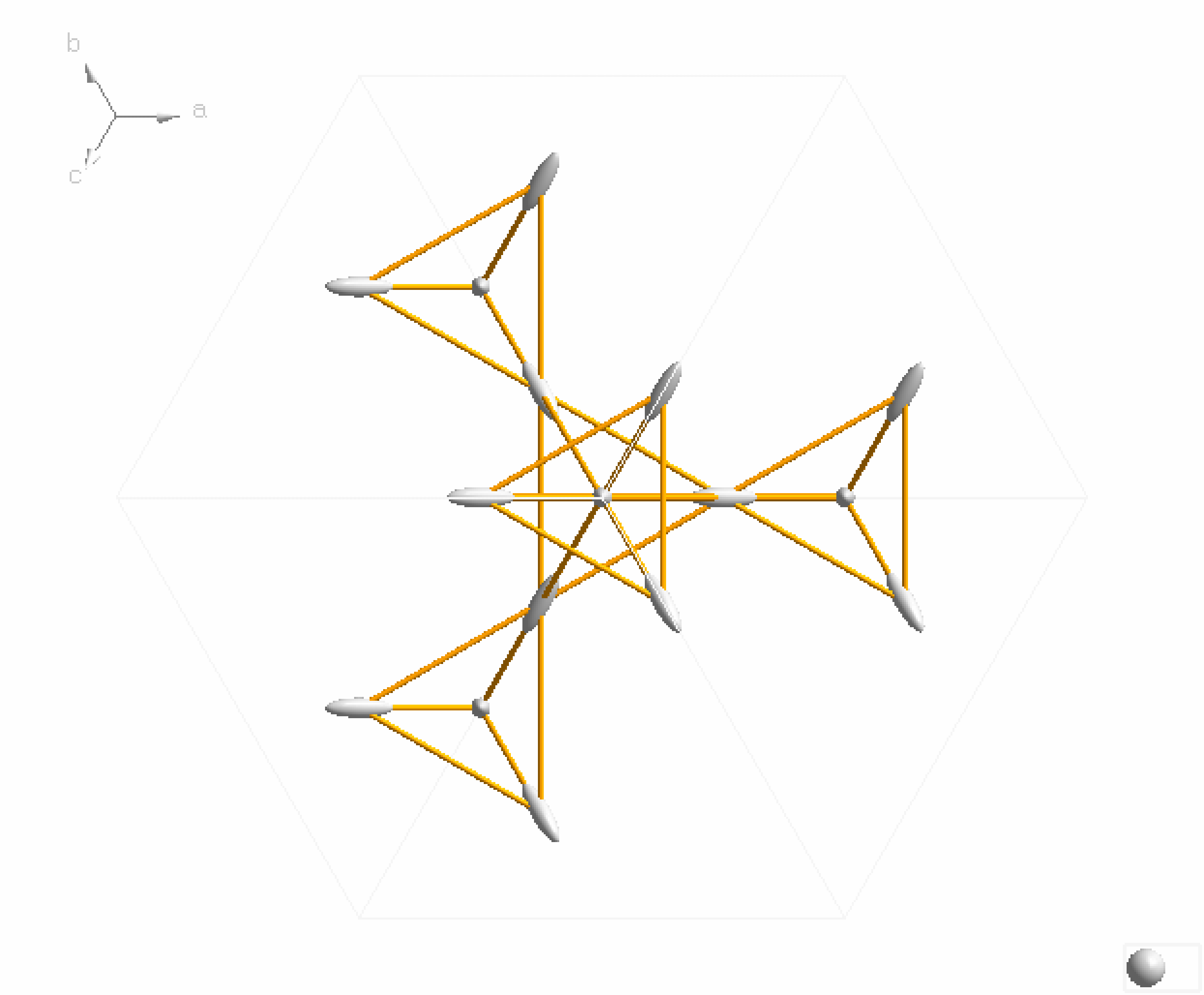

5 K 1 T, 150 FR

Ising versus XYanisotropy “as seen” by PND.

H. Cao, A. Gukasov et al. ***PRL 103****, 056402 (2009)*

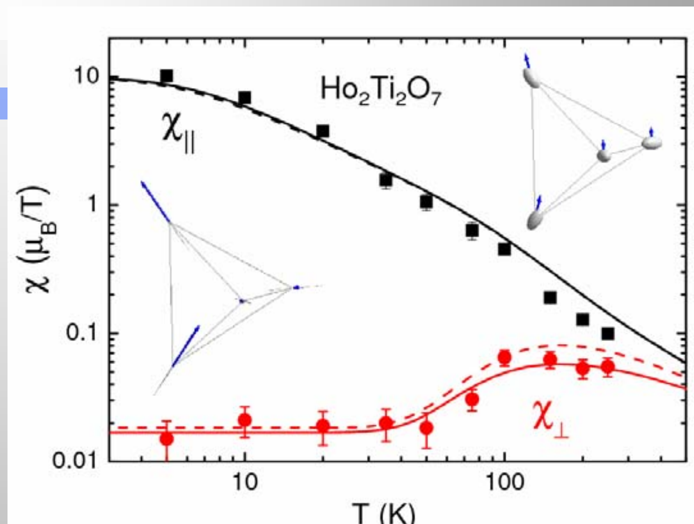

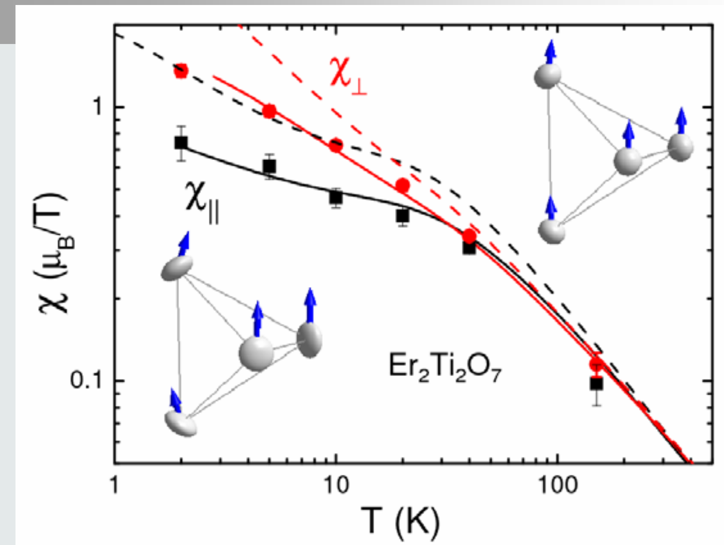

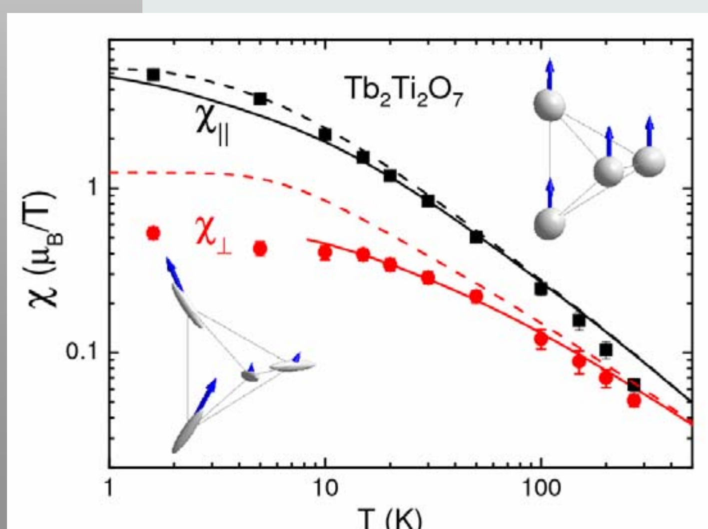

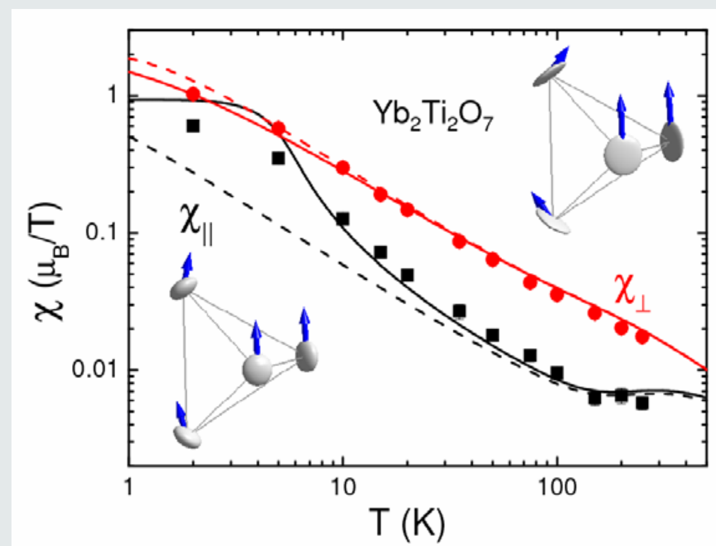

IOP Publishing Journal of Physics: Condensed Matter
J. Phys.: Condens. Matter **22** (2010) 276003 (11pp) doi:10.1088/0953-8984/22/27/276003

Static magnetic susceptibility, crystal field and exchange interactions in rare earth titanate pyrochlores

B Z Malkin[1], T T A Lummen[2,4], P H M van Loosdrecht[2], G Dhalenne[3] and A R Zakirov[1]

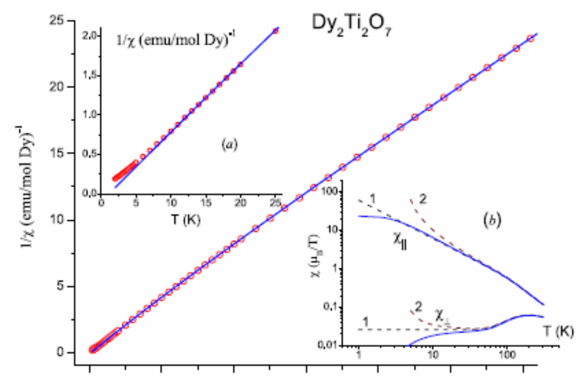

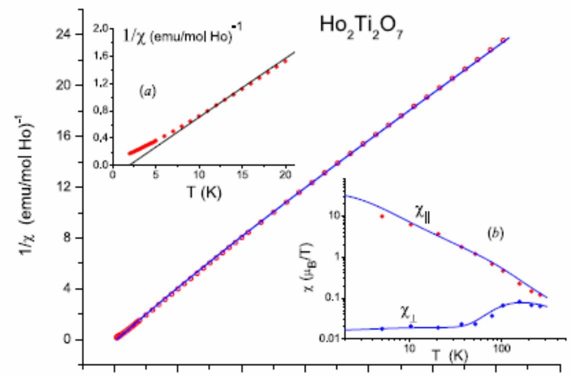

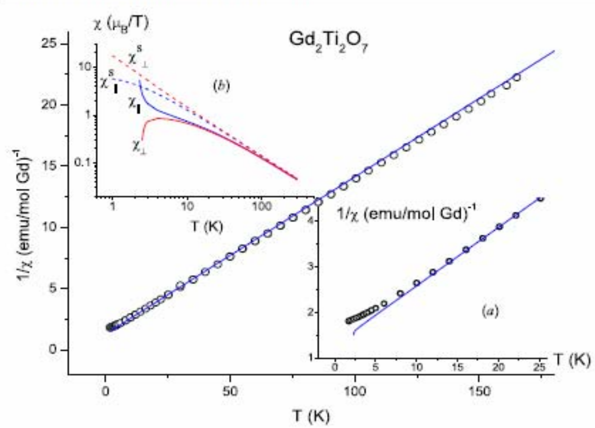

Figure 1. Measured (symbols) and calculated (solid curve) inverse bulk susceptibility of $Gd_2Ti_2O_7$. Inset (*a*) shows the data below 25 K. Inset (*b*): calculated components of the single ion (dashed curves) and the renormalized site susceptibility (solid curves) tensors.

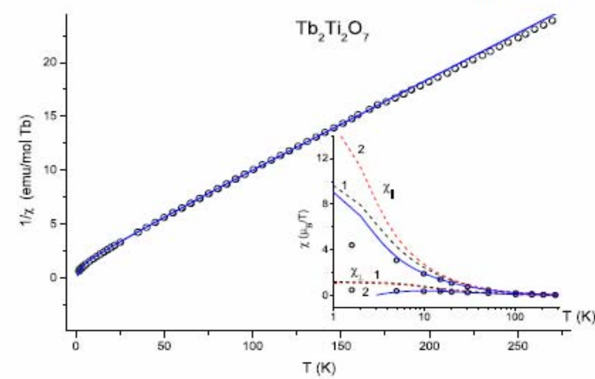

Figure 2. Measured (symbols) and calculated (solid curve) inverse bulk susceptibility in $Tb_2Ti_2O_7$ single crystal (the disk with the demagnetizing factor $N = 1.92$). Inset: site susceptibilities measured in [27] (symbols) and calculated single ion susceptibilities in the crystal field (dotted curves 1), renormalized susceptibilities due to dipole–dipole interactions (dotted curves 2) and due to dipole–dipole and anisotropic exchange interactions (solid curves).

Can we measure ASPs on Powder samples?

powder Tb2Sn2O7 on Super-6T2,

(measuring time 200 sec)

100k 5T

2k 5T

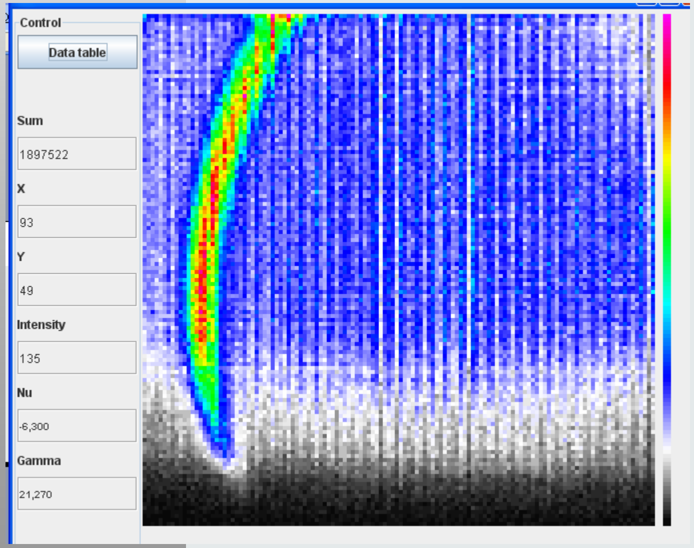

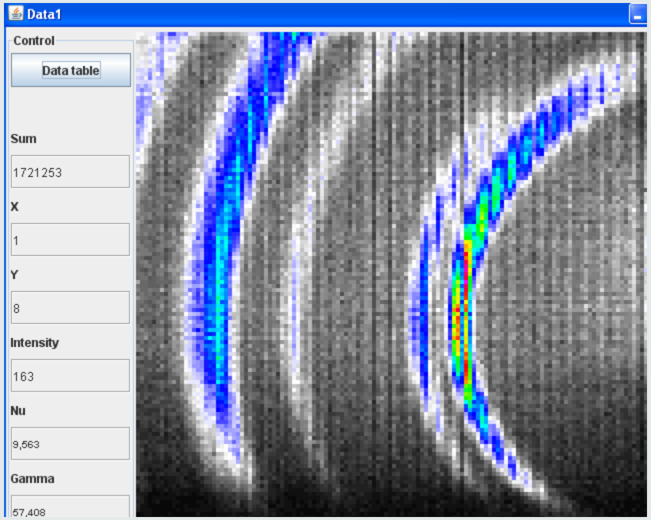

24°

Can we measure ASPs on Powder samples?

powder $Tb_2Sn_2O_7$

100k 5T **2k 5T**

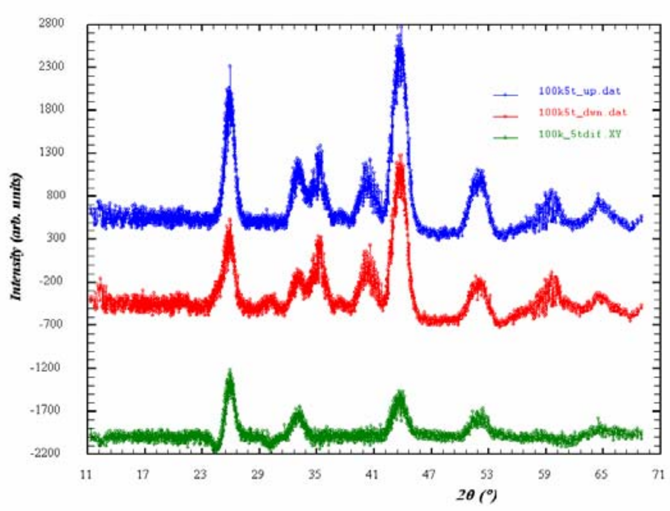

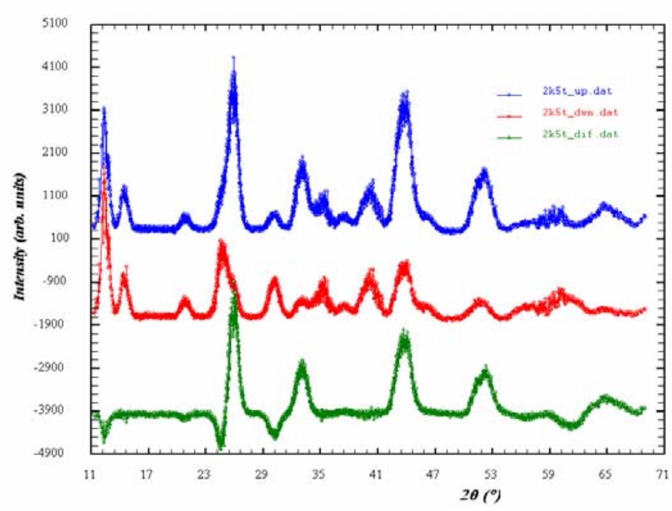

IOP FTC
IOP PUBLISHING JOURNAL OF PHYSICS: CONDENSED MATTER
J. Phys.: Condens. Matter **22** (2010) 502201 (5pp) doi:10.1088/0953-8984/22/50/502201

FAST TRACK COMMUNICATION

Determination of atomic site susceptibility tensors from neutron diffraction data on polycrystalline samples

A Gukasov[1] and P J Brown[2]

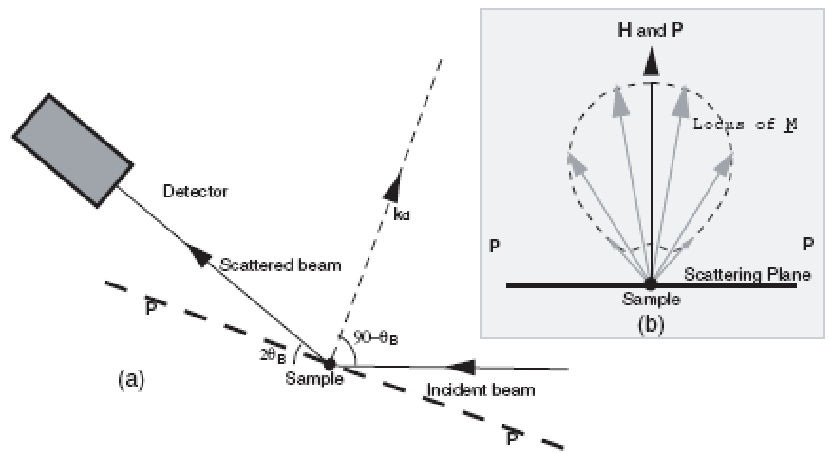

Figure 1: (a) Section in the scattering plane perpendicular to the polarisation and magnetic field direction showing the geometry for scattering by a polycrystalline sample. (b) The shaded inset shows the plane perpendicular to the scattering vector k_d of a reflection and indicates the locus of the magnetic interaction vectors of different contributing grains

Can we measure ASPs on Powder samples?

$$A = \frac{I^+ - I^-}{I^+ + I^-} = \frac{2\Re\left(N(\mathbf{k})\mathbf{M}_\perp(\mathbf{k})^* \cdot \mathbf{P}\right)}{|N(\mathbf{k})|^2 + |\mathbf{M}_\perp(\mathbf{k})|^2}$$

$$\begin{aligned}
\langle|\mathbf{M}_\perp(\mathbf{k})|^2\rangle &= \frac{H^2}{\pi}\int_{-\frac{\pi}{2}}^{\frac{\pi}{2}} |\mathbf{M}_\perp(\mathbf{k})|^2 d\psi \\
&= \frac{H^2}{\pi}\left[\left(\frac{\Xi_{11}^2 + \Xi_{22}^2}{2} + \Xi_{12}^2\right)\psi + \left(\frac{\Xi_{12}(\Xi_{11} + \Xi_{22})}{2}\right)\cos 2\psi\right]_{-\frac{\pi}{2}}^{\frac{\pi}{2}} \\
&= H^2\left(\frac{\Xi_{11}^2 + \Xi_{22}^2}{2} + \Xi_{12}^2\right) \qquad (7)
\end{aligned}$$

and the mean value of $\mathbf{M}_\perp(\mathbf{k}) \cdot \mathbf{P}$ is

$$\begin{aligned}
\langle \mathbf{M}_\perp(\mathbf{k}) \cdot \mathbf{P}\rangle &= \frac{PH}{\pi}\int_{-\frac{\pi}{2}}^{\frac{\pi}{2}} \left(\Xi_{11}\cos^2\psi + 2\Xi_{12}\sin\psi\cos\psi + \Xi_{22}\sin^2\psi\right) d\psi \\
&= \frac{PH}{\pi}\left[\left(\frac{\Xi_{11} + \Xi_{22}}{2}\right)\psi + \Xi_{12}\cos 2\psi\right] = PH\left(\frac{\Xi_{11} + \Xi_{22}}{2}\right)
\end{aligned}$$

CHILSQ program in CCSL (P J Brown)

Can we measure ASPs with upolarized neutrons?

Extinction rule for pyrochlore impose (00h)=4n

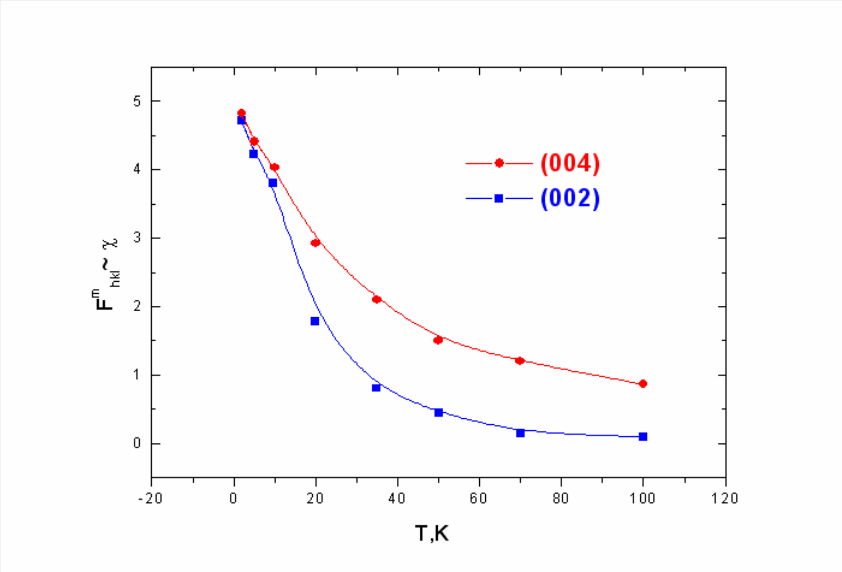

$I_m(400) \sim \chi_{11}$ Heisenberg behavior

$I_m(200) \sim \chi_{12}$ Ising or XY behavior

PND PROVIDES

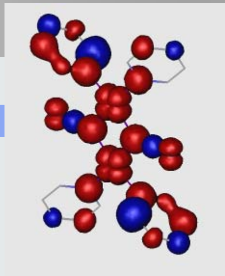

- Spin Densities

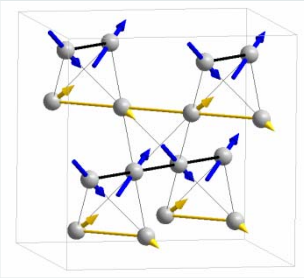

- Magnetic structure refinement

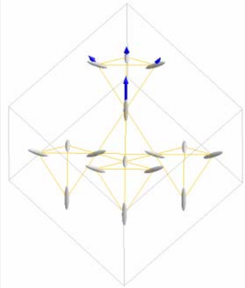

- Atomic Susceptibility Parameters

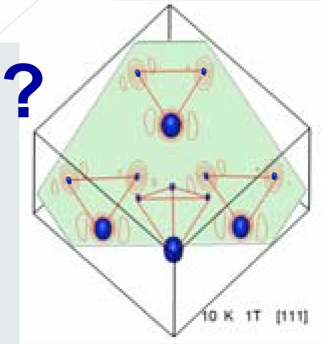

- Non-collinear Magnetization Densities ?

Rectangular 2D Space Group

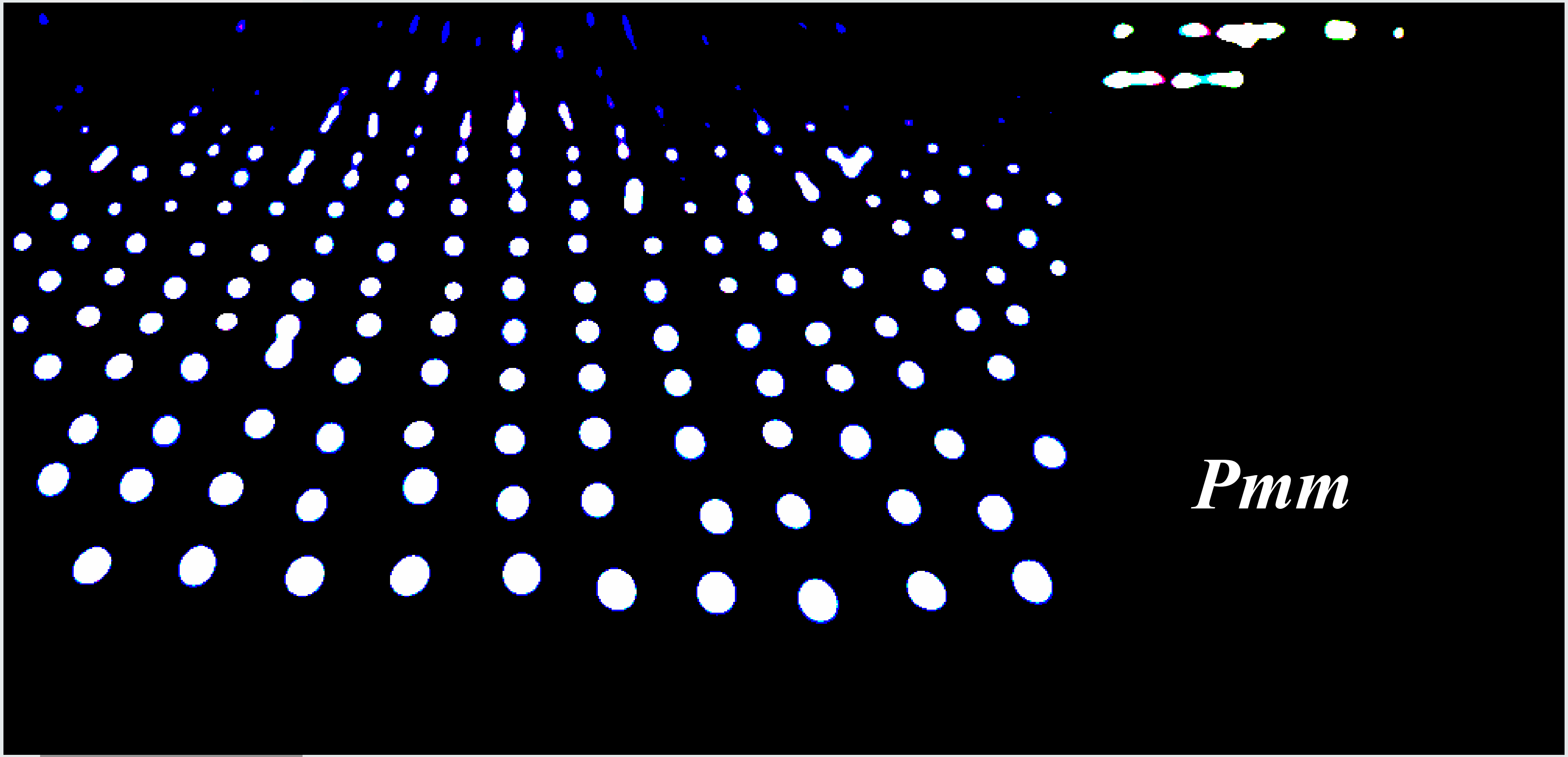

Rectangular 2D Space Group *Pmm*

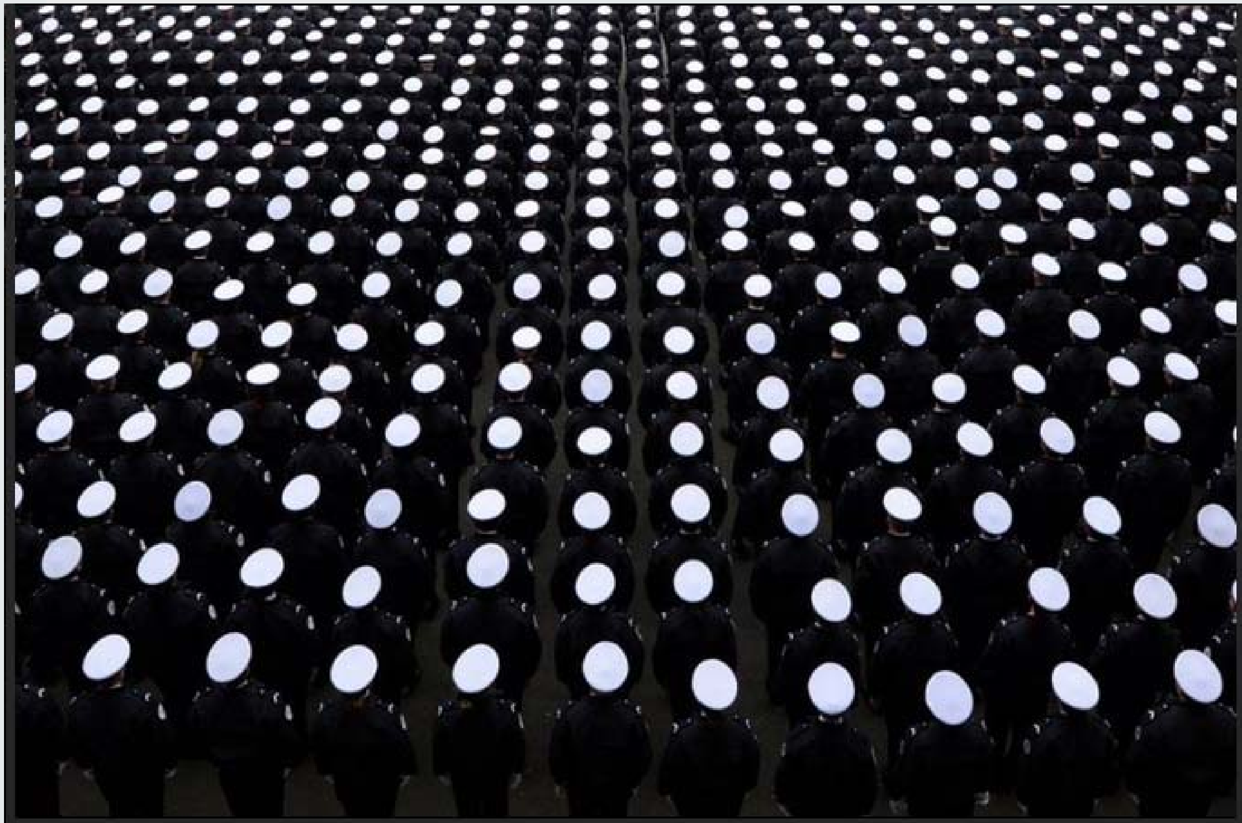

Les images de la semaine

7 DÉCEMBRE 2013 À 09:29

Hommage à Mandela, violences en Centrafrique, manifestations en Ukraine et en Thaïlande, la loi sur la prostitution adoptée, Michelle Obama paniquée et la Valise Vuitton démontée... La sélection des images marquantes de l'actualité.

Pmm

4 décembre. Cérémonie d'accueil à la préfecture de police de Paris de la 226e promotion de gardiens de la paix et du personnel nouvellement affecté. Photo Pierre Andrieu. AFP

Photo-excitation setup at 5C1 diffractometer

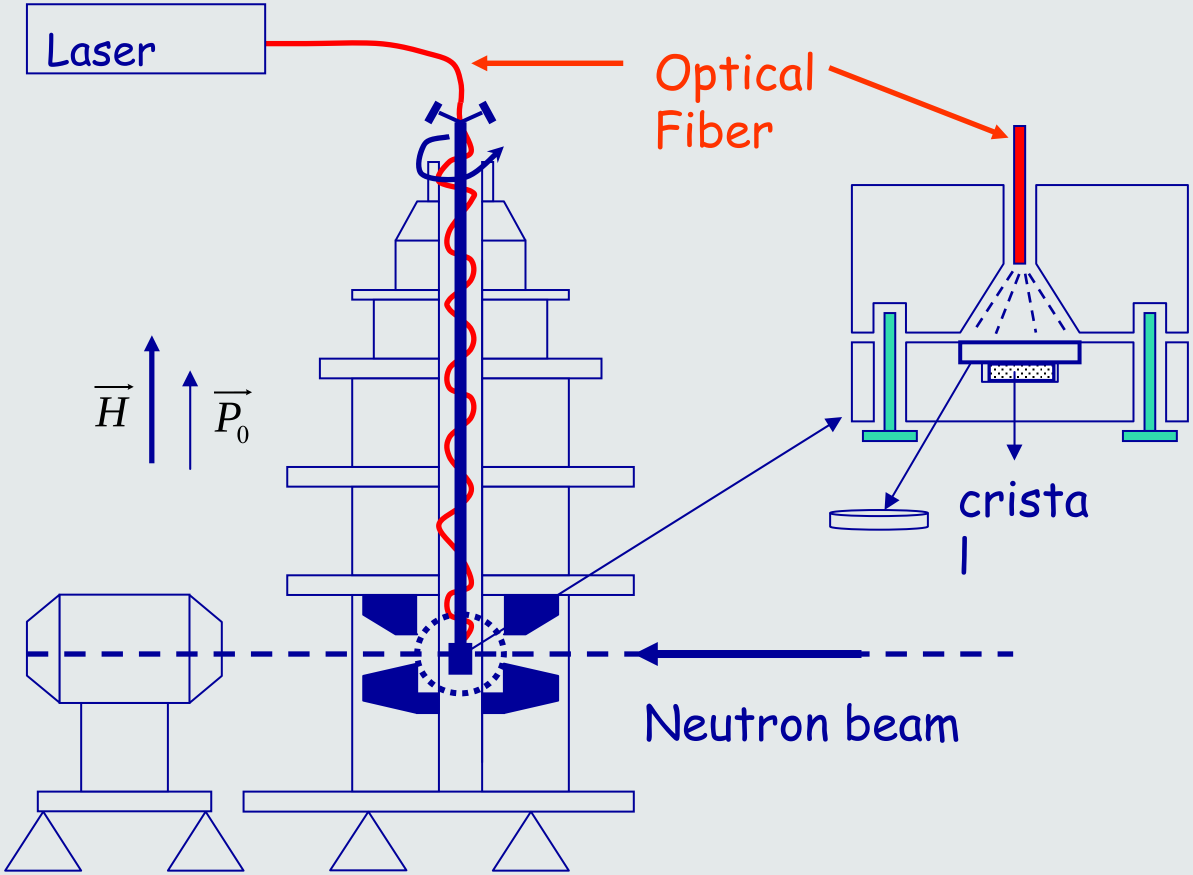

Light Induced Excited Spin State Trapping (LIESST) in Fe(ptz)$_6$](BF$_4$)$_2$

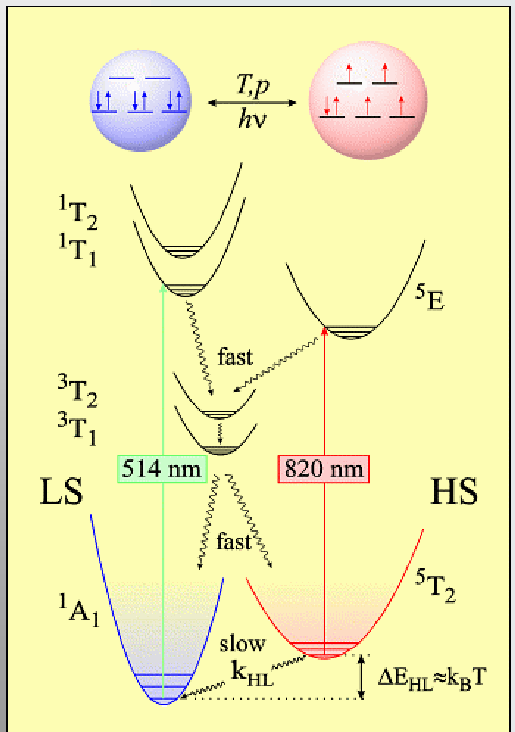

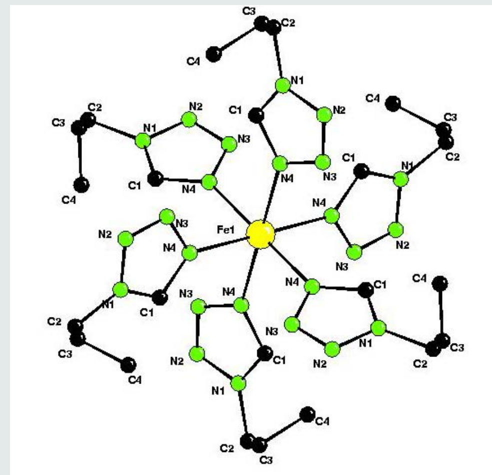

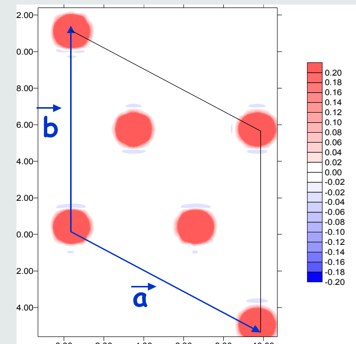

$\lambda \sim 514$ nm

S. Decurtins et al. Inorg. Chem. 24 (1985) 2174

Very Intense Polarized Neutron DIFFRACTOMETER (5C1) at LLB

project started in 2006

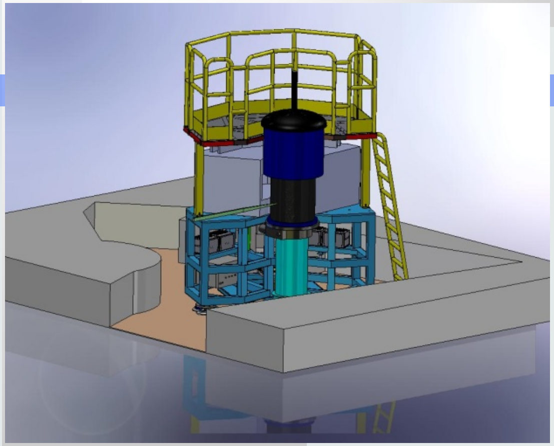

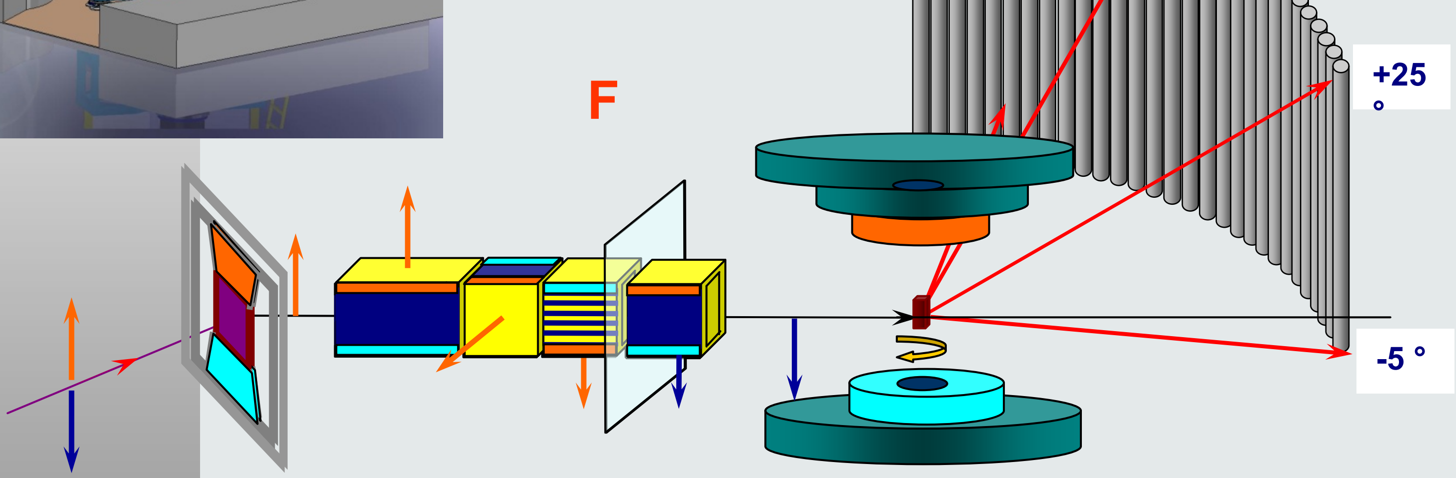

25°x90°

0.7 rad

PHYSICAL REVIEW B 89, 085115 (2014)

Towards a model of a dynamical Jahn-Teller coupling at very low temperatures in $Tb_2Ti_2O_7$

P. Bonville*
CEA, Centre de Saclay, DSM/IRAMIS/Service de Physique de l'Etat Condensé, 91191 Gif-sur-Yvette, France

A. Gukasov, I. Mirebeau, and S. Petit
CEA, Centre de Saclay, DSM/IRAMIS/Laboratoire Léon Brillouin, 91191 Gif-sur-Yvette, France

VIP Neutron DIFFRACTOMETER (5C1)
deliverd in 2010

WISH diffractometer, ISIS TS2

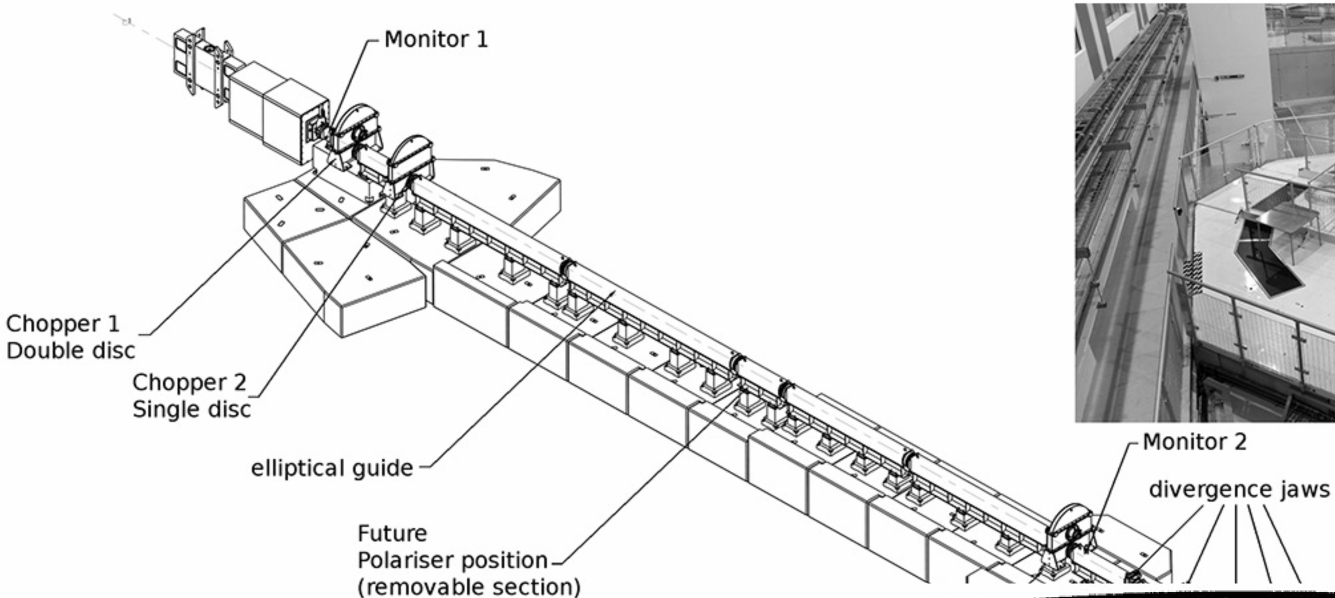

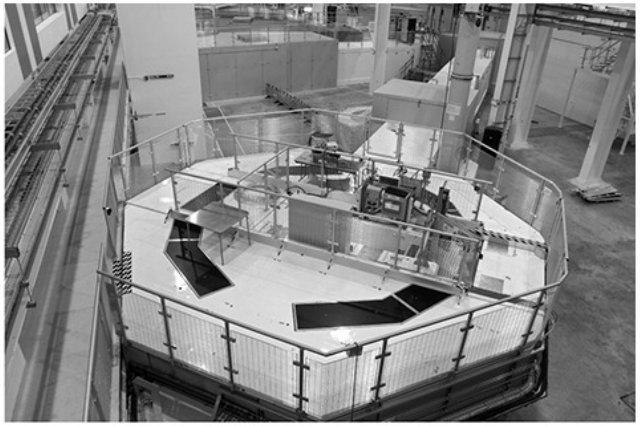

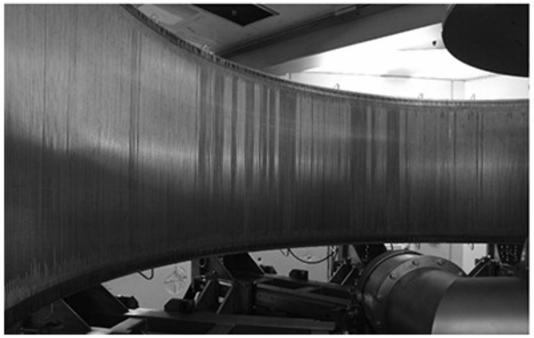

Cap2010

New 7C2
Liquid and Amorphous Diffractometer

B. Beuneu, B. Homatter (february 2012)

- 256 **position sensitive tubes**

(Ø ~ 1.2cm) 30b ^{3}He

efficiency 76 % for 0.7Å

× 5

height 47 cm

× 5

} **25**

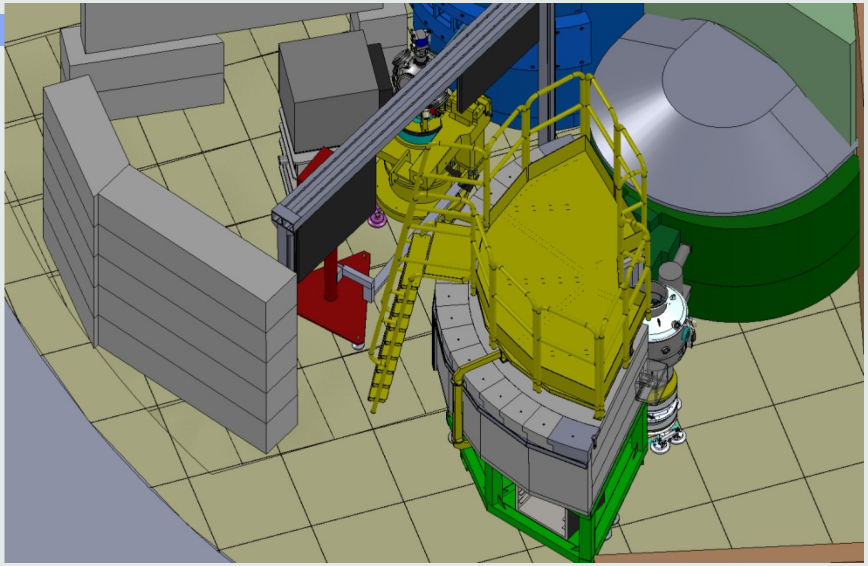

- **modular geometry**:

blocks of 16 paired tubes (2 tubes make one detector: less electronics and cables)

Opens to: 0.58Å measurements, more complex environments (HT), smaller samples, ...

LAUE DIFFRACTOMETERS

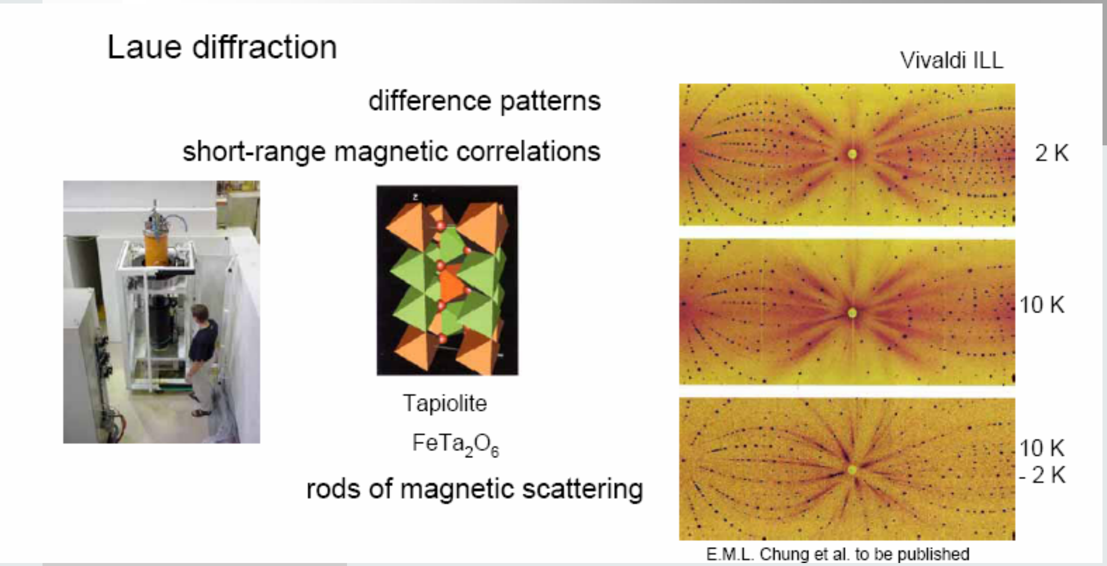

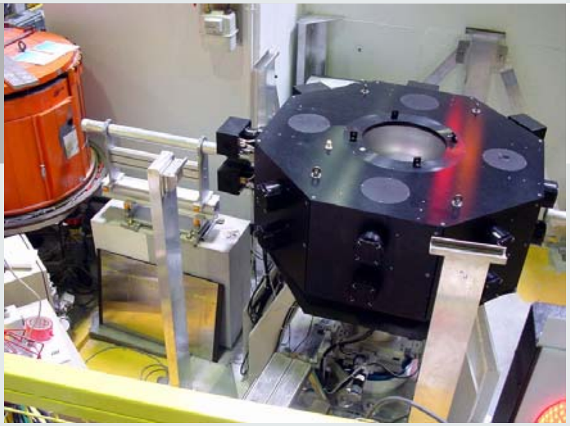

Advantages:

- Large angular covering (9 rad) High Luminosity, Small crystals

Problems:

- High Background, hkl overlapping,
- Specrum Normalisation, Wavelength dependent corrections

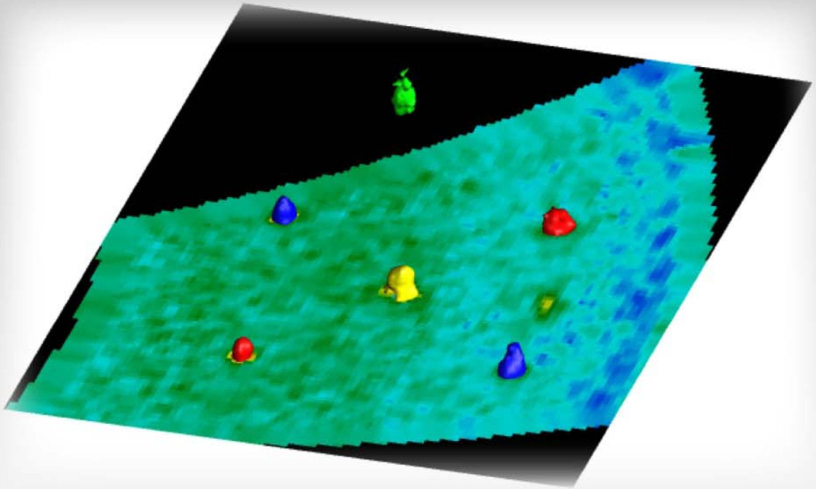

PSD4SC

Position Sensitive Detectors for Single Crystal

Relais de Courlande, LOGES-EN-JOSAS ,

November 12-14 , 2008

SPIN DENSITY ON LIGANDS O^{2-} AND FORMFACTOR OF Ru in Sr2RuO4

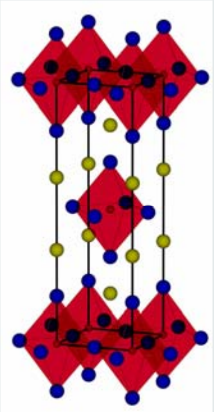

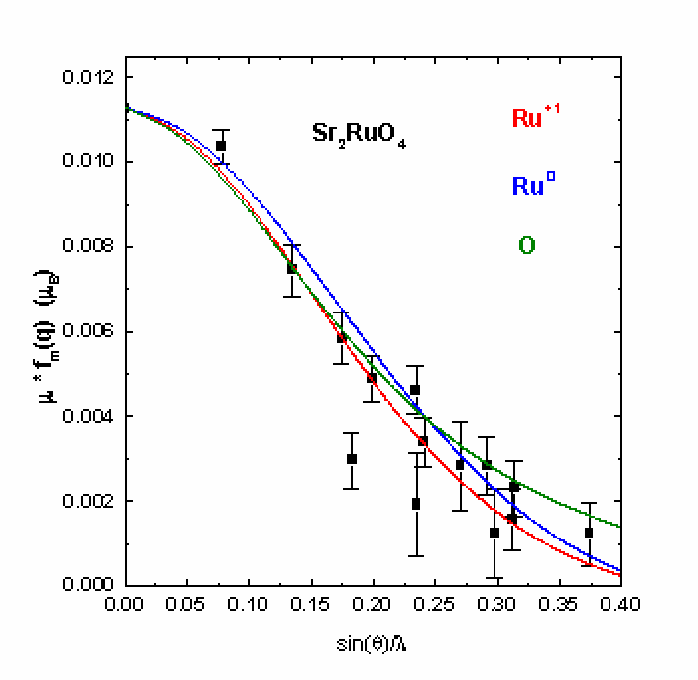

ANOMALOUS SPIN DENSITY ON OXYGEN IN $Ca(Sr)_2RuO_4$

A Gukasov, M Braden, R J Papoular, S Nakatsuji and Y Maeno
PRL, 89, 087202-1, 2002

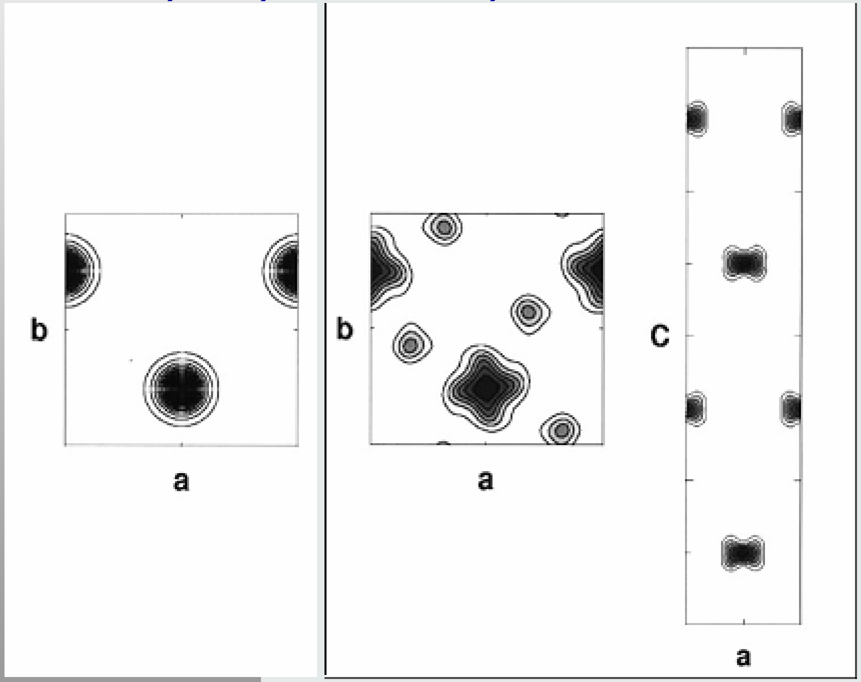

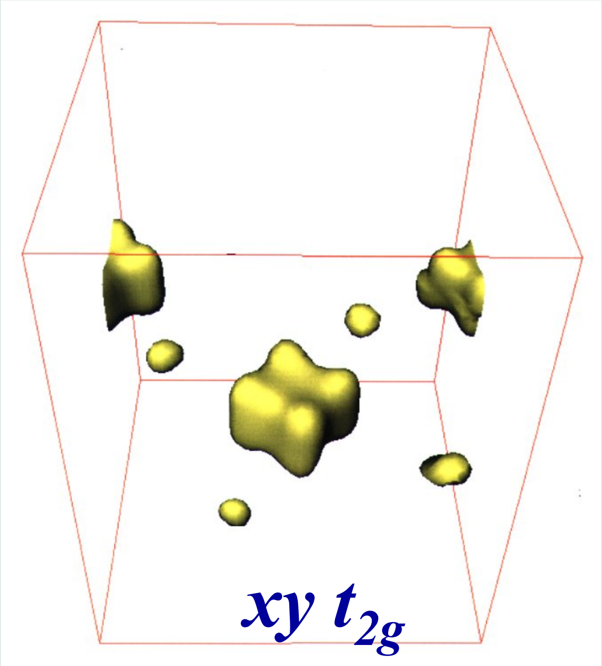

Ru^{4+} 0.36(1)μ_B **O^{2-} 0.070(2)μ_B ≈ 19% of Ru**

PSD4SC

Position Sensitive Detectors for Single Crystal

Diffuse Scattering in $Tb_2Ti_2O_7$ at 160mK

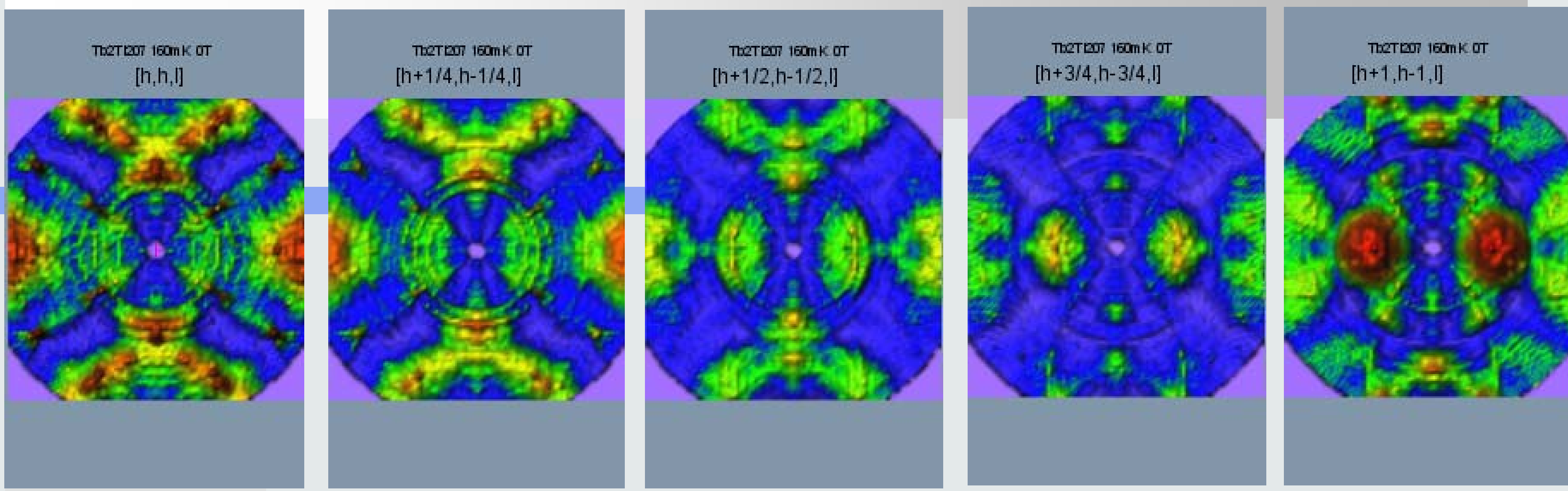

2D cuts in BZ with step δ= (0.25,-0.25,0) along the [1-10] axis

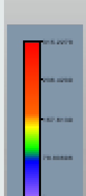

Tb2Ti2O7 H II[1-10], [hhl] cut

160mK, H=0T

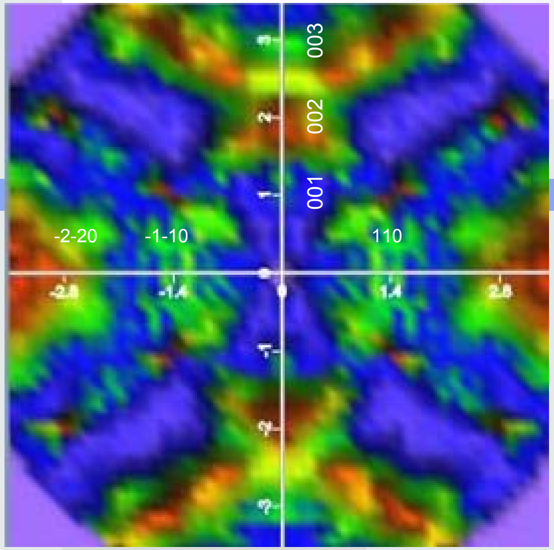

160mK, H=1T

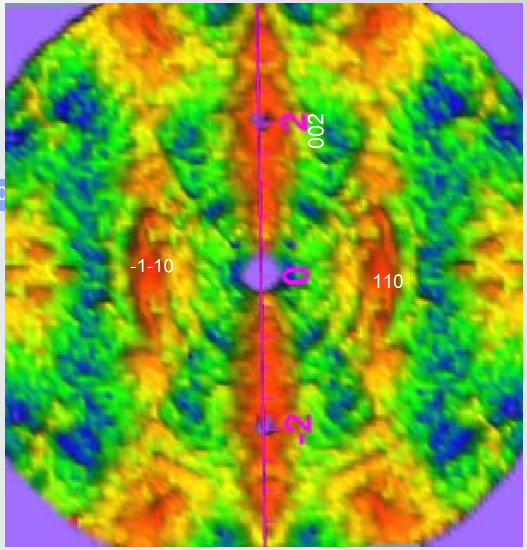

160mK, H=4T

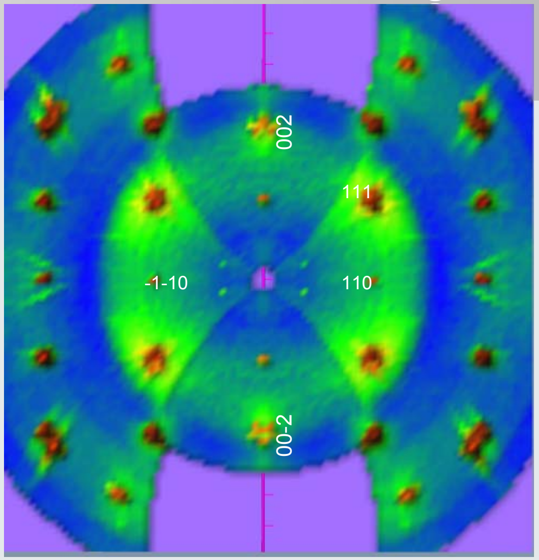

Data Treatment (II)

- Final peak extraction using Res. Parameters
- Corrections (efficiency, Lorenz etc.)
- I (hkl) , FR(hkl)

Evolution of Tb Anisotropy in $TbMnO_3$.

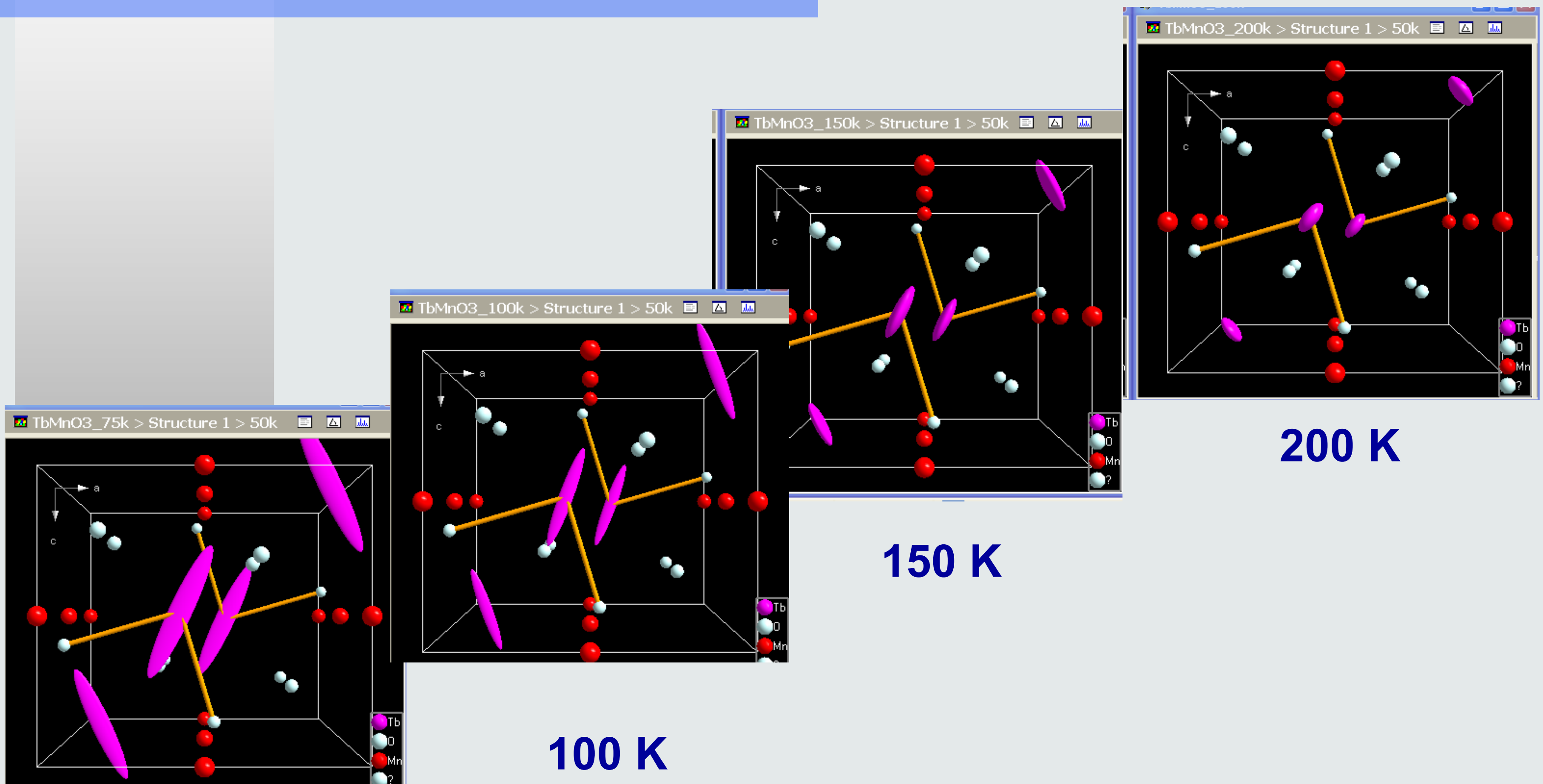

75 K

100 K

150 K

200 K

Crystal Structure of Ladder-Chain Compound $Sr_{14}Cu_{24}O_{41}$;

Sublattice CuO_2 a=11.4698, b=13.3527, c_1=2.7268 (*Amma*)

Sublattice $Sr_2Cu_2O_3$ a=11.4698, b=13.3527, c_2=3.9235 (*Fmmm*)

The $\gamma = c_1/c_2 = 0.698(8) \approx 0.7$

close to the commensurate value $\gamma = 7/10$.

(h k l) chain reflections

(h k 0.7*l) ladder reflections

(hk0) common reflections of both

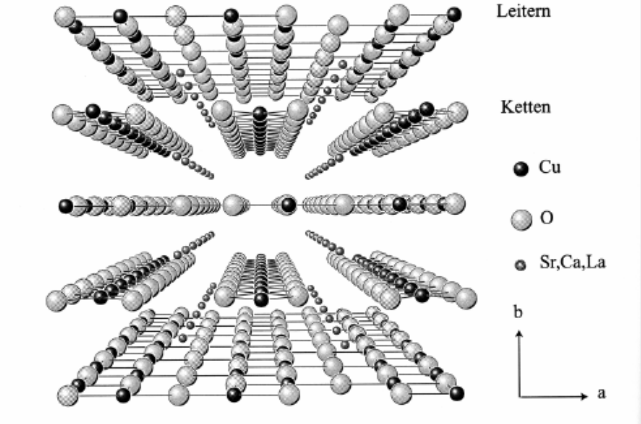

Reciprocal –space view

CuO_2 *Amma* : *k+l =2n*

$Sr_2Cu_2O_3$ *Fmmm* : *k, l=2n*

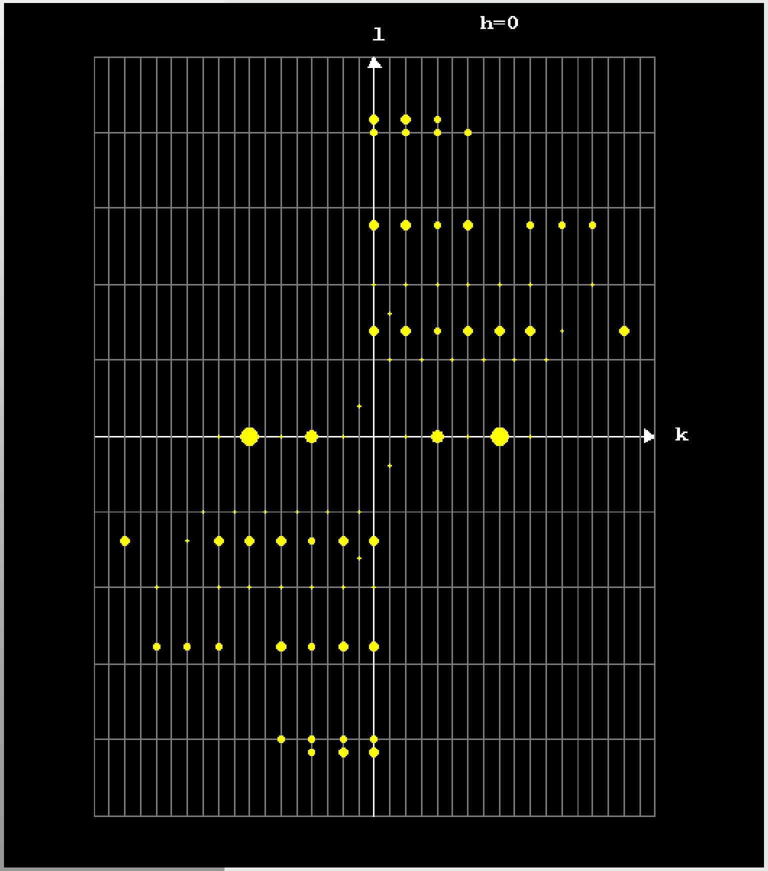

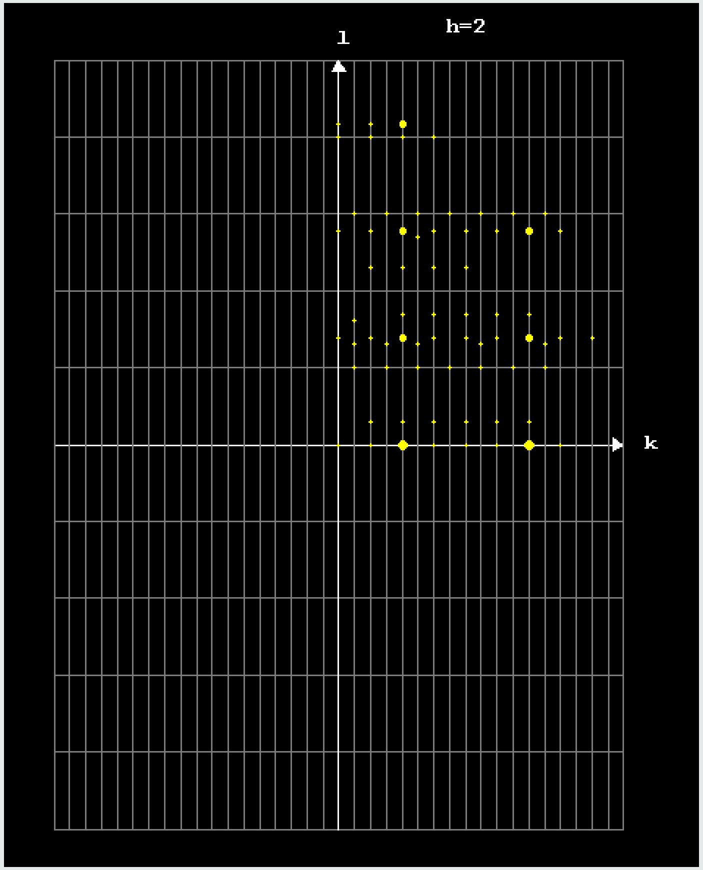

Reciprocal –space view

CuO_2 *Amma* : *k+l =2n*

$Sr_2Cu_2O_3$ *Fmmm* : *k, l=2n*

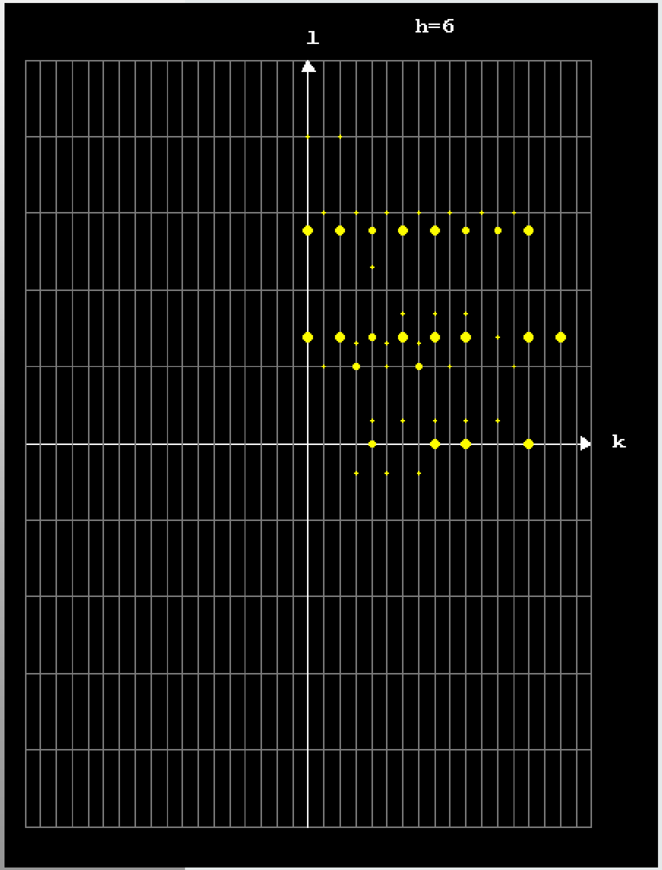

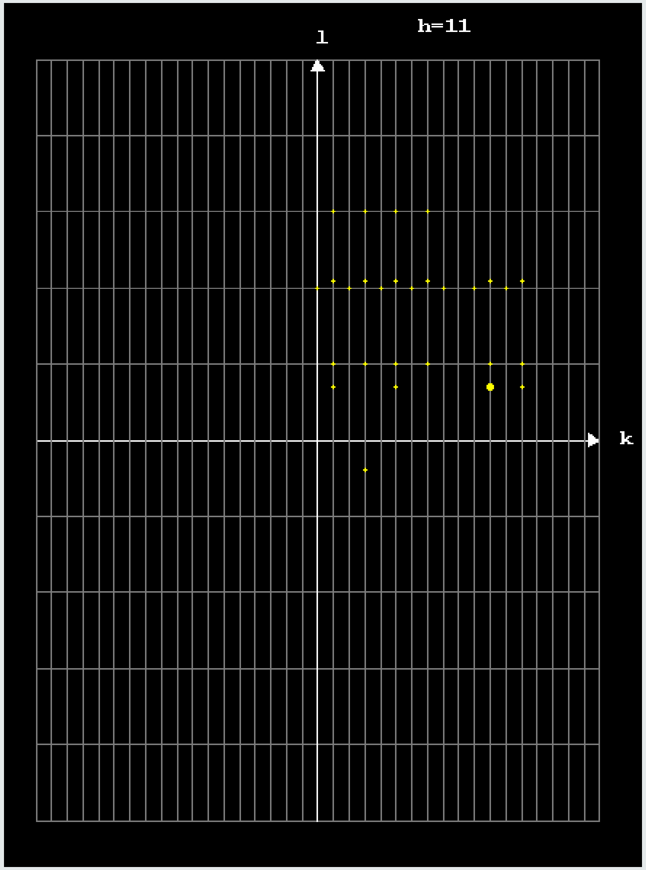

satellite (composite) reflections from interaction of lad-ch

Crystal Structure of Ladder-Chain Compound $Sr_{14}Cu_{24}O_{41}$;

$$q_{hklm} = \boldsymbol{h}a^* + \boldsymbol{k}b^* + \boldsymbol{l}c_1^* + \boldsymbol{m}c_2^* = \boldsymbol{h}a^* + \boldsymbol{k}b^* + (\boldsymbol{l} + \gamma\boldsymbol{m})c_1^*$$

Crystal of cylindrical shape of about
4x3x2.5 mm^3 ~20 mm^3

Measured reflections 1172, indep. 688., obs. ($I \geq 3$ s(I)) 502

	hkl0	*hk0m*	*(hkl±1)*	*(hkl±2)*
R_{F2}	6.25	3.11	11.86	36.66

$Sr_{14}Cu_{24}O_{41}$, Super-Space Group refinement

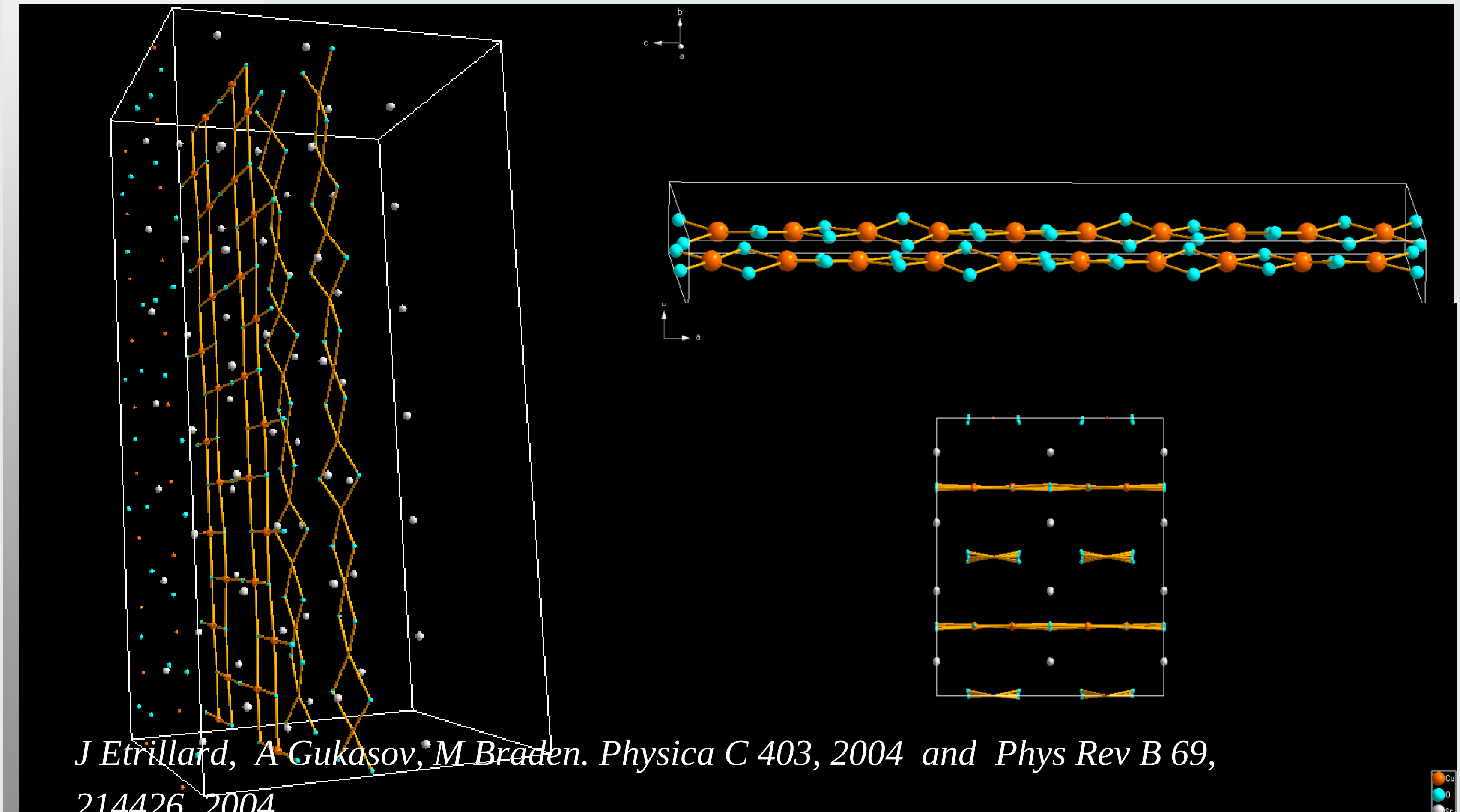

J Etrillard, A Gukasov, M Braden. Physica C 403, 2004 and Phys Rev B 69, 214426, 2004

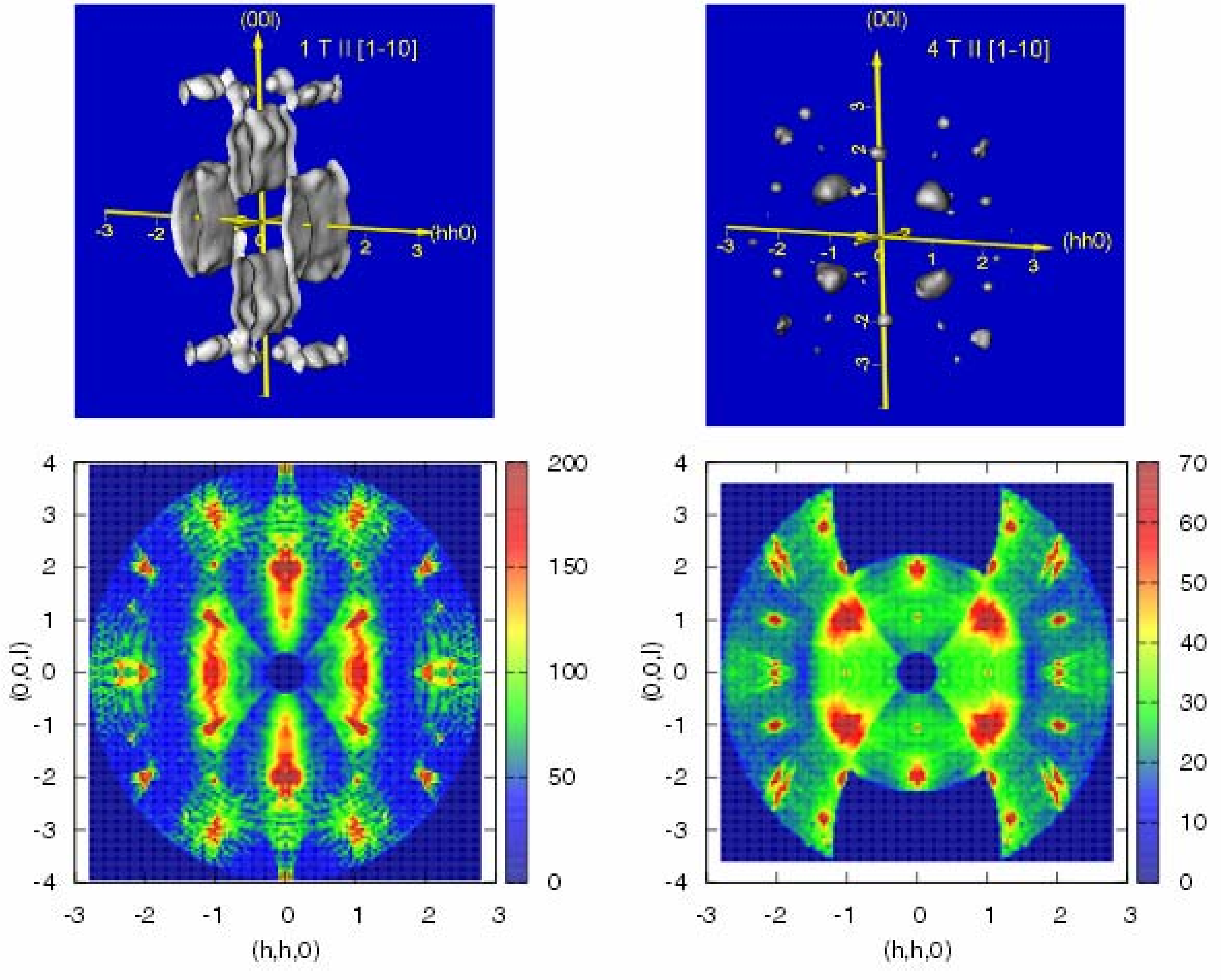

FIG. 2. (Color online) Neutron diffuse scattering maps in reciprocal space at 0.16 K in $Tb_2Ti_2O_7$ with a field applied along $[1\bar{1}0]$. (Top) 3D equal intensity surfaces for a magnetic field of 1 (left) and 4 T (right). (Bottom) Cuts in the (hhl) plane of the maps at 1 (left) and 4 T (right).